UNIVERSITY OF TURKU

PRECLINICAL EVALUATION OF NOVEL RADIOPHARMACEUTICALS FOR POSITRON EMISSION TOMOGRAPHY IMAGING OF ANIMAL MODELS OF MULTIPLE SCLEROSIS

Petri Elo

TURUN YLIOPISTON JULKAISUJA – ANNALES UNIVERSITATIS TURKUENSIS
SARJA - SER. D OSA - TOM. 1509 | MEDICA - ODONTOLOGICA | TURKU 2020

UNIVERSITY OF TURKU

PRECLINICAL EVALUATION OF NOVEL RADIOPHARMACEUTICALS FOR POSITRON EMISSION TOMOGRAPHY IMAGING OF ANIMAL MODELS OF MULTIPLE SCLEROSIS

Petri Elo

TURUN YLIOPISTON JULKAISUJA – ANNALES UNIVERSITATIS TURKUENSIS
SARJA - SER. D OSA – TOM. 1509 | MEDICA – ODONTOLOGICA | TURKU 2020

University of Turku

University of Turku
Faculty of Medicine
Clinical Physiology and Isotope Medicine
Drug Research Doctoral Programme
Turku PET Centre

Supervised by

Professor Anne Roivainen, PhD
Turku PET Centre
University of Turku
Turku University Hospital
Turku, Finland

Academician Sirpa Jalkanen, MD, PhD
Institute of Biomedicine
MediCity Research Laboratory
University of Turku
Turku, Finland

Professor Laura Airas, MD, PhD
Department of Neurology
Turku University Hospital
Turku, Finland

Reviewed by

Professor Ville Leinonen, MD, PhD
Department of Neurosurgery,
Kuopio University Hospital and University of Eastern Finland,
Kuopio, Finland

Adj. Professor Susanna Narkilahti, PhD
Faculty of Medicine and Health Technology,
Tampere University,
Tampere, Finland

Opponent

Associate Professor Andrea Varrone, MD, PhD
Centre for Psychiatry Research,
Department of Clinical Neuroscience,
Karolinska Institutet and Karolinska University Hospital,
Stockholm, Sweden

The originality of this thesis has been checked in accordance with the University of Turku quality assurance system using the Turnitin OriginalityCheck service.

ISBN 978-951-29-8181-6 (PRINT)
ISBN 978-951-29-8182-3 (PDF)
ISSN 0355-9483 (Print)
ISSN 2343-3213 (Online)
Painosalama Oy, Turku, Finland 2020

To loved ones

UNIVERSITY OF TURKU
Faculty of Medicine
Department of Clinical Medicine
Clinical Physiology and Isotope Medicine
PETRI ELO: Preclinical evaluation of novel radiopharmaceuticals for positron emission tomography imaging of animal models of multiple sclerosis
Doctoral Dissertation, 148 pp.
Drug Research Doctoral Programme
September 2020

ABSTRACT

Multiple sclerosis (MS) is the most common autoimmune disease of central nervous system (CNS) that causes chronic neurological impairment and clinical disability. Neuroinflammation is a major element in MS pathology and is present throughout the disease course contributing to clinical symptoms and irreversible neuronal damage. Magnetic resonance imaging (MRI) is the preferred imaging modality to diagnose MS. However, traditional clinical diagnosis tools are not accurate for comprehensive pathological assessment or short-term treatment evaluation. Therefore, new medical imaging methods are needed for better understanding of the disease process.

The goal of this work was to evaluate novel vascular adhesion protein-1 (VAP-1) and folate receptor (FR) targeted radiotracers and compare them with translocator protein 18-kDa (TSPO) targeted radiotracer for positron emission tomography (PET) using rat models of MS. PET studies were performed using ^{68}Ga-DOTA-Siglec-9, ^{18}F-FOL, ^{68}Ga-FOL and ^{11}C-PBR28 radioligands to assess their ability to monitor neuroinflammation, disease progression and efficacy of therapies. MRI, histology, immunofluorescence and immunohistochemistry were performed to validate novel findings and to support PET data.

VAP-1-targeting ^{68}Ga-DOTA-Siglec-9 was able to visualize acute neuro-inflammatory lesions *ex vivo*, but lacked the sensitivity to detect treatment effect and early MS-like lesions. FR-targeting ^{18}F-FOL could also visualize the lesions and, most importantly, was able to outperform ^{11}C-PBR28 by differentiating between acute and chronic lesions. ^{68}Ga-FOL was not sensitive enough to detect treatment effect or lesion progression although it could visualize the MS-like lesions.

In conclusion, FR targeting radioligands provide more specificity to PET imaging of MS-like lesions. FR is a potential target for *in vivo* imaging and development of therapies for MS patients.

KEYWORDS: Multiple sclerosis, PET, neuroinflammation, folate receptor, vascular adhesion protein-1

TURUN YLIOPISTO
Lääketieteellinen tiedekunta
Kliininen laitos
Kliininen fysiologia ja isotooppilääketiede
PETRI ELO: Uusien positroniemissiotomografia kuvantamisen radiolääkeaineiden prekliininen arviointi MS-taudin eläinmalleilla
Väitöskirja, 148 s.
Lääketutkimuksen tohtoriohjelma
Syyskuu 2020

TIIVISTELMÄ

Multippeliskleroosi eli MS-tauti on yleisin keskushermoston autoimmunisairaus, joka aiheuttaa kroonisia neurologisia toimintahäiriöitä ja kliinistä toimintakyvyn alenemaa. Tulehdus on merkittävä osatekijä MS-taudissa ja esiintyy koko taudin ajan vaikuttaen kliiniseen oirekuvaan ja pysyvään hermosolujen rappeutumiseen. Magneettikuvaus on ensisijainen kuvantamismenetelmä MS-taudin diagnostiikassa. Perinteiset kliiniset diagnosointimenetelmät eivät kuitenkaan ole tarpeeksi tarkkoja kokonaisvaltaisen diagnoosin tai lyhyen ajan hoitovasteen arvioinnissa. Siksi uusia lääketieteellisiä kuvantamismenetelmiä tarvitaan ymmärtääksemme paremmin MS-taudin kulkua.

Tämän tutkimuksen tarkoituksena oli arvioida uusien verisuonen pinnan tartuntamolekyyli-1:een (VAP-1), ja folaattireseptoriin (FR) kohdentuvien radioaktiivisten PET merkkiaineiden käyttökelpoisuutta verrattuna 18-kDa:n translokaatio proteiiniin (TSPO) kohdentuvaan merkkiaineeseen MS-taudin rottamalleissa. PET tutkimukset tehtiin ^{68}Ga-DOTA-Siglec-9, ^{18}F-FOL, ^{68}Ga-FOL ja ^{11}C-PBR28 merkkiaineilla, jotta voitaisiin arvioida näiden merkkiaineiden kykyä seurata tulehdusreaktiota, taudin etenemistä ja lääkehoitojen vastetta. Magneettikuvausta, histologiaa, immunofluoresenssia ja immunohistokemiaa käytettiin uusien löydösten validointiin ja PET löydösten tukemiseen.

VAP-1:een kohdentuva ^{68}Ga-DOTA-Siglec-9 pystyi havaitsemaan akuutin vaiheen tulehdukselliset leesiot, mutta ei lääkkeen hoitovastetta tai uusia MS-taudin kaltaisia leesioita. FR:iin kohdentuva ^{18}F-FOL kykeni myös havaitsemaan leesioita ja ennen kaikkea onnistui erottamaan akuutin ja kroonisen vaiheen leesiot toisistaan paremmin kuin ^{11}C-PBR28. Myös ^{68}Ga-FOL havaitsi leesioita, mutta ei osoittanut lääkehoidon vastetta tai leesioiden etenemistä.

Yhteenvetona voidaan todeta, että FR:iin kohdentuvat merkkiaineet tarjoavat lisää spesifisyyttä MS-taudin kaltaisten leesioiden PET-kuvantamiseen. FR on lupaava kohde sekä MS-taudin *in vivo* kuvantamiselle että lääkehoitojen kehittämiselle.

AVAINSANAT: Multippeliskleroosi, PET, tulehdus, folaattireseptori, verisuonen pinnan tartuntamolekyyli-1

Table of Contents

Abbreviations

^{11}C-PBR28	N-acetyl-N-(2-[^{11}C]methoxybenzyl)-2-phenoxy-5-pyridinamine
^{18}F-FOL	Aluminum [^{18}F]fluoride-labeled 1,4,7-triazacyclononane-1,4,7-triacetic acid conjugated folate
^{68}Ga-FOL	[^{68}Ga]gallium-labeled 1,4,7-triazacyclononane-1,4,7-triacetic acid conjugated folate
ARR	Annual relapse rate
BBB	Blood-brain barrier
BCG	Bacillus Calmette-Guérin
CD	Cluster of differentiation
CDMS	Clinically definite multiple sclerosis
CFA	Complete Freund's adjuvant
CIS	Clinically isolated syndrome
CNS	Central nervous system
CSF	Cerebrospinal fluid
CT	Computed tomography
DAB	3,3'-Diaminobenzidine
DIS	Dissemination of lesions in space
DIT	Dissemination of lesions in time
DVR	Distribution volume ratio
EC2319	Folate aminopterin drug of Endocyte
EAE	Experimental autoimmune encephalomyelitis
EDSS	Expanded disability status scale
*f*DTH-EAE	Focal delayed-type hypersensitivity experimental autoimmune encephalomyelitis
FITC	Fluorescein isothiocyanate
*f*MOG-EAE	Focal myelin oligodendrocyte glycoprotein experimental autoimmune encephalomyelitis
FOV	Field of view
FR	Folate receptor
FR-α	Folate receptor-α
FR-β	Folate receptor-β

Gd	Gadolinium
H&E	Hematoxylin-eosin
HEPES	2-[4-(2-hydroxyethyl)piperazin-1-yl] ethanesulfonic acid
HEV	High endothelial venule
HPLC	High-performance liquid chromatography
iNOS	Inducible nitric oxide synthase
i.v.	Intravenous(ly)
ICAM-1	Intercellular adhesion molecule-1
IFA	Incomplete Freund's adjuvant
IgG	Immunoglobulin G
IFN-γ	Interferon-γ
LFB	Luxol fast blue
LJP1586	Z-3-Fluoro-2-(4-methoxybenzyl) allylamine hydrochloride
MBP	Myelin basic protein
MRC-1	Mannose receptor C-type 1
MRI	Magnetic resonance imaging
MS	Multiple sclerosis
NAGM	Normal appearing grey matter
NAWM	Normal appearing white matter
NFP	Neurofilament protein
OX-42	Cluster of differentiation 11b/c
PBR	Peripheral benzodiazepine receptor
PBS	Phosphate-buffered saline
PET	Positron emission tomography
PLP	Proteolipoprotein
PML	Progressive multifocal leukoencephalopathy
PPMS	Primary progressive multiple sclerosis
PRMS	Progressive relapsive multiple sclerosis
PSL/mm^2	Photostimulated luminescence per square millimeter
ROI	Region of interest
RRMS	Relapsing-remitting multiple sclerosis
s.c.	Subcutaneous(ly)
Siglec-9	Sialic-acid binding immunoglobulin-like lectin 9
SPECT	Single photon emission computed tomography
SPMS	Secondary progressive multiple sclerosis
SSAO	Semicarbazide-sensitive amine oxidase
SUV	Standardized uptake value
sVAP-1	Soluble vascular adhesion protein-1
TAC	Time-activity curve
TB	Mycobacterium tuberculosis

TE	Echo time
TFA	Trifluoroacetic acid
TNF-α	Tumor necrosis factor-α
TLR	Toll-like receptor
TR	Time of repetition
TSE	Turbo spin-echo
TSPO	Translocator protein 18-kDa
UV	Ultra violet
VAP-1	Vascular adhesion protein-1
WM	White matter

List of Original Publications

This dissertation is based on the following original publications, which are referred to in the text by their Roman numerals I - III and on supplementary unpublished data:

I Petri Elo, Sina Tadayon, Heidi Liljenbäck, Jarmo Teuho, Meeri Käkelä, Kalle Koskensalo, Virva Saunavaara, Jenni Virta, Tibor Z. Verez, Aida Kiviniemi, Antti Saraste, Päivi Marjamäki, Laura Airas, Sirpa Jalkanen, Anne Roivainen. Vascular adhesion protein-1 is actively involved in the development of inflammatory lesions in rat models of multiple sclerosis. *J Neuroinflammation,* 2018; 15: 128.

II Petri Elo, Xiang-Guo Li, Heidi Liljenbäck, Semi Helin, Jarmo Teuho, Kalle Koskensalo, Virva Saunavaara, Päivi Marjamäki, Vesa Oikonen, Jenni Virta, Chen Qinshou, Philip S. Low, Juhani Knuuti, Sirpa Jalkanen, Laura Airas, Anne Roivainen. Folate receptor-targeted positron emission tomography of experimental autoimmune encephalomyelitis. *J Neuroinflammation,* 2019; 16: 252.

III Petri Elo, Xiang-Guo Li, Heidi Liljenbäck, Maria Gardberg, Olli Moisio, Maxwell G. Miner, Jenni Virta, Antti Saraste, Madduri Srinivasarao, Michael Pugh, Yingjuan June Lu, Philip S. Low, Juhani Knuuti, Sirpa Jalkanen, Laura Airas and Anne Roivainen. Efficacy of a new folate aminopterin treatment in a rat model of multiple sclerosis. Manuscript submitted for publication.

1 Introduction

Multiple sclerosis (MS) is the most common chronic central nervous system (CNS) autoimmune disease that causes progressive disability already in young adults. MS has multiple identified disease components including neuroinflammation, demyelination and neurodegeneration, which is believed to be the pathological correlate for permanent clinical disability in MS (Kutzelnigg & Lassmann, 2014, Compston & Coles, 2008). Despite decades of research, the etiology of MS is not fully understood. MS is not a hereditary disease, but there are several genetic and environmental factors that increase the risk of developing MS. The clinical features of MS differ between affected individuals, the relapsing-remitting MS (RRMS) being the most common form of MS. In RRMS the disease is characterized by acute worsening of neurological symptom followed by full or partial recovery. In addition to RRMS, there are several progressive forms of MS. Typically, the progressive form of MS originates from RRMS shifting to secondary progressive MS (SPMS) or alternatively the MS starts as a progressive form already at the onset of the disease, and is diagnosed as primary progressive MS (PPMS) (Compston & Coles, 2008).

MS continues to pose a major challenge for clinicians, as there is no specific diagnostic marker for MS but the diagnosis is based on clinical, magnetic resonance imaging (MRI) and laboratory evaluations of the patient (Sormani & Bruzzi, 2013). The diagnostic evaluation of MS includes gadolinium (Gd)-enhanced and T2-weighted MRI of CNS lesions, confirmation of clinical relapses rates, and evaluation of clinical disability using the Expanded Disability Status Scale (EDSS) method. MRI is currently used as a standard tool for MS diagnosis and can detect white matter (WM) demyelinating lesions dominant in RRMS (Rovira & Leon, 2008). However, all forms of MS involve an inflammatory component, which is already observed at the onset of disease and becomes more prominent and diffuse during the disease progression affecting clinical symptoms, disease progression and lesion load (Ransohoff, 2012). It is clear that currently used diagnostic methods are incapable to evaluate disease progression or measure the inflammatory activity associated with MS. There is also no sensitive method for predicting the progression or observing therapeutic effects in MS patients (Rovira & Leon, 2008). Due to this, several MS patients could undergo ineffective therapy due to incomplete or false diagnosis

reducing their long-term quality of life. In addition, the mechanisms of new MS lesions formation are difficult to examine (Pirko & Johnson, 2008). Tissue samples from early lesions are challenging to obtain from living MS patients and majority of existing lesion samples are collected from chronic lesions in *post-mortem* studies. Hence, new non-invasive medical imaging methods and markers capable for evaluating early pathology in MS lesions are of high importance in the diagnostic field of MS.

MS is uniquely a human disease, but experimental autoimmune encephalomyelitis (EAE) has been used as a fairly reliable animal model for studying the inflammatory component of MS (Ransohoff, 2012). From a wide range of EAE models, the clinically most relevant focal delayed-type hypersensitivity experimental autoimmune encephalomyelitis (*f*DTH-EAE) model can be used in experiments comparing lesion size, progression, and inflammatory activity (Serres et al., 2009). In addition, focal myelin oligodendrocyte glycoprotein experimental autoimmune encephalomyelitis (*f*MOG-EAE) is representative of acute cortical demyelination and widespread inflammation in the CNS simultaneously recapitulating many of the hallmarks of antibody-mediated inflammatory lesions in human MS (Serres et al., 2009).

Vascular adhesion protein-1 (VAP-1) and folate receptor-β (FR-β) are both inflammation specific markers and could potentially be exploited as targets for imaging inflammation in MS. VAP-1 is an endothelial cell surface molecule and primary amine oxidase enxyme. During inflammation it is translocated from the intracellular storage granules to the luminal side of vessels. This controlling of the leukocyte extravasation is a key element in inflammatory reactions (Salmi et al., 1993). FR's are mainly upregulated on malignant cells in cancer and in inflammatory conditions, but the FR-β isoform is overexpressed on activated (not resting) macrophages during inflammatory conditions (Low et al., 2007)

This thesis examines the emerging role of positron emission tomography (PET) imaging in the diagnostic field of chronic inflammatory CNS diseases such as MS. PET is non-invasive, quantitative and repetitive molecular imaging technique using targeted molecular probes labeled with positron-emitting radionuclides to evaluate rates of biochemical processes in living tissues (Kiferle et al., 2011). Molecular imaging of inflammation is a promising technique to identify high-risk individuals. However, more specific markers than the currently used glucose analogue, fluorodeoxyglucose ^{18}F-FDG, are needed to assess inflammation (Autio et al., 2013). Novel molecular imaging targets such as FR-β and VAP-1 have been validated for molecular imaging of inflammation and cancer (Aalto et al., 2011, Autio, et al., 2013). They could potentially overcome the limitations of traditionally used translocator protein 18-kDa (TSPO) targeted PET imaging in patients with MS (Turk et al, 2002, Imaizumi et al., 2007). Therefore, we investigated the utility of VAP-1

targeting PET radiotracer, ^{68}Ga-DOTA-Siglec-9, and FR-targeting PET radiotracers, ^{18}F-FOL and ^{68}Ga-FOL, for monitoring inflammatory activity, lesion progression and therapy response using animal models of MS.

2 Review of the literature

2.1 Multiple sclerosis

2.1.1 Epidemiology of MS

MS is an autoimmune disease of CNS that causes chronic inflammation, myelin destruction, axonal loss and progressive neurological disability in affected individuals (Compston & Coles, 2008). It has been estimated that there are approximately 2.8 million MS patients worldwide and the number is increasing. The prevalence and incidence of MS is highest especially in Northern Europe, Scandinavia, UK, US and Canada. On the other hand, MS is rather rare in the rest of the world and the lowest number of MS patients are located in counties close to the equator line (Browne et al., 2014). This trend is reflected in part to improved survival, and also to better diagnosis and reporting of new of MS patients in developed countries, but does not completely explain these changes (Browne et al., 2014). Environmental factors such as low exposure to sunlight, low vitamin D levels in serum, viral infections, high standard of living and genetic susceptibility genes (modifications particularly in "human leukocyte antigen" gene region) are greatly affecting to the increased risk of developing MS. The female-to-male sex ratio for MS incidence has previously been 2:1, but is currently around 4:1. Notably, this supports the view that hormonal factors are assumed to contribute to the formation and regulation of the disease course in MS (Orton et al., 2006).

2.1.2 Diagnosis standards and criteria of MS

The conventional clinical diagnosis standards for MS consist of clinical findings, new Gd-enhanced or T2 lesions detected by MRI, and evaluation of permanent clinical disability using EDSS (Polman et al., 2011). The clinical findings may include impaired vision, problems with balance, sensory disturbances, motor weakness, speech difficulties or fatigue depending on the location of the inflammatory lesion in the CNS. These symptoms are typically the first signs that may generate a suspicion of patient having MS, although similar symptoms are present in various other diseases (Compston & Coles, 2008). Therefore, these

clinical findings are not sufficient for definite MS diagnosis. Often these signs are accompanied with demyelinating plaques in the brain and/or spinal cord that can be demonstrated using MRI. These observations first present as a clinically isolated syndrome (CIS) with mono- or multifocal demyelinating lesions typically in brainstem or in optic nerve and a majority of these CIS patients develop clinically definite MS (CDMS) over time (Chan et al. 2007). As 95% patients with CDMS have shown to exhibit brain abnormalities, MRI is currently considered as an essential tool for evaluating the pathological changes that complete the diagnosis for MS. On the other hand, MRI has shown to be low in specificity showing variety of MS-like abnormalities in the brain indicating that the association of clinical disability and MRI findings are not optimal (Chan et al. 2007, Bakshi et al., 2008, Mollison et al., 2017). In addition to MRI, laboratory measurements of immunoglobulin G (IgG) or oligoglonal band from cerebrospinal fluid (CSF) are used to support the diagnosis of inflammatory lesions observed in MS and aid in the differential diagnosis (Polman et al., 2011).

When the MS patient has progressed to a degree where there is permanent disability and deficit in neurological function, the disability can be evaluated using the EDSS (Kurtzke et al., 1983). It was invented and developed to assess the clinical severity of MS by evaluating the eight functional systems of the CNS: pyramidal, cerebellar, brain stem, sensory, bowel and bladder, visual, cerebral and others. The rating scale starts from 0 and gradually increases to 10; 0 refers to no permanent disability and 10 corresponds to a death due to MS (Kurtzke et al., 1983). The lower scale values ranging from 0 to 4 in EDSS measure impairments based on the neurological examination. The Mid-range values in EDSS from 4–6 mainly describe the walking ability of a patient, while the upper range of the scale (> EDSS 6) focuses on handicaps of patients with MS. EDSS is also widely used as an endpoint in clinical trials and as a tool to assess the effectiveness of therapeutic interventions in clinical trials (Meyer-Moock et al., 2014).

The current diagnostic criteria for MS is described in the McDonald criteria (McDonald et al., 2001, Polman et al., 2011, Polman et al., 2005) and presented in Table 1. It is originally based on diagnostic criteria set out by Poser and Schumacher (Poser et al., 1983, Schumacher et al., 1965) but has been updated and improved according to scientific advancements over time. These diagnostic criteria for MS include clinical and paraclinical laboratory assessments, demonstration of dissemination of lesions in space (DIS) and dissemination of lesions in time (DIT) (Polman et al., 2011). Although, MR imaging is not required for the diagnosis, it is greatly emphasized that MRI would be used to support the clinical findings and to exclude any alternative diagnoses that exhibits similar symptoms compared to MS.

Some criticisms has been pointed towards these guidelines due to their ineffective utilization among Asian people, because of differences in clinical

features. Asian-type MS patients are typically characterized with fewer Gd-enhancing brain lesions and greater amount of Gd-enhancing spinal cord lesions compared to western-type MS patients. Therefore, the diagnostic criteria of MS is more likely to be met in an MS patient with the western-type MS (Chan et al., 2007, Yamasaki et al., 1996). In addition, pathological hallmarks are suggested to be more decisive in the diagnosis, which might improve McDonald's criteria even further (Chan et al., 2007).

Table 1. The 2017 revised McDonald diagnostic criteria for MS according to the International Panel on Diagnosis of MS (Modified from Thompson et al., 2018).

Clinical presentation	Additional data needed for MS diagnosis
≥2 attacks; objective clinical evidence of ≥2 lesions	None
≥2 attacks; objective clinical evidence of 1 lesion as well as clear-cut historical evidence of a previous attack involving a lesion in a distinct anatomical location	None
≥2 attacks; objective clinical evidence of 1 lesion	Dissemination in space demonstrated by an additional clinical attack implicating a different CNS site or by MRI
1 attack; objective clinical evidence of ≥2 lesions	Dissemination in time demonstrated by an additional clinical attack or by MRI OR demonstration of CSF-specific oligoclonal bands Dissemination in space demonstrated by an additional clinical attack implicating a different CNS site or by MRI
1 attack; objective clinical evidence of 1 lesion (clinically isolated syndrome)	Dissemination in time demonstrated by an additional clinical attack or by MRI OR demonstration of CSF-specific oligoclonal bands

2.1.2.1 Magnetic resonance imaging

Conventional MRI can be effectively used to confirm the pathological changes underlying the clinical symptoms in MS. It is routinely used in the MS diagnosis because of its sensitivity for identifying demyelinating brain lesions, especially WM plaques, in T2-weighted sequences and T1-weighted contrast enhanced (e.g. Gd) sequences as hyperintense lesions and due to good availability of MRI scanners in major clinical practices.

Several individual MRI parameters have been shown to exhibit predictive and diagnostic values for disease activity and disease progression in MS. The appearance of new T1-weighted contrast enhanced lesion and new T2 hyperintense lesions are indicative of disease activity during a relapse in RRMS, during when the blood-brain barrier (BBB) is compromised and inflammatory reaction is intensified due to the influx of inflammatory cells from periphery to the CNS. In addition, brain atrophy can serve as a reliable marker for determining clinical progression. Increased grey matter athropy is believed to correlate with clinical disability in all subtypes of MS, whereas increased total brain atrophy and lesion volume changes combined can predict permanent neurological deficits (Popescu et al., 2013).

However, there are certain limitations for MR imaging when evaluating MS patients in clinical setting. It is increasingly clear that MRI is insufficient for complete and accurate diagnosis of the disease. MRI is incapable to accurately evaluate disease progression, predict the subtype of MS or inflammatory activity (Confavreux et al., 2000). There is also no sensitive method for observing short-term therapy effects in MS patients. Longitudinal follow-up imaging of an individual MS patient could reveal patient's response to a particular therapy or determine the progression of the disease, but this frequently requires several months or even years of time to evaluate (Fazekas et al., 2007 & Rovira & Leon, 2008, Sormani & Bruzzi, 2013). Despite the drawbacks of conventional MRI in diagnosing MS, new discoveries related to non-conventional MRI-derived metrics have proven alternative tools to monitor the effects of new treatments and to measure multiple aspects of MS pathology (Rovira & Leon, 2008). These tools include the use of advanced techniques like proton magnetic resonance spectroscopy, magnetization transfer MRI and diffusion-weighted MRI, which are capable to detect more subtle MS related tissue abnormalities, such as, axonal damage and tissue integrity (Fazekas et al., 2007).

2.1.3 Subtypes of MS

MS is considered as a very diverse disease with multiple aspects, such as virus infections, genetic risk factors and environmental factors, are affecting the incidence, clinical fenotype, progression, disease burden and manifestations of the symptoms (Marrie, 2004). The clinical occurrence of MS varies greatly between the affected individuals and they might follow a variable patterns of clinical symptoms (Marrie, 2004, Lublin & Reingold, 1996). Still the clinical course of the disease can be defined by either episodic acute periods of clinical attacks with rapid worsening in neurological performance, gradual progressive decline in neurological functions with increasing permanent disability, or combinations of both characteristics. These observed features have promoted the categorization of MS into four clinically

different subtypes (Lublin & Reingold, 1996). These clinical subtypes are presented in Figure 1.

The first and the most common subtype is RRMS and 70–90 % of MS patients suffer from this subtype (Sumelahti et al., 2003). It is defined by disease relapses with full or partial recovery and periods between disease relapses that are characterized by a lack of disease progression (Lublin & Reingold, 1996). These periods are referred as remissions that typically consist of no disease activity (Confraveux et al., 2000), but there has been growing evidence that disease progression might occur even during the remission periods (Siffrin et al., 2010). The relapses usually last a relatively short period of time (months) and occur unpredictably during which the progression of the disease is very fast and the neurological function deteriorates rapidly (Young et al., 2006). Most of the RRMS patients respond to currently approved treatments for MS, which are mainly categorized as anti-inflammatory drugs (Frischer et al., 2009).

RRMS will eventually develop to SPMS, where the disease progression in characterized as a gradual progression of the disease and permanent deficits in neurological function after the initial relapsing-remitting phase with approximately 60–70% of patients transforming to SPMS within 20 years of disease onset (Compston & Coles 2008, Rovaris et al., 2006). It is distinguished from the RRMS by lack of remission periods where the progression is usually absent (Lublin & Reingold, 1996). The transition from RRMS to SPMS is typically assessed retrospectively once the patient has established a period of continuous worsening of neurological symptoms and permanent impairment. This time period can last up to a year (Rovaris et al., 2006). The most reliable pathological correlates for neurological disability in progressive phase of MS are considered axonal injury and neurodegeneration. After this transitioning, most of the currently available disease modifying therapies have very little impact on the disease course. In addition, the monitoring of pathological changes in SPMS becomes more challenging. Specific clinical biomarkers that could determine the onset of transition from RRMS to SPMS have shown little prognostic value and conventional MRI seems to poorly monitor MS once patient have entered to secondary progressive phase (Wingerchuk & Carter, 2014, Lublin et al., 2014). However, increased gray matter atrophy has been claimed to predict clinical progression in progressive phase of MS, but this evidence remains controversial (Jacobsen & Farbu, 2014). Although the progression is difficult to determine in SPMS, the clinical symptoms show less variation than during RRMS and therefore are easier to predict.

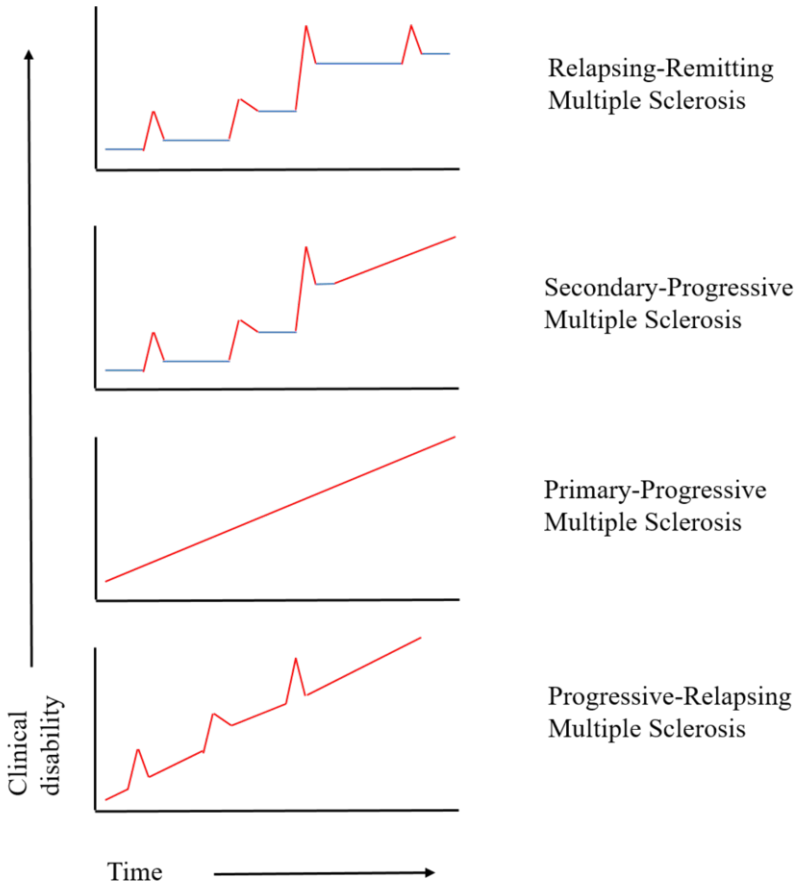

Figure 1. MS subtypes according to clinical course.

PPMS is a lot rarer compared to RRMS and SPMS subtypes of MS. It occurs in roughly 10–15% of MS patients and consist of gradual progression in neurological disability already from the onset of the disease (Miller & Leary, 2007). The onset of the primary progressive subtype is typically later in life compared to other types of MS patients, but the disease usually progresses faster and appears more severe than SPMS (Kremenchutzky, 2003). PPMS entirely lacks remission periods or minor remissions might appear at very most. The pathological changes closely resemble the pathologies occurring is SPMS, with diffuse axonal loss, microglial activation and neurodegeneration occurring in gray matter and normal appearing white matter (NAWM) (Miller & Leary, 2007). Although there is some evidence that PPMS represents a distinct form of MS with significantly milder inflammatory component compared to other progressive forms of MS (Lassmann et al., 2012, Lublin et al., 2014). Similar to SPMS, most of the currently available disease modifying therapies

show lack of efficacy in altering the disease course for PPMS with the exception of ocrelizumab, a monoclonal antibody selectively depleting B cells that has shown lower rates of clinical and MRI progression than placebo (Montalban et al., 2017).

The rarest subtype definition according to clinical course of MS is progressive relapsing MS (PRMS) and it is usually the most severe in regards to clinical symptoms and progression (Miller & Leary, 2007). It involves gradual decline in neurological function already from the onset of the disease, like in other progressive forms of MS, but the progression is superimposed with clinical attacks or relapses. Patients suffering from PRMS most commonly experience a severe relapse with only diminutive recovery, if at all (Miller & Leary, 2007). Mitoxantrone has shown efficacy towards reducing progression in SPMS and PRMS (Hartung et al., 2002).

2.1.4 Pathogenesis of MS

The pathogenesis of MS has still remained unknown, although several complex mechanisms have been suggested to trigger the pathological changes occurring in MS. However, multiple individual components of the disease have been identified and these have greatly improved our understanding of MS. MS involves a strong inflammatory component that is present already at the onset of disease and subsequently becomes more prominent and diffuse affecting heavily on clinical symptoms, disease progression and lesion load on later stages of MS (Frohman et al., 2006, Ferguson et al., 1997). Demyelination, the destruction of myelin sheath covering axons, occurs already in early stages of MS and remains as a relevant pathological mechanism throughout the disease progression. It is thought that demyelination and inflammation in MS partially occur as a discrete events (Lassmann, 1999). In general, it is thought that inflammation and demyelination over time lead to neuronal damage, axonal loss and eventually to neurodegeneration, which is believed to be a pathological correlate for permanent clinical disability in MS (Fisniku et al., 2008).

2.1.4.1 Neuroinflammation

Most of the research and currently available effective therapeutic strategies are focused on the immunological mechanisms present in MS. Therefore, the nature of inflammatory response in MS is the best known aspect of the disease (Lassmann et al., 2007). Initially, the inflammation in the MS was considered to be a result of autoreactive T-cells and macrophages reacting against myelin antigens in CNS and causing a chronic inflammatory response leading to demyelination and further neuronal damage (Bruck et al., 1995). This provided a very useful concept for the development of first therapies, such as INF-1α and INF-1β, for MS as these therapies

modulated the immune response by directly altering the overall concentration of inflammatory cytokines to express predominantly anti-inflammatory cytokines (Th2 cells) reducing the neuroinflammation (Kieseier, 2011). In early pathology of acute MS or RRMS, the composition of inflammatory infiltrates in focal plaques of WM lesions mainly consist of MHC I CD8+ T cells and mostly remain as CD8+ and macrophage dominated lesions regardless of the disease stage or activity (Lassmann et al., 2007). In active phases of lesions, the inflammatory response is amplified via BBB disruption allowing leukocyte transmigration from periphery to CNS parenchyma during inflammation (Alvarez et al., 2011).

In progressive phases of MS, such as SPMS and PPMS, the nature of inflammation slightly shifts from active inflammatory demyelinating lesions to inflammatory infiltrates composed of T cells and activated microglia. These chronic lesions typically show slow and gradual expansion of the lesions without any significant demyelinating activity. At this stage, NAWM has profound expression of activated microglia and diffuse inflammatory processes associated with axonal injury and neuronal damage not just in WM, but also in cortical gray matter of the brain (Lassmann et al., 2007, Allen et al., 2001). The BBB is commonly restored with perivascular infiltrates distinguishable in blood vessels in the brain and MRI images display lack of Gd-enhancement, indicating that inflammation can be compartmentalized in the CNS behind repaired BBB (Alvarez et la,. 2011, Hochmeister et al., 2006). In addition, these chronic type lesions are classified to 3 different categories according to their inflammatory cell compositions and demyelinating activity (Kutzelnigg et al., 2005). Chronic active lesions contain large amount of macrophages and microglia in a ring shape structure around the lesions with ongoing demyelination at these sites, whereas the core of the lesion has less of myelin degradation products and inflammatory cells. The second type of chronic lesions are considered to grow more slowly and have inactive core with some macrophages and microglia surrounding the core, as well as some macrophages located at the edge of the lesion combined with slowly occurring demyelination. On the other hand, the inactive lesions shown completely inactive core and non-existent microglial activation and macrophage recruitment throughout the lesion structure (Kutzelnigg et al., 2005, Kutzelnigg and Lassmann, 2014). These chronic lesions are most typical in progressive phases of MS, such as SPMS and PPMS, compared to active lesions, which are abundantly present in focal inflammatory lesions during RRMS.

In addition to the absence of demyelinating lesions and microglial activation, the chronic inactive lesions undergo astroglial scar formation by astrocytes (Kuhlmann et al, 2017). Therefore, astrocytes have typically been viewed as bystander cells that only contribute to the glial scar formation in MS lesions once they are completely demyelinated, but the latest data refers to astrocytes having active role in MS lesions

development (Brosnan and Raine, 2013, Ponath et al., 2017). It is believed that they recruit lymphocytes and promote tissue damage during inflammation. In the acute lesions, the astrocytes tend to exhibit hypertrophic morphology, possibly due to disruption of astrocyte-oligodendocyte connections, where the cell soma is enlarged and glia limitants is retraced from the basal lamina surrounding the blood vessel in perivascular areas throughout the lesion. This contributes to BBB leakage and specific cytokine secretion enabling further recruitment of immunce cells from periphery to sustain the inflammation. These reactive astrocytes are present at the border of demyelinating lesions and are also detected in adjacent NAWM already at early phases of lesions development (Brosnan and Raine, 2013, Horng et al., 2017). However, astrocytes have also shown to confine inflammatory activity and contribute to tissue repair especially in the chronic demyelinated lesions. The formation of glial scar is considered as a barrier for other inflammatory cells and toxins protecting the damaged tissue from further damage. It also helps to support demyelinated axons and restoration of BBB function. Furthermore, neuroprotective toll-like receptors (TLRs) are prominently expressed in astrocytes in late stage chronic lesions, which is though to attenuate inflammation and support tissue repair mediated by TLR signaling pathways (Sofroniew, 2010, Sofroniew, 2015). Despite the diverse functions of astrocytes, they appear to act similarly between different lesions.

However, each of these acute or chronic lesions can exhibit different lesion patterns that can be distinguished from each other. Pattern I lesions are dominant in T-cells and macrophages that are accompanied with demyelinating plaques and more common pattern II lesions have antibody and complement mediated inflammatory responses against myelin sheath. It has been demonstrated that the pattern II lesions are most common and are found from acute lesions. In contrast, Patterns III and IV are rarely observed in MS patients and are fundamentally different patterns compared to patterns I and II (Compston and Coles, 2008 & Lucchinetti et al., 2000). Pattern III lesions display characteristics of oligodendrocyte dystrophy and mitochondrial dysfunction leading to CNS inflammation and pattern IV lesions likewise show primary oligodendrocyte malfunction that rather originates from viral- or toxin-induced damage to myelin sheath and oligodendrocyte cells (Lucchinetti et al., 2000).

2.1.4.2 Neurodegeneration

Neurodegeneration in MS has originally believed to arise from inflammation causing demyelination in the axons, axonal damage, and disturbances in the remyelinating capacity and subsequent axonal loss. This extent of axonal injury correlated with the degree of inflammation and neuronal degeneration in MS brain (Trapp et al., 1998,

Ferguson et al., 1997). But this general view has been challenged by recent advancements in MS research (Frischer et al., 2009). Neuropathological studies have shown that profound axonal loss is occurring in NAWM, which can develop independently from axonal injury in demyelinating lesions (Evangelou et al., 2005, DeLuca et al., 2006). Furthermore, ongoing axonal injury is also observed in chronic inactive lesions in MS patients and demyelination associated with axonal and neuronal degeneration, is seen in the cortical lesions of progressive MS patients. Both of these pathological features were present in the absence of parenchymal inflammatory T- or B-lymphocytes (Bo et al., 2003). Compartmentalized inflammation (inflammation becomes trapped within the brain compartment) has been suggested as an explanation for driving disease progression and neurodegeneration in chronic phases of MS (Frischer et al., 2009). However, it is clear that axonal damage and loss can be considered as a hallmark of neurodegeneration and permanent disability (Compston and Coles, 2008).

2.1.4.3 Demyelination and remyelination

Originally it has been described by Charcot (1880) that lesions in MS are strongly associated with inflammation causing essential structural changes like demyelination and axonal damage. Although the essential components of MS have been known for a century, major achievements have improved our understanding about demyelination in MS. Currently it is believed that demyelination actually can occur independently of inflammation (Lassmann et al., 1999). This view is supported by the findings that inflammation is not restricted to demyelinating plaques as T-cell infiltrates and macrophages are recruited to the sites of demyelination after the initial steps of myelin damage (Gay et al., 1997) and active demyelination can be found even from patients that do not represent inflammatory cells in the active demyelination plaques (Prineas et al., 2001). Demyelinating lesion in MS are typically found in WM, but are located in cortical areas in the brain as well. This cortical demyelination is a characteristic feature of progressive type of disease (Kutzelnigg et al., 2005). Especially pattern III and IV lesions in MS demonstrate the discrete events of antibody-mediated demyelination and oligodendrocytes dystrophy related demyelination that is found in part from MS patients (Lucchinetti et al., 2000). In addition, evidence suggests that increased oligodendrocyte apoptosis in MS is not restricted to pattern III and IV lesions, but can be considered as important feature in all patterns of new lesion formation (Barnett & Prineas, 2004). For example, pattern I and II lesions show loss of oligodendrocytes at the active border of lesions with partial recurrence of oligodendrocytes in the inactive center of the lesions indicating remyelinating capacity, whereas rarer pattern III and IV

demyelinating lesions exhibited loss of oligodendrocytes without remyelinating axons (Lucchinetti et al., 2000).

While the evidence for the driving force of oligodendrocyte apoptosis in MS remain controversial, profound mitochondrial disturbances in the mitochondrial respiratory chain has been identified as an important component in mitochondrial dysfunction (Mahad et al., 2008). In contrast, the number of mitochondria and their enzyme activity is demonstrated to be increased in demyelinated axons in inactive lesions. This might be interpreted as a compensatory mechanism in response to the initial injury in mitochondria or to the increased energy demand of demyelinated axons to maintain myelin status (Witte et al., 2009). Thus, the resulting energy deficiency due to mitochondrial injury can significantly contribute to the independent demyelination processes present in all MS patients (Lassmann, 2014). The location of demyelinating lesions can contribute to the clinical symptoms of the disease. Cognitive deficits have been shown to correlate with extensive hippocampal demyelination in MS (Geurts et al., 2007).

Plaque formation in MS is a dynamic process highlighted by the existence of remyelinating lesions (Prineas & Parratt, 2012). Oligodendrocytes in recently demyelinated tissue exhibit a phenotype, which is known to respond to M2 polarized macrophages promoting new myelin formation in demyelinated axons (Miron et al., 2013). Often times in pattern I and II lesions the recently remyelinated axons experience repeated rounds of demyelination until the oligodendrocytes progenitor cells, responsible for remyelination capacity, are exhausted from the vicinity of demyelinating axons. On the other hand, pattern III and IV lesions show loss of oligodendrocytes at the sites of demyelination and therefore are sparce of remyelination (Lucchinetti et al., 1999).

2.1.5 Experimental autoimmune encephalomyelitis (EAE)

MS is uniquely a human disease that varies with respect to symptoms, pathogenesis and progression of the disease between individuals. It is, therefore, extremely difficult to create a comprehensive animal models that would closely mimic all features of MS (Ransohoff, 2012). EAE is the mostly used animal model that has provided vast amounts of information especially on the inflammatory component and immune cells functions in MS, and few of the current disease-modifying therapies, such as natalizumab, glatiramer acetate and mitoxantrone have been developed originally in EAE (Mix et al., 2010).

It is noteworthy that the clinical course of the EAE is affected by several individual factors like antigen, administration route and animal species (Gold et al., 2006). For example, immunization with myelin oligodendrocyte glycoprotein (MOG) creates acute EAE in C57BL mice presenting no options to evaluate relapses,

whereas immunization with myelin basic protein (MBP) or proteolipoprotein (PLP) results in chronic relapsing-remitting active EAE when induced in Swiss James Lambert mice (Mix et al., 2010). Active models of EAE require subsequent activation of immune response via injection of pertussis toxin, Complete Freund's Adjuvant (CFA) or Incomplete Freund's Adjuvant (IFA). Usually lesions in EAE are created in random and variable fashion that are located throughout the brain and spinal cord leading to severe inflammation in the CNS, but in focal delayed-type hypersensitivity (*f*DTH) model of EAE in Lewis rat the individual lesion is created focally (Anthony et al., 1998). It first resembles the characteristics of acute EAE and then progresses to chronic progressive lesion that closely mimics the lesions observed in progressive MS. Regarding lesion pathology, DTH lesion includes BBB breakdown, demyelination, T cell and macrophage infiltration at the acute phase of the disease and widespread microglial activation with demyelination and recruitment of peripheral immune cells at the chronic phase of the disease (Airas et al., 2015 and Serres et al., 2009). Therefore, the clinically more relevant *f*DTH-EAE can be used to compare lesion size, inflammatory activity and progression (to some extent) without the interference of newly formed neighboring lesions (Anthony et al., 1998 and Serres et al., 2009). The different features of common EAE models are displayed in Table 2.

The nature of the inflammatory response and the lesion progression in EAE differs to some extent from MS. Whereas patients with MS are commonly characterized with CD8+ T cell and macrophage dominated inflammatory lesions, the inflammatory response in EAE is CD4+ T cell dominated (Sriram and Steiner, 2005, Ransohoff, 2006). Secondly, inflammation is a primary event in EAE causing CD4+ T cells and CD8+ T cells to target CNS myelin antigens, such as MBP, PLP and MOG followed by demyelination events. In MS the inflammation process is believed to be induced as a consequence of damage to oligodendrocytes or microglia, respectively, leading first to persistently demyelinating axons and subsequent inflammatory reaction in attempt to repair the damaged myelin and axons (Prineas & Parratt, 2012).

EAE models are lacking the ongoing myelin destruction and function deterioration observed in MS. Second, studying chronic remyelination cannot be investigated in EAE and the lesions in EAE are mainly occurring in WM. Thirdly, EAE models are poor in studying B cell activity in CNS inflammatory process, with the exception of *f*MOG-EAE that causes antibody-mediated acute inflammation with cortical demyelination (Merkler et al., 2006 and Hauser et al., 2008). These features of EAE are still limiting the capability of preclinical studies in discovering the pathological mechanism driving the permanent neuronal dysfunction and clinical disability typical for MS patients.

2.1.6 Currently available disease-modifying treatments

Although there is still no curative treatment for MS, most of the currently approved disease-modifying treatments have shown efficacy in reducing inflammation, formation of new T2 or T1 Gd-enhancing lesions, annual relapse rate (ARR) and slow disease progression (Corboy et al., 2003, Thorkildsen et al., 2016). As majority of patients have the RRMS subtype, the therapies are primarily indicated for treating clinical conditions often preceeding CDMS, such as radiologically isolated syndrome and CIS that eventually tend to develop to RRMS (Niino, 2012). There is evidence that these available immunotherapies appear to have maximum efficacy when initiated early in the course of the disease also improving the long term disability prognosis (Freedman et al., 2013). However, the neurodegenerative component of MS cannot be effectively treated with any current medications. In contrast to therapy options for RRMS, there is currently no effective treatments for reducing the clinical disability in progressive forms of MS (Leary & Thompson, 2005), with the exception of an anti-CD20 therapy, which has an impact on lowering the clinical disease progression rate in patients with PPMS (Montalban et al., 2017). Although partially efficacious in PPMS, the anti-CD20 therapies pose an increased risk of secondary antibody deficiency that might lead to significant complications like serious infections associated with hypogammaglobulinemia (Tallantyre et al., 2018). All approved therapies for MS are displayed in a Table 3.

There has been over 20 years of experience in the use of therapies that are able to alter the disease course in RRMS (Hauser et al., 2013, Thorkildsen et al., 2016). Currently the focus of the development of new therapies has changed towards not only reducing inflammatory activity and ARRs in MS, but halting clinical disability and preventing new disease activity in all subtypes of MS (Havrdova et al., 2010).

Up to date, several first-line treatments have been developed including interferon beta, teriflunomide, glatiramer acetate, dimethyl fumarate, diroximel fumarate and siponimod (Thorkildsen et al., 2016, FDA news release, 2019). In general, the first-line medications have shown efficacy in reducing the ARR by about 30%, reducing the progression of disability in RRMS and disease activity measured with MRI, while the most common side effects present transitory flu-like symptoms like fever, chills, headache and back pain (Ebers, et al., 1998, Comi et al., 2001).

For second-line medications, the treatment effect is more drastic. The effect in reducing the occurrence of commonly used primary endpoints in clinical MS trials is normally 25–50% compared to first-line treatments. However, these medications may be associated with grater risks of developing severe CNS complications, such as progressive multifocal leukoencephalopathy (PML), compared to first-line therapies (Thorkildsen et al., 2016). These second-line therapies for example include fingolimod, natalizumab, alemtuzumab, cladribine, mitoxantrone and ocrelizumab (Thorkildsen et al., 2016, FDA news release, 2019, Montalban et al., 2017).

Table 2. Characteristics of commonly used EAE animal models in preclinical research of MS.

EAE models	induction	activation	development of symptoms	lesion pathology	intended use	clinical symptoms
Active EAE with whole brain immunization, *1)*	Repeated injections (i.m.) of brain emulsions and extracts in water-oil emulsion	—	days	Sings of meningitis, demyelination	virus-induced paralysis	local or systemic paralyses, death
Active EAE with whole myelin, *2)*	With MBP/PLP emulsified in CFA	—	10-21 days	no/little demyelination, CD4+cells, disseminated acute lesions	inflammation and relapses in EAE	weight loss, leg paralysis, tremor
Active EAE with MBP-peptides or MBP-specific lymph node cells, *3)*	Injection (s.c.) of MBP-peptides or lymph node cells and TB	Injection (i.p.) of pertussis toxins	11-18 days	no/little demyelination, CD4+cells, disseminated acute lesions	inflammation, relapses and therapies in EAE	loss of righting reflex, limb paralysis
Active EAE with MOG, *4)*	Immunized with MOG or MOG-peptides in CFA supplemented with TB	Injection (i.v.) of pertussis toxins	10-25 days	widespread demyelination, encephalitogenic T cells, (CD3+), macrophages and astrocytes	development of immunotherapies	loss of righting reflex, limb paralysis
AT-EAE with Th17 cells or lymph node cells, *5)*	Injection of myelin-reactive CD4+ or Th17 cells	—	14-18 days	minimal demyelination, spinal cord lesions, widespread inflammation, encephalitogenic T cells and B cells	primarily evaluation of pathology in EAE and in MS	limb paralysis, loss of coordinated movement
AT-EAE with myelin targeted CD8+ cells, *6)*	Injection of myelin-reactive CD8+ cells	—	3-14 days	more lesions in the brain, milder inflammation, CD8+ cells, lymphocytes and macrophages	pathology in EAE and in MS	ataxia, weight loss, paralysis, death

Table 2. Continued

EAE models	induction	activation	development of symptoms	lesion pathology	intended use	clinical symptoms
Chronic progressive EAE with pertussigen, *7)*	mouse spinal cord in CFA containing TB	pertussi-gen	11 days – 3 months	T lymphocytes, macrophages, CD4+ dominated lesions, mononuclear cells	Chronic CNS inflammation evaluation	weight loss, limb paralysis, tremor
Transgenic EAE, *8)*	Transgenic modification (for example IL-12, TNF-α, INF-γ)	—	1-6 months	Inflammatory demyelinating lesions in the CNS, neutrophilic granulocytes, macrophages and T lymphocytes	Individual cytokines in EAE pathogenesis	tremor, ataxia, epilepsy
Focal MOG-EAE, *9)*	Immunization (s.c.) with MOG-peptides	cytokines (corpus callosum)	1-18 days	B cells, complement activation, microglia and macrophages, T lymphocytes	B cells in CNS inflammation, relapses	loss of weight, epilepsy, incoherence
Focal DTH-EAE, *10)*	BCG injection in striatum	Injection of CFA with TB	11 days – 6 months	microglia and macrophages, T lymphocytes, CD4+ dominated lesions	acute & chronic CNS inflammation	mild incoherence and weight loss

From studies: *1)* = Freund et al 1947, *2)* = Laatsch et al 1962, *3)* = Wekerle et al 1994, *4)* = Genain et al 1995, *5)* = Paterson et al 1960, *6)* = Huseby et al 2001, *7)* = Munoz et al 1984, *8)* = Goverman et al 1993, *9)* = Merkler et al 2006 and *10)* = Serres et al 2009.

Table 3. Currently available disease-modifying therapies for MS. Modified from Thorkildsen et al 2016 and supplemented from fda.gov (news release, 2019).

Therapy (administration)	Suggested mode of action	Approved indication
Interferon β 1-a/b (i.m. or s.c.)	Inhibition of T-lymphocyte proliferation	CIS, RRMS & active SPMS
Glatiramer acetate (s.c.)	Promotes Th2 and Treg differentiation for anti-inflammatory effect	CIS, RRMS & active SPMS
Teriflunomide (p.o.)	Inhibition of *de novo* pyrimidine synthesis leading to reduced number of circulating lymphocytes	CIS, RRMS & active SPMS
Dimethyl fumarate (p.o.)	Anti-inflammatory effects mediated through NRF2 transcriptional pathway	CIS, RRMS & active SPMS
Diroximel fumarate (p.o.)	Anti-inflammatory effects mediated through NRF2 transcriptional pathway with improved gastrointestinal tolerability	CIS, RRMS & active SPMS
Fingolimod (p.o.)	S1PR mediated inhibition of autoreactive lymphocyte transmigration from the lymph nodes to the CNS.	CIS, RRMS & active SPMS
Siponimod (p.o.)	Similar to Fingolimod, but more selective modulation of S1PR, modulates $S1PR_1$ and $S1PR_5$ subtypes	CIS, RRMS & active SPMS
Natalizumab (i.v.)	Monoclonal anti-VLA-4 antibody against α4-integrin, inhibiting the migration of inflammatory cells into the CNS.	CIS, RRMS & active SPMS (monotherapy)
Alemtuzumab (i.v.)	Monoclonal anti-CD52 antibody, antibody dependent cellular cytolysis and complement-mediated lysis causing depletion and repopulation of lymphocytes	RRMS
Mitoxantrone (i.v.)	Interacts with nuclear DNA and targets proliferating immune cells, inducing apoptosis of T- and B lymphocytes and macrophages.	RRMS, SPMS & PRMS
Cladribine (p.o.)	Deoxyadenosine analog phosphorylation resulting in preferential and sustained reduction of peripheral T and B lymphocytes	CIS, RRMS & active SPMS
Ocrelizumab (i.v.)	Monoclonal anti-CD20 antibody, selective depletion of CD20-expressing B cells	CIS, RRMS, SPMS & PPMS

2.2 Positron emission tomography

PET imaging is a promising technique to identify disease processes in living patients. It offers a valuable approach to diagnosis, therapy planning and *in vivo* monitoring and it can especially be exploited for imaging cancer and inflammation (Autio et al., 2013). Although MRI has been considered as a gold standard for diagnosing and evaluating the brain abnormalities related to MS, PET imaging has also a valuable potential to explore relevant aspects of neuroinflammation, neurodegeneration and visualize extralesional pathological processes that are present in progressive forms of MS (Airas et al., 2015, Barkhof, 2002). In addition, Gd-enhanced and T2-weighted MRI at 6 to 12 months after an effective therapy initiation is required to demonstrate the reduction in pathological hallmarks of MS (Miller et al., 1996). This efficacy could optimally be observed in MS patients after weeks with PET imaging.

2.2.1 Principles of PET imaging

PET imaging is non-invasive, three dimensional (3D), quantitative and repetitive molecular imaging technique using targeted probes labeled with positron-emitting radionuclides to visualize and measure rates of biochemical processes in tissues of living subjects (Kiferle et al., 2011). In a PET radioligand, these probes are usually chemically incorporated with a short-lived radionuclide such as ^{11}C, ^{13}N, ^{15}O, ^{18}F and ^{68}Ga, which will eventually cause (γ) radiation at the target site detectable with PET camera. Over time, the radioligand accumulates at this target site and can be quantified as a function of time within a region of interest (ROI).

In more detail, the radionuclides used in PET imaging are radioactive isotopes that undergo a radioactive beta plus (β^+) decay, where proton is converted into a neutron and at the same time the proton is emitting a positron and neutrino. These emitted protons travel in a tissue releasing their kinetic energy until the proton collides with an electron. This annihilation of proton and electron will result in an emission of two gamma γ-photons, which will travel roughly in opposite direction (180, 25°) with 511 keV energy. This event is detected by scintillation detector crystals located in a rim shaped structure in a PET camera around the imaged object (Cherry et al., 1997, Turkington et al., 2001). The detectors trace the location of the initial annihilation site along the line of response. It is noteworthy that most annihilation events are rejected, because both annihilated photons of a single event may not hit the detector. As only linear annihilation events are included in the PET image production, nonlinearity of annihilation, among crystal size and positron range are significantly restricting the spatial resolution of a PET image (Ching et al., 2012). Finally, photomultiplier tubes are used to improve the acquired signals and image reconstruction algorithms form the final image for analysis.

Typically PET data is acquired either from static or dynamic images. In static PET imaging, the image data is collected over a single time frame to visualize the radioligand distribution in an imaged object. These static imaging protocols are beneficial as they offer clinical applicability, where the relative tracer uptake is of interest (e.g. cancer diagnosis). However, static imaging protocols may cause bias if only a single image is considered to represent the overall tracer metabolism (Muzi et al., 2012). On the other hand, dynamic PET imaging utilizes the time-activity curves (TAC's) that represent the amount of radioactivity in each pixel as a function of time during the time course of the imaging. Therefore, dynamic PET imaging provides better assessment tools on the tracer uptake, kinetics and retention than static PET imaging and is often used as a PET data acquisition method during new PET radioligand studies (Kiessling et al., 2017, Muzi et al., 2012).

2.2.2 PET radioligands in the imaging of MS patients

PET imaging studies of MS have utilized the neuroinflammatory reactions generally involved in neurodegenerative and neoplastic brain disorders (Chauveau et al., 2008). CNS is characterized as an immunoprivileged site with the presence of BBB and reduced immunosurveillance due to lack of normal lymphatic drainage. Therefore, the cellular response in neuroinflammation alters from the immune response occurring in periphery (Bailey et al., 2006). Neuroinflammation involves the activation of cells such as astrocytes, microglia and peripheral infiltrated macrophages, which all express elevated levels of TSPO formerly referred to as the peripheral benzodiazepine receptor (PBR). TSPO is a membrane protein in an outer mitochondrial membrane that is expressed in various cell and tissues types throughout the body, but the basal expression of TSPO under normal conditions in CNS is very low. Hence, TSPO is considered as a marker of inflammation in the brain (Harberts et al., 2012). Majority of the PET radioligans are consequently targeting TSPO and radiolabeling of TSPO ligands have allowed the imaging of TSPO expression in neuroinflammatory conditions, and established the concept of PET imaging in diagnosing MS (Schweitzer et al., 2010, Luus et al., 2010). ^{11}C-labeled tracer ^{11}C-(*R*)-PK11195 (^{11}C-N-methyl-N-[1-methylpropyl]-1-[2-chlorophenyl]-isoquinoline-3 carboxamide, ([^{11}C]PK11195) was the first tracer to be consistently used in PET imaging studies, because of its usefulness in animals and clinical studies of neuroinflammation. Despite the popularity, it possesses numerous limitations including low binding affinity, high lipophilicity, poor signal-to-noise ratio, lack of selectivity and capability to visualize subtle levels of TSPO expression (Dickens et al., 2014, Ching et al., 2012). In addition to [^{11}C]PK11195, [^{11}C]Ro5-486 is also considered to belong to first generation TSPO radioligands. However, the

binding affinity of [^{11}C]Ro5-4864 is both temperature- and species-dependent drastically limiting its use in further human studies (Farges et al., 1994).

The development of second generation TSPO radioligands has attempted to solve these issues related to first generation TSPO radioligands with various stages of success (Schweitzer et al., 2010). In general, the second generation TSPO radioligands exhibit improved specificity, affinity, lower lipophilicity, lower nonspecific binding and metabolism compared to e.g. [^{11}C]PK11195 (Imaizumi et al., 2007). These TSPO ligands have typically constructed from other structural classes like acetamides, vinyl alkaloids or pyrazolopyrimidines (Alam et al., 2017). The most important first, second and new generation TSPO radioligands in human studies have been summarized in Figure 2.

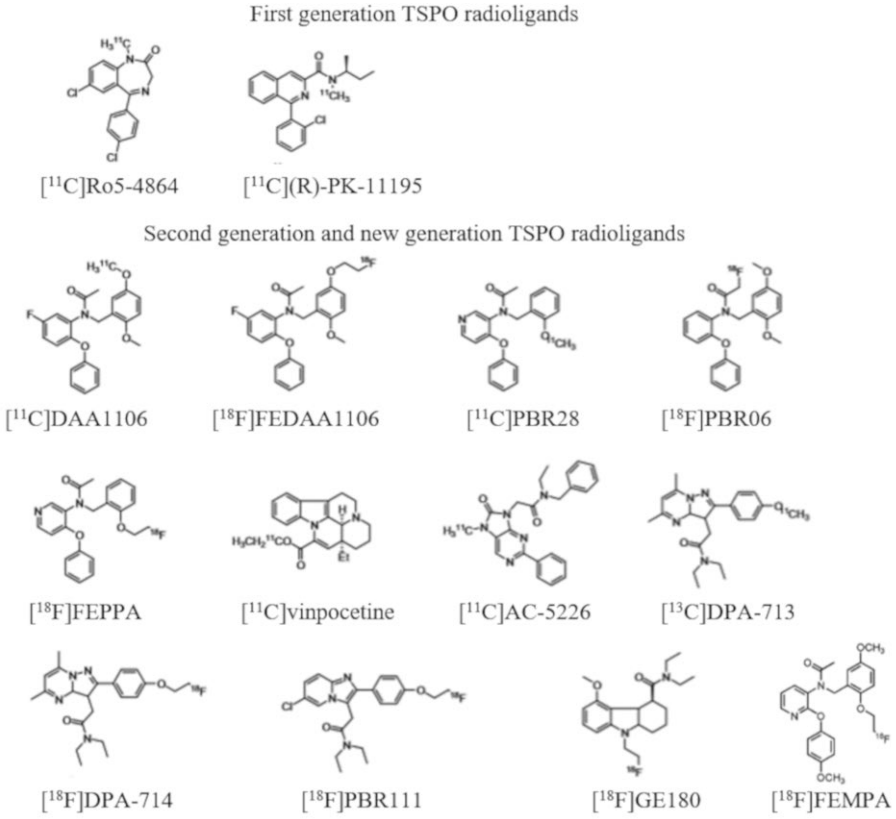

Figure 2. First and second generation TSPO radioligands in clinical studies. (Modified from Alam et al., 2017).

2.3 New imaging targets and radioligands for PET imaging of MS

Despite the recent developments, TSPO targeting radioligands are not microglia or macrophage specific markers by definition, which has given rise to the development of new generation radioligands that use alternative targets for imaging microglia and macrophages (Lavisse et al., 2012). The goal with the new PET imaging agents is either to target microglia or macrophage-specific markers, detect the independently occurring neurodegeneration or to trace the source of progressive disability in MS (Rissanen et al., 2013, De Paula Faria et al., 2014). Therefore, several novel targets for imaging MS have been identified and they are represented in Table 4.

2.3.1 Vascular adhesion protein -1

An example of an alternative molecular target for PET imaging of MS or EAE is VAP-1. Each of the MS subtypes, RRMS, SPMS, PPMS, RPMS, comprises of inflammation that is present already at the onset and is more heavily involved on later stages as the disease progresses. In all cases, residential immune cells in the CNS are insufficient to completely regulate the pathogen defense (Siffrin et al., 2010). Therefore, amplification of immune response from the periphery is considered as substantial in pathogenesis of MS (Airas et al., 2006). This immune cell recruitment requires interaction between leukocyte ligands and its receptors on endothelial cell wall mediated by several adhesion molecules from which VAP-1 plays a crucial role in this process (Carlos et al., 1994).

VAP-1 is a 170-kD endothelial cell surface molecule with dual function: both adhesive and enzymatic properties. It is mainly responsible for controlling the transmigration of leukocytes to the sites of inflammation and conversion of primary amines into corresponding aldehydes. Under normal condition, VAP-1 is stored in intracellular storage granules located in the vessel wall. Although during inflammation, VAP-1 is rapidly upregulated by the endothelial cells and it is translocated from the intracellular granules to the luminal surface of the endothelium (Salmi et al, 1993, Castillo et al., 1998).

Leukocyte transmigration is also mitigated by BBB breakdown, where the leukocytes can passively migrate to CNS parenchyma without active transportation by adhesion molecules (Alvarez et al., 2011). One might suspect that in MS the BBB remains active for adhesion molecules like VAP-1 once the BBB has initially been compromised during a relapse in RRMS. Based on this assumption, VAP-1 targeted PET radioligands could constitute as a promising approach for PET imaging of MS.

Table 4. PET radioligands applied in MS patients or animal models of MS (Modified from De Paula Faria et al., 2014 and supplemented from Auvity et al., 2020).

Target	MS characteristic	PET tracer	Application of PET imaging
TSPO	Neuroinflammation	[^{11}C]PK11195	Clinical
TSPO	Neuroinflammation	[^{11}C]PBR28	Clinical
TSPO	Neuroinflammation	[^{11}C]vinpocetine	Clinical
TSPO	Neuroinflammation	[^{18}F]FEDAA1106	Preclinical
TSPO	Neuroinflammation	[^{11}C]DAC	Preclinical
TSPO	Neuroinflammation	[^{18}F]DTPA714	Preclinical
TSPO	Neuroinflammation	[^{18}F]PBR111	Preclinical
Glucose metabolism	Neuroinflammation and neurodegeneration	[^{18}F]FDG	Clinical
A_{2A} receptors	lymphocytes and macrophages	[^{11}C]TMSX	Clinical
A_1 receptors	Downregulation in MS	[^{11}C]DPCPX	Preclinical
A_1 receptors	Downregulation in MS	[^{11}C]MPDX	Preclinical
Choline metabolism	De- and remyelination	[^{11}C]Choline	Clinical
Choline metabolism	De- and remyelination	[^{11}C]BMB1	Preclinical
Myelin	De- and remyelination	[^{11}C]CIC	Preclinical
Myelin	De- and remyelination	[^{11}C]MeDAS	Preclinical
Myelin	De- and remyelination	[^{11}C]PIB	Clinical
Cholinergic neurons	Neurodegeneration	[^{11}C]MP4A	Clinical
Amylod-β deposits	Damaged white matter	[^{18}F]Florbetaben	Clinical

2.3.1.1 ^{68}Ga-DOTA-Siglec-9

The translocation of VAP-1 to the luminal side of blood vessels is a key element in controlling leukocyte trafficking during inflammatory conditions (Salmi et al, 1993). This process can be utilized in *in vivo* PET imaging. It has also been discovered that sialic-acid binding immunoglobulin-like lectin 9 (Siglec-9) is a leukocyte ligand of VAP-1 and ^{68}Ga-labelled Siglec-9 motif facilitates *in vivo* imaging of inflammation. Gallium-68-labelled 1,4,7,10-tetraazacyclododecane-N,N′,N″,N‴-tetraacetic acid conjugated sialic acid-binding immunoglobulin-like lectin 9 (^{68}Ga-DOTA-Siglec-9) has successfully been used for imaging of peri-implant infections in rats, tumor melanoma models, animal models of atherosclerosis and inflammation (Aalto et al., 2011, Ahtinen et al., 2014, Siitonen et al., 2019, Silvola et al., 2016). In addition, the inhibition of VAP-1 activity in

non-clinical studies has shown to reduce EAE symptoms in mice once the disease has progressed to a relapse phase (O'Rourke et al., 2007). Therefore, ^{68}Ga-DOTA-Siglec-9 could be considered as a promising approach for PET imaging of neuroinflammation related conditions such as MS.

2.3.2 Folate receptor –β

Folic acid (folate) is considered as a necessary ingredient for normal cell survival, proliferation and function (Hilgenbrink & Low, 2005). In healthy cells, the folate is usually acquired via either a reduced folate carrier and/or the proton-coupled folate transporter (Sirotnak & Tolner, 1999, Qiu et al., 2006). Nevertheless, the remaining folate uptake system is the high-affinity cell surface folate receptor (FR), a glycosyl phosphatidyl inositol–anchored glycoprotein (38–45 kDa) that binds preferentially to folic acid with approximately 1000-fold higher affinity for folate than other folate transportation pathways. This FR is largely upregulated on malignant cells in cancer, atherosclerosis and in inflammatory conditions (Low et al., 2007). Generally, there are four different isoforms (folate receptor-α, (FR-α), -β, -γ and –δ) of FRs recognized, which two of them are specific for pathological conditions. Whereas, FR-α isoform is upregulated primarily on tumor cells that require excessive amounts of folate for abnormal cell proliferation (Elnakat & Rathnam, 2004), the FR-β is overexpressed on activated (not resting) macrophages during inflammation conditions, such as in rheumatoid arthritis, Crohn's disease, atherosclerosis, inflammatory osteoarthritis and in animal models of EAE, and therefore constitutes as an excellent marker for inflammatory conditions (Low & Anthony, 2004, Turk et al., 2002). In contrast to previous FR isoforms, FR −γ and –δ isoforms are detected in normal and malignant hematopoietic cells and are not consequently considered as a promising targets for therapeutic interventions or imaging agents (Elnakat & Rathnam, 2004).

However, FR-α and FR-β have been targets for the development of folate-based imaging and therapeutic agents because the concept of folate-conjugation provides multiple advantages compared to conventional agents including relatively easy and straight-forward conjugation process, finite availability of FR in healthy tissues, very high affinity (K_D = 10 nM) for FR-α and FR-β isoforms and consequently low toxicity (Low et al., 2007).

Although FR-β expression is relatively little studied in MS or EAE, it would provide a potential target for diagnosing MS, because macrophages and microglia are known to be fundamental for MS and EAE pathogenesis. Growing amount of research supports the view of functionally different polarization phenotypes in inflammatory reactions in MS or EAE (Janssen et al., 2018, Lassmann et al., 2007, Bogie et al., 2014). In these conditions, microglia and macrophages are considered

to be polarized into proinflammatory M1 or immunomodulatory M2 dominant polarization patterns where M1 proinflammatory alterations have developed to induce inflammatory reactions, pathogen-defense and propagate disease process. M2 phenotype is characterized by immunoregulatory functions, tissue remodeling, remyelination, debrief cleaning or inducing and maintaining recovery from chronic inflammation (Miron et al., 2013, Sica & Mantovani, 2012). Based on the expression patterns of FR-β on either M1 or M2 polarized macrophage phenotypes, FR-β-targeted folate-conjugated *in vivo* imaging agents could further facilitate in capturing the heterogeneity of dynamic activation patterns occurring in neuroinflammation.

2.3.2.1 Al^{18}F-NOTA-Folate

Various folate-targeted *in vivo* PET imaging compounds have shown promise in imaging activated macrophages that are relevant in the pathogenesis and immune response in several inflammatory conditions (Hilgenbrink & Low, 2005, Low et al., 2007). Especially, aluminum [^{18}F]fluoride-labeled 1,4,7-triazacyclononane-1,4,7-triacetic acid conjugated folate ([^{18}F]AlF-NOTA-Folate, ^{18}F-FOL) has recently been successfully studied as a PET imaging agent for targeting FRs in tumor xenografts and inflammatory atherosclerotic lesions (Chen et al., 2016, Silvola et al., 2018). It has shown to pose improved radiopharmaceutical properties over ^{99m}Tc-EC20, a clinically established folate-targeted single photon emission computed tomography (SPECT) imaging agent, providing a viable alternative tool for imaging FR-positive conditions (Chen et al., 2016). In addition, there is evidence that FR-β-mediated interventions attenuate symptoms and histopathological changes in EAE (Lu et al., 2014). However, it still remains to be evaluated whether ^{18}F-FOL would present a promising new tool for the *in vivo* imaging of neuroinflammation in rats with EAE or humans with MS.

2.3.2.2 ^{68}Ga-NOTA-Folate

The rapid development of PET imaging is partially restricted by the requirement of onsite cyclotron for radioligand production, which is relevant especially with 18-fluorine labeled radioligands (McBride et al., 2009). Hence cyclotron independent production of radiotracers with ^{68}Ga-labelling, which is performed with ^{68}Ge/^{68}Ga generator, would be a welcomed approach for imaging folate-receptor positive conditions. As [^{68}Ga]gallium-labeled 1,4,7-triazacyclononane-1,4,7-triacetic acid conjugated folate (^{68}Ga-NOTA-Folate, ^{68}Ga-FOL) has previously demonstrated the ability to detect folate-receptor positive tumors in tumor xenograft mice (Aljammaz et al., 2014), it would be a tempting approach to evaluate the utility of ^{68}Ga-FOL in

visualizing inflammatory activity, disease progression and monitoring FR-β targeted therapy effects in EAE rat models and potentially in clinical trials in patients with MS in the future.

3 Aims

The overall aims of this study were to evaluate novel molecular imaging methods for monitoring neuroinflammation, disease progression and efficacy of therapy using animal models of MS. The specific aims for each sub study is described below:

1. To investigate the role of VAP-1 and feasibility of VAP-1-targeted ^{68}Ga-DOTA-Siglec-9 PET in monitoring neuroinflammation and efficacy of treatment in EAE rats.
2. To evaluate the ability of a novel FR-targeted PET radioligand, ^{18}F-FOL, to detect activated macrophages/microglia in a rat EAE model and to compare it with TSPO radioligand for monitoring neuroinflammation and progression of the disease.
3. To study efficacy of folate aminopterin treatment on EAE rats and feasibility of FR-targeted ^{68}Ga-FOL PET radioligand to detect neuroinflammation.

4 Materials and methods

4.1 EAE rat models

There are several types of EAE models that vary in respect to nature, severity and duration of the inflammation and method of establishment. In this work, I have focused only on two specific clinically relevant EAE models that enable the evaluation of individual lesion formation, ascertainment of BBB integrity during its disease course, easier measurement of therapy efficacy on individual lesion and monitoring of lesion development by *in vivo* PET imaging. Animal experiments that were performed related to this work were approved by the national Animal Experiment Board of Finland and the Regional State Administrative Agency for Southern Finland (license numbers: ESAVI/3046/04.10.07/2014 and ESAVI/2979/2018) and were conducted according to the relevant European Union directive.

4.1.1 *Focal* delayed-type hypersensitivity EAE (*f*DTH-EAE)

*F*DTH-EAE rat model was established in two phases. The disease was induced with the intrastriatal injection of heat-killed Bacillus Calmette-Guérin (BCG) that created the initial and transitory inflammatory response. Subsequently the BCG accrual was activated with peripheral injection of CFA supplemented with *Mycobacterium tuberculosis* (TB) to complete the $CD4^+$ cell and macrophage-mediated immune response against the BCG site.

When inducing the *f*DTH-EAE, the rats were first anesthetized with isoflurane anesthetic mixed with air (induction: 4–5% isoflurane and 500 mL-700 mL/min air, maintenance: 2.0–2.5% isoflurane and 400 mL-500 mL/min air) and set on a heating pad to maintain rat body temperature during the procedure. The rats were administered with subcutaneous (s.c.) injection of 100 µL analgesic (buprenorphine, 0.05 mg/kg/day, Temgesic, Indivior, Berkshire, UK) once just before the operation and 24 h after the operation and local anesthetic (Emla, AstaZeneca, Södertälje, Sweden) was applied in the ears of rat to attenuate the pain caused from fixing the head into the stereotactic frame. Then the rat's head was placed on a fixed coordinate system for stereotactic surgery and a one centimeter incision was made to the scalp

to enable the drilling of a 1.0 mm diameter hole 1.0 mm anterior and 3.0 mm lateral from the bregma at the depth of 4.0 mm from the surface of the cortex with a special dentist drill. The injection of two µL BCG (BCG, a kind gift from Professor Daniel Anthony, Department of Pharmacology, University of Oxford, UK) suspension (5×10^5 organisms in 1 µL of saline) was then performed with a Hamilton micro-syringe (Hamilton Bonaduz AG, Bonaduz, Switzerland) over time period of 10 minutes. After the injection, the wound was closed with stiches and disinfected with alcohol. The rats were allowed to recover on the heating pad until recovered from anesthesia.

Four weeks from the BCG induction into the striatum, the lesion was activated with intradermal injection of 100 µL of heat-killed TB (H37Ra, InvivoGen, San Diego, CA, USA) in an emulsion of CFA (CFA)/saline emulsion (100 µL, Sigma Aldrich, St. Louis, MO, USA) into the hind limbs of the rat. Before the procedure, the rats were anesthetized with mixture of isoflurane and air as with stereotactic operation and set on a heated cradle for sustaining the body temperature during anesthesia. The rats were allowed to recover after the operation as previously described. Saline injected rats were used as controls.

4.1.2 *Focal* myelin oligodendrocyte glycoprotein EAE (*f*MOG-EAE)

Likewise with *f*DTH-EAE, *f*MOG-EAE model was also set up in two phases. However, the *f*MOG-EAE rats were first MOG-immunized under anesthesia by injecting s.c. 150 µL of rat MOG (35–55) peptide (Sigma Aldrich, St. Louis, MO, USA) emulsified in IFA (Sigma-Aldrich, St. Louis, MO, USA) to the base of the tail. Then 21 days post MOG-immunization, the rats were placed into the stereotactic frame and drilled as described earlier and operated by a stereotactic injection of 2-µL cytokine mixture including 1 µg recombinant rat interferon-γ (IFN-γ, Sigma-Aldrich, St. Louis, MO, USA) and 1.45 µg of recombinant rat tumor necrosis factor-α (TNF-α, Sigma-Aldrich, St. Louis, MO, USA) into the corpus callosum at the depth of 2.5 mm from the surface of the cortex over a 10 min period to induce a targeted focal EAE lesion. The sham-operated rats were injected with 2 µL of saline. This sensitation procedure combined with injection of cytokine mixture will create more diffuse inflammatory lesions that exhibit transient cortical demyelination and have B cells involved in the pathogenesis, which is a common feature in patients with MS (Frohman et al., 2006, Lucchinetti et al., 2000, Serres et al., 2009, Racke et al., 2008).

4.2 Radiochemistry

4.2.1 Radiosynthesis of ^{68}Ga-DOTA-Siglec-9

DOTA-Siglec-9 is a cyclic peptide consisting of residues 283−297 from the Siglec-9 and it has a polyethylene glycol derivative linker (8-amino-3,6-dioxaoctanoyl) in between the peptide (Peptide Specialty Laboratories, Heidelberg, Germany) and DOTA chelate. The cyclic rings in DOTA-Siglec-9 are covalently bound with disulfide-bridged cysteines. For labeling purposes, ^{68}Ga was acquired from a 68Ge/68Ga generator (Eckert & Ziegler, Valencia, CA, USA) by elution with 0.1 M hydrochloric acid. ^{68}Ga eluate (0.5 mL, 320 ± 30 MBq) was mixed with 2-[4-(2-hydroxyethyl)piperazin-1-yl] ethanesulfonic acid (HEPES) to adjust the pH to approximately 4.1. 3 nmol of DOTA-Siglec-9 dissolved in deionized water was added and the then heated at 100°C for 15 min. Overall radiochemical purity for ^{68}Ga-DOTA-Siglec-9 was > 95% throughout the Study I and the specific radioactivity at the end of synthesis was 180 ± 140 MBq/nmol. The radiochemical purity of ^{68}Ga-DOTA-Siglec-9 was evaluated by radiodetector-coupled high-performance liquid chromatography (HPLC) (Jupiter C18 column, 4.6 × 150 mm, 300 Å, 5 µm; Phenomenex, Torrance, CA, USA). For the HPLC-analysis, solvent A was water including 0.1% trifluoroacetic acid (TFA) and B solvent consisted of 0.1% TFA and acetonitrile. A to B gradient was set from 82/18 percent during first 2 min to transition from 82/18 to 40/60 during time period from 2 to 11 min and remained at 40/60 from 11 to 14min. At 14 min, the gradient was returned back to 82/18 over 1 min time frame. Finally, the gradient was set to 82/18 at 15 min to 20 min. The flow rate was adjusted to 1 mL/min and ultra violet (UV) detection to 215 nm.^{68}Ga-DOTA-Siglec-9 is presented in Figure 3.

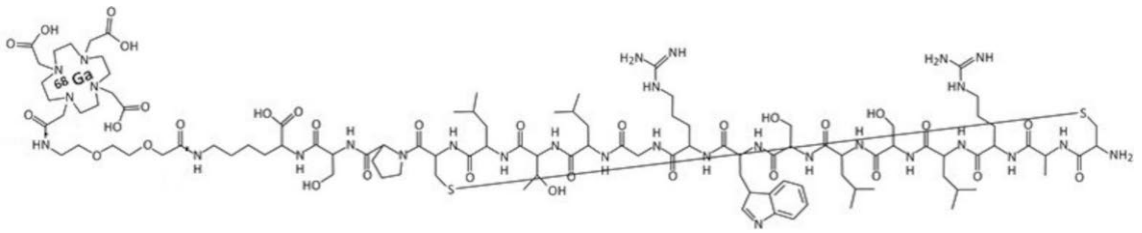

Figure 3. The chemical formula of [^{68}Ga]-DOTA-Siglec-9 (Modified from Virtanen et al., 2015).

4.2.2 Radiosynthesis of Al^{18}F-NOTA-Folate (^{18}F-FOL)

Synthesis of 1,4,7-triazacyclononane-1,4,7-triacetic acid (NOTA)-folate conjugate was prepared according to a previously published method (Chen et al., 2016). The radiolabeling was initiated by eluation of ^{18}F-fluoride (3.2–3.4 GBq) in saline

(50 µL) and then transformed to a reaction vessel containing sodium acetate buffer (pH 4.0, 1 M, 25 µL) and aluminium chloride ($AlCl_3$) (2 mM). The reaction mixture was kept at room temperature for 3 min and the NOTA-folate (250 µg) in water (50 µL) and acetonitrile (125 µL) was added. The reaction vessel was heated at 100 °C for 15 min. The reaction mixture was diluted with water containing 0.1% formic acid (1 mL) and subjected to HPLC purification with a semi-preparative C18 column (Jupiter 250 × 10 mm, Phenomenex Inc., Torrance, CA, USA) with both UV (254 nm) and radioactivity detection. Water containing 0.1% formic acid was used as a solvent A and solvent B contained acetonitrile and mixture of 0.1% formic acid. The elution was programmed as A/B gradient from 92/8 to 79/21 over 20 min with a flow rate of 4 mL/min. A solution of potassium bicarbonate ($KHCO_3$) in water (1 M) was added to adjust the collected HPLC fraction to pH 5.5 and the solvents were evaporated. The residue was formulated in phosphate-buffered saline (PBS) containing 8% ethanol and 7% polypropylene glycol. The total synthesis time was 77–88 min starting from end of bombardment. Another HPLC analysis was performed at the end product on an analytical C18 column (Jupiter 250 × 4.6 mm, Phenomenex Inc., Torrance, CA, USA) using both UV (254 nm) and radioactivity detection as previously. This time, solvent I was water containing 0.1% TFA and solvent II was acetonitrile containing 0.1% TFA. The I/II elution gradient was programmed from 90/10 to 75/25 over 15 min with a flow rate of 1 mL/min. The radiochemical purity was >95% and molar activity was 52 ± 22 GBq/µmol. The decay-corrected radiochemical yields were 28 ± 7%, respectively. The final compound is shown in Figure 4.

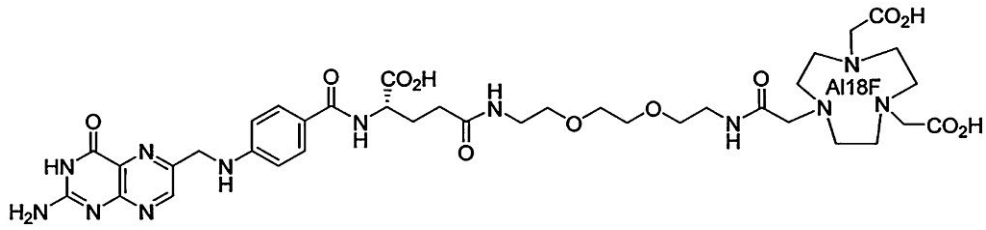

Figure 4. The chemical formula of Al[^{18}F]-NOTA-Folate, ^{18}F-FOL (Modified from Chen et al., 2016).

4.2.3 Radiosynthesis of ^{11}C-PBR28

The radiochemical synthesis of N-acetyl-N-(2-[^{11}C]methoxybenzyl)-2-phenoxy-5-pyridinamine (^{11}C-PBR28) is adapted from the published method (Wang et al., 2009). Cyclotron-produced [^{11}C]methane was halogenated by gas phase reaction into [^{11}C]methyl iodide, converted online into [^{11}C]methyl triflate and introduced in a solution of desmethyl precursor (dm-PBR28, 0.30–0.40 mg, PharmaSynth AS,

Tartu, Estonia) in acetone (200 µl) and sodium hydroxide (0.5 M sodium hydroxide (NaOH), 2.5 µl) at 0 °C.

After 3 minutes reaction at 80 °C, the reaction product was purified using a semi-preparative HPLC column (ACE C18-HL, 5 µm, 10 × 250 mm, Advanced Chromatography Technologies Ltd, Aberdeen, Scotland) and acetonitrile (CH_3CN) in 0.02 M potassium dihydrogenphosphate (KH_2PO_4) (43:57) mobile phase at 7 ml/min flow rate. The eluent was monitored for 254 nm UV absorbance and radioactivity. Collected product fraction was diluted and loaded into a solid phase extraction C18 cartridge (Sep-Pak Light, Waters Corp., Milford, MA) and the cartridge was washed. Dilution and washing were done using five percent ethanol in water solution.

The product was extracted with ethanol from the SPE cartridge, diluted with 0.1 M phosphate buffer solution into < 10% ethanol level and finally sterile filtered (Millex GV, 0.22 µm polyvinylidene fluoride membrane, 33 mm, Merck Millipore).

Determination of identity, radiochemical purity, and mass concentration was performed using analytical HPLC column (Kinetex XB-C18, 2.6 µm, 3.00 × 50 mm, Phenomenex Inc., USA), CH_3CN in 0.02 M KH_2PO_4 (35:65) mobile phase, 1 mL/min flow rate, 5 min run time and detectors in series for UV absorption (210 nm) and radioactivity. [^{11}C]PBR28 was produced with >99.9% radiochemical purity and averaged molar activity of 680 ± 270 MBq/nmol at the end of synthesis. [^{11}C]PBR28 is displayed in Figure 5.

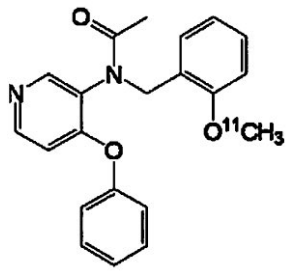

Figure 5. The chemical structure of [^{11}C]-PBR28 (Modified from Imaizumi et al., 2007).

4.2.4 Radiosynthesis of ^{68}Ga-NOTA-Folate (^{68}Ga-FOL)

The precursor compound of NOTA-folate was synthesized as earlier described and radiolabeled with gallium-68. ^{68}Ga was obtained from a ^{68}Ge/^{68}Ga generator (Eckert & Ziegler, California, USA) by elution with 0.1 mol/L aqueous hydrochloric acid. 68Ga eluate (1.0 mL) was added to a mixture of 2-[4-(2-hydroxyethyl)piperazin-1-yl]ethanesulfonic acid (120 mg), gentisic acid (0.3 mg) and NOTA-Folate (17 µg) in 120 µL TraceSELECT grade water. The reaction mixture was heated at 80°C for

10 min. After cooling down with an ice bath to approximately r.t, aqueous NaOH solution (1 M) was used to adjust the pH to neutral. Radiochemical purity of ^{68}Ga-FOL was determined with HPLC on a reversed phase column (Jupiter C18 column, 4.6 × 150 mm, 300 Å, 5 µm; Phenomenex, Torrance, CA, USA). The HPLC conditions were as follow: flow rate was 1 mL/min; solvent A was 0.1% TFA/water and solvent B was 0.1% TFA/acetonitrile. A/B gradient: 0–0.5 min, 95/5; 0.5–15 min, from 95/5 to 75/25. The HPLC system consisted of LaChrom Instruments (Hitachi; Merck, Darmstadt, Germany) and of a Radiomatic 150TR radioisotope detector (Packard, Meriden, CT, USA). ^{68}Ga-FOL was prepared in high radiochemical purity (>95%). Duration of radiosynthesis was approximately 17 min. ^{68}Ga-FOL is displayed in Figure 6.

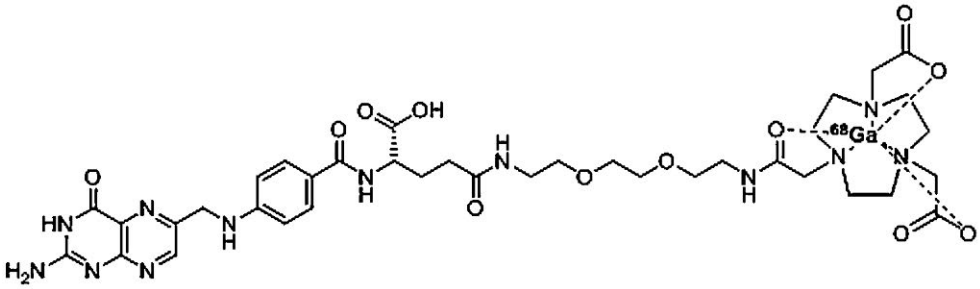

Figure 6. Chemical structure of [^{68}Ga]-NOTA-Folate (^{68}Ga-FOL).

4.3 PET studies

4.3.1 *In vivo* multimodal PET/CT imaging

In all of the studies, *in vivo* PET/computed tomography (CT) images were acquired with Inveon multimodality small animal PET/CT scanner (Siemens Medical Solutions, Knoxville, TN, USA). The detector of the Inveon small animal PET/CT scanner consist of 80 crystal rings, which include 25600 crystals in total. Its spatial resolution ranges between 1.2 mm^3 and 1.6 mm^3 depending on the radioisotope used (Goertzen et al., 2012). This PET/CT generates an axial field of view (FOV) of 12.7 cm and transaxial field of 10 cm. To start the *in vivo* PET/CT data acquisition, the animals were anesthetized on a heating pad using a mixture of isoflurane and air as previously described and a cannula was placed into the tail vein prior to radiotracer injection. A 10-min CT scan was performed prior to PET imaging for anatomical references and attenuation correction. Depending on the study, either 60-min, 45-min or 30min-dynamic PET acquisition was started after an intravenous (i.v.) tail vein injection. (Study I, ^{68}Ga-DOTA-Siglec-9, 45 min-dynamic, 34 ± 5.1 MBq,

n = 32; Study II, ^{18}F-FOL, 60-min dynamic, 38.9 ± 2.7 MBq, n = 21 and ^{11}C-PBR28, 30 min-dynamic, 34.1 ± 3.5 MBq, n = 12; Study III, ^{68}Ga-FOL, 30 min-dynamic, 45 ± 1 MBq, n = 40). The PET data was reconstructed using an ordered subsets expectation-maximization 2-dimensional maximum a posteriori algorithm to yield 6 × 10, 9 × 20, 4 × 60, 4 × 180, and 2 × 300 s time frames. For the *in vivo* PET data analysis, the PET images were aligned to the corresponding CT and MRI data sets and analyzed with Carimas v2.9 (Carimas, Turku PET Centre, Turku, Finland) with the exception of the study III where MRI data was absent. Representative PET/CT and MRI images were captured using Inveon Research Workplace v4.1 (Siemens Medical Solutions). The quantitative PET data was analyzed by defining a ROI in the injected lesioned hemisphere and this ROI was then mirrored onto the contralateral non-injected hemisphere to function as an internal reference region. These results were expressed as standardized uptake value (SUV) ratios according to the following equation:

$$\text{SUV ratio} = \text{SUV}_{\text{max,Lesion}}/\text{SUV}_{\text{mean, Contralateral}}$$

In this equation, SUV values are defined as radioactivity concentration in a ROI (MBq/mL), which is normalized for injected radioactivity dose (MBq/mL) and animal body weight (kg).

4.3.2 *Ex vivo* autoradiography & gamma counting

After the *in vivo* PET/CT imaging, the anesthetic was increased to a terminal level (4–5% isoflurane; and oxygen, 500–700 mL/min) and blood was extracted from the left ventricle of the heart via cardiac puncture. Cervical dislocation was performed to confirm the euthanasia. Then, the rats brains were carefully dissected, frozen in a cold isopentane at a temperature of −70°C, and sectioned (20 µm for *ex vivo* autoradiography and 10 µm for histology) in a microtome (Leica CM 3050S cryostat, Leica Biosystems, Nussloch, Germany). Coronal brain sections were cut from striatum (at lesion site) and cerebellum and placed on to positively charged glass slides (Superfrost Ultra Plus, Thermo Fisher, Pittsburgh, PA, USA). The sections cut for autoradiography (20µm sections) were then exposed to a phosphor imaging plate (BAS-TR2025, Fuji Photo Film Co, Ltd., Tokyo, Japan) for periods of 220 min (i.e., two physical half-lives of ^{18}F), 40 min (i.e., two physical half-lives of ^{11}C) or 140 min (i.e., two physical half-lives of ^{68}Ga) depending on the isotope and scanned with a phosphor imaging plate reader (BAS-5000, Fuji; 25 µm internal resolution) to acquire the data. Finally, both the 10 µm and 20 µm sections were frozen at −20°C for histological, immunohistochemical and immunofluorescence evaluation. The acquired *ex vivo* autoradiography data were analyzed with AIDA Image analyzer v4.55 software (Raytest Isotopenmessgeräte GmbH, Straubenhardt, Germany) by

drawing the ROIs in the lesions hemisphere and mirroring the corresponding ROI to contralateral hemisphere for obtaining the count densities as photostimulated luminescence per square millimeter (PSL/mm^2) of ^{18}F-FOL, ^{11}C-PBR28 or ^{68}Ga-FOL binding within ROIs. Cortical ROI's were also determined to cover the extent of radiotracer binding surrounding the lesion. The following equation was used for data quantitation and formation of the bound-to-free ratio of the radioligand:

$$[(\text{PSL/mm}^2\ _{\text{Lesion}} - \text{PSL=mm}^2\ \text{Contralateral}) = \text{PSL/mm}^2\ _{\text{Contralateral}}]$$

For the *ex vivo* gamma counting, the excised tissues including the brain were weighted and measured with a gamma counter (Triathler 3″, Hidex, Turku, Finland) to obtain the biodistribution of the radioactivity.

4.3.3 *In vitro* studies

In vitro binding of ^{18}F-FOL and ^{68}Ga-FOL in *f*DTH-EAE lesions were determined to evaluate the specificity of radiotracers to FR. Firstly, the 20 µm brain tissue cryosections were pre-incubated in sterile PBS at room temperature for 15 min, and thereafter with 0.2 nM ^{18}F-FOL or ^{68}Ga-FOL in sterile PBS. One group of slides was incubated with ^{18}F-FOL or ^{68}Ga-FOL and other groups received a 100-fold molar excess of folate glucosamine ($C_{25}H_{30}N_8O_{10}$; molecular weight, 602.56) prior to applying the radiotracer for 30 min. After the incubation period, the slides were washed with ice-cold PBS, placed in ice-cold distilled water, briefly dried, and predisposed to a phosphor imaging plate (BAS-TR2025, Fuji Photo Film Co, Ltd., Tokyo, Japan) for 220 min (^{18}F-FOL) or 140 min (^{68}Ga-FOL). Finally, the imaging plates were scanned with the imaging plate reader (BAS-5000, Fuji; 25µm internal resolution). The *in vitro* autoradiography data was analyzed as described above regarding *ex vivo* autoradiography experiments.

4.3.4 *In vivo* stability of ^{18}F-FOL and ^{68}Ga-FOL

For measuring the stability of ^{18}F-FOL and ^{68}Ga-FOL, blood samples from healthy Lewis rats (Study II, n = 12, Study III, n = 16) were collected at 2–60 min after ^{18}F-FOL injection and at 5-30 min after ^{68}Ga-FOL injection into heparinized tubes. A gamma counter (1480 Wizard 3″; Perkin Elmer/ Wallac, Turku, Finland) was used to measure the radioactivity concentration of whole blood and plasma samples. To separate plasma proteins from plasma, equal volume of acetonitrile was added to each sample followed by centrifugation 2100×g at room temperature for 4 min. Post centrifugation, the plasma supernatant was filtered through a 0.45 µm Minispike filter (Waters Corporation, Milford, MA, USA) for HPLC analysis. This HPLC analysis was conducted using a semipreparative C18 column (Jupiter Proteo 90Å,

4 µm, 250 × 10mm, Phenomenex Inc., Torrance, CA, USA) for both the ultraviolet (254 nm) and radioactivity detection of the plasma samples. Solvents A and B were of same content as with HPLC analysis of radiotracer synthesis. However, the elution was programmed with modifications as follows: flow rate was 5 mL/min, 8% B during 0–1 min, from 8 to 23% B during 1–14 min, and from 23 to 8% B during 14–15 min. The fraction of intact tracer remaining in the plasma was determined by comparing this fraction with ^{18}F-FOL or ^{68}Ga-FOL standard depending on the study. By utilizing the population-based information of plasma radioactivity, the dynamic PET images of *f*DTH-EAE rats were analyzed by the Logan method of reversible modelling. The data was corrected for metabolites using an image-derived input function from the ROI defined on the left ventricle of the heart.

4.4 MRI studies

In the Study I and II, MRI data was acquired using clinical Philips Achieva 3T device (Philips Medical Systems, Koninklijke, The Netherlands) combined with rat-dedicated brain coil (Rat Brain Array 4, RAPID Biomedical GmbH, Rimpar, Germany). Anesthesia was initiated as described for *in vivo* PET imaging. Then, a cannula was inserted into the tail vein for the administration of 100 µL of the Gd-contrast agent (DOTAREM 279.3 mg/mL, Guerbet, Roissy, France) 10 min prior to the post T1-weighted imaging for ascertainment of BBB status. First, scout images were acquired to determine the area to be scanned from the brain. Pre and post T1-weighted spin-echo sequences were obtained by using the time of repetition (TR) of 600 ms and echo time (TE) of 14 ms. The T2-weighted images were obtained using the turbo spin-echo (TSE) sequence, which included parametric values as TR 4000 ms, TE 75 ms and TSE factor 10. The FOV was 45 mm × 45 mm × 21.6 mm for the T2-weighted images and 50 mm × 50 mm × 17.6 mm for the T1-weighted images. MRI data were analyzed in the study I using Inveon Research Workplace v4.1 software (Siemens Medical Solutions, Malvern, PA, USA) and used only as an anatomical reference for drawing ROI's in PET images in the study II. In the study I, post T1-weighted and T2-weighted images were first thresholded according to the signal intensity in non-injected brain hemispheres. Post T1-weighted and T2-weighted hyper-intnsity MR images were assessed by defining ROIs on the area of Gd-enhancement and the ROI's were mirrored on the contralateral intact brain hemisphere. The results were expressed as lesion to contralateral intact brain hemisphere ratios.

4.5 Experimental designs

In the Study I, both *f*DTH-EAE and *f*MOG-EAE rats were divided into two groups and PET/CT imaged on day 3 ($n = 8$) and on day 14 ($n = 8$). A subset of *f*MOG-EAE rats were intraperitoneally administered daily with a selective semicarbazide-sensitive amine oxidase (SSAO) inhibitor Z-3-fluoro-2-(4-methoxybenzyl) allylamine hydrochloride, (LJP1586, SYNthesis med chem, Monash Institute of Pharmaceutical Sciences, Melbourne, Australia), 5 mg/kg ($n = 8$) and imaged as mentioned for other groups. Sham-operated rats ($n = 8$) were used as controls. For the Study II, *f*DTH-EAE rats were imaged with ^{18}F-FOL ($n = 15$) or ^{11}C-PBR28 ($n = 8$) at day 14 and re-evaluated with ^{18}F-FOL ($n = 6$) or ^{11}C-PBR28 ($n = 4$) at day 90 before the sacrifice. In the study III, *f*DTH-EAE rats ($n = 60$) were divided into six groups according to the intervention, disease duration and health status. The first two groups of *f*DTH-EAE rats imaged at day 14 ($n = 20$) were administered s.c. with folate aminopterin drug of Endocyte (EC2319) (500 nmol/kg/day) or saline on days 0, 3, 7, 10 after the disease induction. The rats studied for the chronic phase were first imaged at day 60 ($n = 20$) and the second time at day 90. Between the baseline and follow-up PET/CT imaging, the *f*DTH-EAE rats were biweekly administered with EC2319 (750 nmol/kg/day) for four weeks. Additional ($n = 20$) healthy rats were also treated with EC2319 (500 nmol/kg/day) or saline as for rats during acute phase group (day 14).

4.6 Immunohistochemistry & Immunofluorescence for pre-clinical experiments

The histological stainings were performed by first fixing the 10µm sections with either acetone or formalin, which was determined based on the optimization data and then stained with hematoxylin-eosin (H&E) or Luxol Fast Blue (LFB) with cresyl violet counterstain using standard procedures. For immunohistochemistry, the sections were post-fixed with periodate-lysine-paraformaldehyde for 20 min and washed three times with PBS. Antigen retrieval was performed after the fixation in a hot citrate buffer (pH 6.0) in order to improve antibody binding. Then the sections were processed with a quenching step in which the 1% hydrogen peroxide (H_2O_2) in methanol is blocking the endogenous peroxidase and washed with PBS. Then the desired primary antibody: anti-cluster of differentiation 11b/c (OX-42), (OX-42, 1:100 dilution, Abcam, Cambridge, UK), anti-inducible nitric oxide synthase (iNOS, 1:500 dilution, Abcam, Cambridge, UK), anti-mannose receptor C-type 1 (MRC-1, 1:2000 dilution, Abcam, Cambridge, UK), anti-cluster of differentiation 68 (CD68) (1:1000 dilution, AbD Serotec, Hercules, CA, USA) and anti-FR-β (1:50 dilution, m909, a kind gift from Professor Philip S. Low, Purdue University, West Lafayette, IN, USA) to study FR-β expression (Feng et al., 2011), was added for a 1h

incubation. The primary antibody incubation was followed by the addition of a secondary antibody: for OX-42, Dako EnVision anti-mouse Ig (Code K4001), for anti-iNOS, Dako EnVision anti-rabbit (Code K4003), for anti-MRC-1, Dako EnVision anti-rabbit (Code K4003), for anti-CD68, Dako EnVision anti-mouse (Code K4001), (4) for anti-FR-β, Dako (Code P0397) Streptavidin, for 30 min. 3,3-diaminobenzidine (DAB, Dako; Code K3468) was used as a chromogen for the detection of antibodies. Counterstaining was conducted with hematoxylin and then sections were mounted with ProLong Gold antifade reagent (Life Technologies P36930).

For neurofilament protein (NFP) and IgG immunohistochemical staining, the cryosections were processed as described above except washes in between the procedures was performed with PBS supplemented with 0.05% Tween-20. Then, the sections were incubated with anti-NFP antibody (M0762, clone 2F11, Dako, Santa Clara, CA, USA) for 1h and followed by the addition of a secondary anti-rat Ig antibody (Dako, K4001). IgG leakage was assessed with incubating the sections with only anti-rat Ig (Dako, K4003). After DAB reaction, sections were further processed as described above.

H&E stained sections were used for evaluating lesion size and quantifying lymphocyte infiltration as lymphocyte count densities per mm^2. For lymphocyte quantification, four non-overlapping areas within the lesion area were chosen according to the highest density of recruited lymphocytes. The amount of activated microglia in the injected hemisphere was determined by drawing ROIs on the subjectively estimated area of increased microglial activation. The degree of demyelination was scored from 0 to 3 or determined by using the automatic color deconvolution method of ImageJ v.1.48 software (National Institutes of Health, Bethesda, MD, USA) based on LFB staining intensity. The percent area of altered NFP expression or IgG leakage were determined by defining ROIs on positive immunostained areas. These areas were defined on four brain sections and averaged for each rat. Finally, the average areas were divided by the total averaged brain area for each rat.

For double immunofluorescence of FRβ and MRC-1 or FRβ and iNOS, the sections were fixed with ice-cold formalin for 3min and washed with PBS. Then, the slides were incubated with primary anti-FRβ (1:50 dilution, m909) and anti-MRC-1 antibodies (1: 2000 dilution, Abcam) or with anti-FR-β and anti-iNOS antibodies (1:500 dilution, Abcam) for 30min at room temperature. Thereafter, the sections were incubated with fluorophore-labeled secondary antibodies (1:100 dilution, Alexa Fluor 488 or Alexa Fluor 594, Invitrogen, Waltham, MA, USA).

For P-selectin and intercellular adhesion molecule-1 (ICAM-1) immunofluorescence, the samples were incubated either with primary anti-P-selectin antibody (Santa Cruz sc-6943; 1:100 dilution) or with anti-ICAM-1 antibody (Santa

Cruz sc-7891; 1:20 dilution) for 30 min in room temperature followed by incubation with fluorescein isothiocyanate (FITC)-conjugated goat anti-rabbit secondary antibody (Sigma F1262-2ML; 1:100 dilution) and the amplification of the signal with anti-Fluorescein-488 (Invitrogen A11096, 5 μg/mL). For VAP-1 immunofluorescence, the sections were incubated only with FITC-conjugated (Sigma F1262; 1:40 +5% normal rat serum) goat anti-rabbit IgG secondary antibody (Life Technologies A11034) for the detection of luminal VAP-1 on the surface on the endothelial cells. For a subgroup of slides, polyclonal anti-VAP-1 antibody (rabbit anti-human VAP-1 that also recognizes rat VAP-1) was applied for 30 min to visualize both intracellular and surface-bound VAP-1 (Kivi et al., 2009). The sections were mounted as described with immunohistochemical stainings.

All immunohistochemical and immunofluorescence stainings were scanned using Pannoramic 250 F scanner or Pannoramic Midi fluorescence scanner (3D Histech, Budapest, Hungary) and analyzed with Case viewer (3D Histech, Budapest, Hungary). The percentages of positive staining area for iNOS, MRC-1, CD68, and FR-β were determined as with immunohistochemical stainings.

4.6.1 Human tissue samples

Human brain tissue samples were obtained to investigate the FR-β, iNOS, MRC-1 and CD68 positivity in healthy human brain and in brains affected with SPMS. For the stainings, human formalin-fixed paraffin embedded samples were acquired from Auria Biobank (Turku University Hospital, Turku, Finland) with the criteria of active or inactive chronic MS plaques located in the brain or spinal cord. On the other hand, normal brain tissue samples were collected from corresponding anatomical areas of the brain compared to samples from patients with MS. The approval for the archival human tissues study was granted by the Auria Biobank scientific steering committee (decision AB19-2623). A separate patient informed consent was not needed according to the Finnish Biobank Law (688/2012). All samples had been attained for histopathologic examination during autopsy between years 2001 and 2013. For the immunofluorescence and for the immunohistochemistry, the samples were stained as described previously for pre-clinical experiments. Positivity for FR-β immunohistochemistry was graded as either negative, weak, moderate, or strong based on the intensity of the staining.

4.7 Statistical analyses

All statistical analyses related to this thesis work were conducted with GraphPad Prism v5.01 or 8.04 software (Graph Pad Software Inc., La Jolla, CA, USA). Non-parametric Kruskal-Wallis tests with Mann-Whitney post hoc tests were used to

evaluate the significance of differences in lesion tracer uptake between the studied groups. Intragroup comparison for histological, immunohistochemistry and immunofluorescence data was also conducted by using non-parametric Kruskal-Wallis tests with Mann-Whitney post hoc tests. To analyze longitudinal PET imaging studies regarding ^{11}C-PBR28, ^{18}F-FOL and ^{68}Ga-FOL, Wilcoxon matched-pairs test was performed. Spearman's correlation was used to analyze relationships between PET data, immunohistochemistry and histology. Results are presented as mean ± standard deviation with two significant numbers. The results that indicate P values under 0.05 were regarded statistically significant in the studies.

5 Results

5.1 MRI analysis of *f*MOG-EAE and *f*DTH-EAE lesions

Lewis rats induced with *f*DTH and *f*MOG lesions were imaged with 3-T MRI combined with rat dedicated brain coil to showcase the availability of clinical MRI for pre-clinical research without the use of high-resolution MRI. Our MRI analysis in the study I revealed that this method could visualize the characteristics of a typical active Type 1 MS-like lesion with significantly increased Gd-enhancement in T1-weighted images indicating BBB disruption and areas of hyperintensity in T2-weighted MRI images ($P < 0.05$). Pre-active lesions that only show small scale damage were not observed T1-weighted Gd-enhanced or T2-weighted images (Figure 7). On the other hand, Type 2 lesions were clearly visible in T1-post Gd-enhanced and T2-weighted MRI showing an acute, widespread and diffuse inflammation already two days after disease induction accompanied by BBB breakdown. After the partial resolvement of *f*MOG-EAE lesions at day 13, the T2-hyperintense area ($P < 0.05$) and Gd-enhanced areas in T1-weighted images ($P < 0.001$) were significantly reduced indicating improved BBB status during remission (Figure 7).

These MRI findings were supported by OX-42 and IgG immunohistochemistry showing low amounts of OX-42 positive microglia for pre-active lesions and significantly higher levels of OX-42 positivity in acute phase of *f*DTH lesions compared to pre-active lesions ($P = 0.039$). IgG staining was minimal during the pre-active phase and was detected in significantly higher levels at acute phase ($P < 0.05$). For the *f*MOG-EAE, the OX-42 immunohistochemistry showed significantly larger areas of OX-42 positive cells compared to remission at day 13 ($P = 0.0024$) and IgG leakage indicated marked improvements at remission when compared to IgG positivity at acute phase ($P < 0.05$).

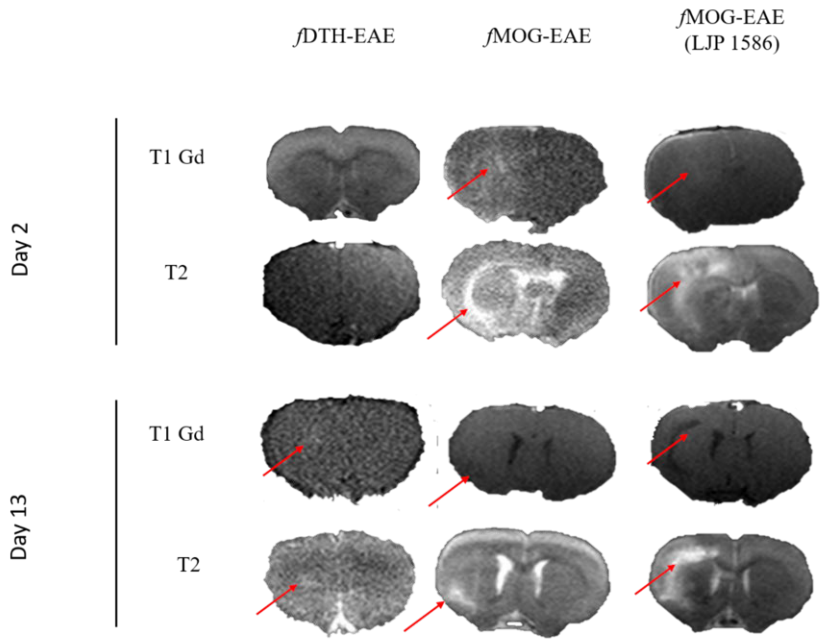

Figure 7. MRI images acquired on days 2 and 13 from *f*DTH-EAE, *f*MOG-EAE and *f*MOG-EAE rats treated with LJP 1586. Red arrows indicate lesion site. Post-contrast T1-weighted images illustrate the BBB status at various stages of disease and demonstrate Gd-enhancement in the lesion during BBB damage. T2-weighted images show the formation and partial resolvement of a hyperintense region. LJP 1586 administration prevents recovery of the hyperintense and Gd-enhanced areas (Modified from Study I).

5.2 Evaluation of VAP-1 expression and ^{68}Ga-Siglec-9 binding in inflammatory EAE lesions

We observed in the study I that luminal VAP-1 expression in *f*DTH-EAE appeared in the lesion vasculature post pre-active lesion development only during active inflammatory phase. Immunofluorescence data only showed occasional VAP-1 positivity in brain tissue and total lack of VAP-1 translocation in the lesion area. This was supported by a weak ^{68}Ga-DOTA-Siglec-9 *ex vivo* autoradiography signal (Figure 8). There was no evidence of demyelination during VAP-1 absence. During the acute inflammatory phase, the immunofluorescence stainings indicated higher signal for luminal VAP-1 compared to the pre-active phase. ^{68}Ga-DOTA-Siglec-9 binding was significantly elevated at the site of *f*DTH-EAE lesion during the acute phase. (3.2 ± 0.59 vs. 0.16 ± 0.22 PSL/mm^2, $P = 0.0031$) (Figure 8). The VAP-1 immunofluorescence signal of endothelial cells in *f*DTH-EAE reminded the structure of regular flat-walled endothelial cell morphology, which is typically found in smaller and thinner venules. The LFB staining now revealed demyelinated areas

present around the lesions although the difference was not statistically significant when compared to pre-active lesions ($P = 0.13$).

When *f*MOG-EAE rats representative of Type 2 immunopathology were examined, the expression patterns of VAP-1 were substantially altered from rats with *f*DTH-lesions (Figure 8). Immunofluorescence stainings exhibited high amounts of positivity for luminal VAP-1 both during acute widespread inflammation and the remission phase. In lines with VAP-1 positivity, ^{68}Ga-DOTA-Siglec-9 binding was significantly elevated in the injected lesion hemisphere at acute phase ($P = 0.017$) and a remission phase ($P = 0.055$) as compared to the sham-operated rats. However at day 14, the ^{68}Ga-DOTA-Siglec-9 binding remained at the same level compared to day 3 ($P = 0.17$). As opposed to endothelial cells in *f*DTH-EAE, the endothelial cells in *f*MOG-EAE lesions displayed characteristics commonly observed in high endothelial venules (HEV)-like vessels (Girard et al., 1995) (Figure 8). There were moderate amount of demyelination at day 3 and no difference in demyelination score between the observed timepoints ($P = 0.72$). It could be stated that luminal VAP-1 expression remained in the lesion vasculature once the *f*MOG-EAE rats had first experienced the acute inflammatory phase with compromised BBB. This pattern was detected by VAP-1 targeted ^{68}Ga-DOTA-Siglec-9 *ex vivo* autoradiography and immunofluorescence with i.v. injected anti-VAP-1 antibody.

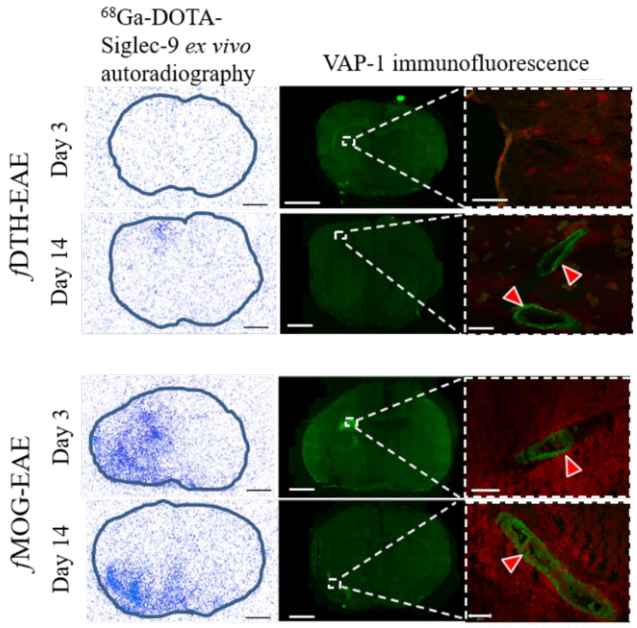

Figure 8. ^{68}Ga-Siglec-9 binding and VAP-1 positivity in *f*DTH and *f*MOG-EAE rats during the timecourse of the disease. Red arrows indicate VAP-1 positivity (green) from the autofluorescence (red). Scale bar is 50 µm (Modified from Study I).

5.2.1 The effect of VAP-1 inhibitor therapy on *f*MOG-lesions

VAP-1 inhibitor treatment with LJP1586 inhibited the recruitment of lymphocytes by 58% ($P = 0.026$) at day 3 in *f*MOG-EAE compared to the number of lymphocytes in untreated rats at day 3. However during the remission phase at day 14, the amount of lymphocytes was restored to the same levels as observed with the untreated *f*MOG-EAE rats ($P = 0.70$). In addition, the administration of LJP1586 lowered the expression of ICAM-1 in the lesion vasculature for *f*MOG-EAE at acute phase until the expression patterns of ICAM-1 appeared to be slightly increased for LJP1586-treated rats compared to untreated *f*MOG-EAE rats. Most importantly, VAP-1 expression tended to decrease in the vasculature of the inflammatory *f*MOG-brain lesions due to LJP1586 intervention both at acute and remission phases of lesion development. The i.v. injected anti-VAP-1 antibody detects the endothelial cell surface VAP-1 and the secondary antibody applied during the immunostaining then detects the primary anti-VAP-1 antibody bound to the luminal side of endothelium, respectively. It is noteworthy that, the lesion size in *f*MOG-EAE was markedly larger at remission phase in the LJP1586-treated rats compared to untreated ($P = 0.039$). P-selectin staining was negative during the entire time course of LJP1586-treated *f*MOG-EAE rats and untreated *f*MOG-EAE rats. In contrast, the LJP1586 treatment had no effect on the amount of OX-42-positive cells, the intensity of LFB staining, IgG leakage revealed by immunohistochemistry or the area of altered NFP expression in *f*MOG-lesions. Despite no difference was observed in IgG stainings between LJP1586-treated *f*MOG-EAE rats in acute and remission phases, a significant reduction of Gd-enhancement in MRI was observed at acute phase of *f*MOG-EAE ($P = 0.0041$).

5.3 FR-β and macrophage marker expression during acute and chronic inflammation in *f*DTH-EAE lesions

In the Study II, the formation of *f*DTH-EAE lesions showed increased positivity for FRβ, CD68, iNOS (marker for M1-like pro-inflammatory macrophages) and MRC-1 (marker for M2-like anti-inflammatory macrophages) as observed from immunohistochemistry. The positivity for FRβ, CD68, iNOS and MRC-1 exsisted during acute phases of inflammation and persisted or significantly intensified once the disease had progressed into chronic phase (Figure 9 A & B, Table 5). In more detail, the staining areas of anti-FRβ ($P = 0.11$), anti-CD68 ($P = 0.23$) and anti-MRC-1 ($P = 0.14$) showed no statistical difference when the inflammation in *f*DTH lesions transitioned from acute to chronic phase. The computational ratio between iNOS and MRC-1 (iNOS/MRC-1) lacked the difference when acute and chronic phases were compared (Figure 9 C, $P = 0.21$). In contrast, the anti-iNOS positivity was

significantly higher in the chronic phase than in the acute phase (P = 0.019). Importantly, a significant proportion of anti-FRβ positivity and ^{18}F-FOL uptake was found to be located in the areas of active demyelination and remyelination in *f*DTH lesions.

The acquired correlation data suggested that the positive area of FRβ had significant negative correlation with CD68 area and iNOS/MRC-1 ratio when data from both time points were included from immnohistochemical stainings. In contrast, the correlation between the positive area of FRβ and MRC-1 was positive. The iNOS positivity and FRβ positivity lacked correlation (Table 5).

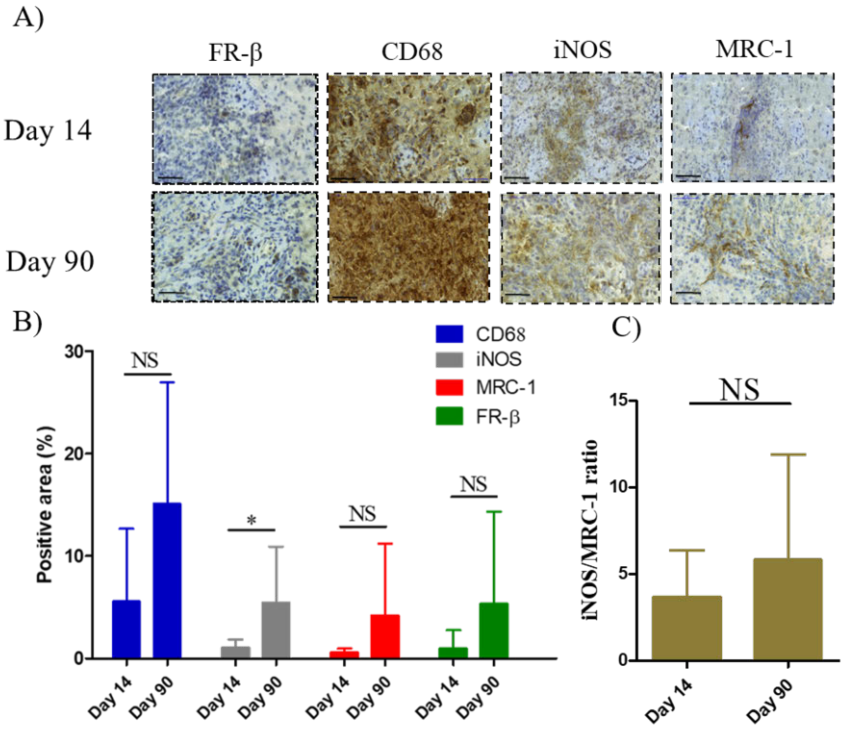

Figure 9. Example image of CD68, iNOS, FRβ and MRC-1 immunostainings for acute (day 14) and chronic (day 90) *f*DTH-EAE and quantification of corresponding immunohistochemical data. (A) FRβ, CD68, iNOS and MRC-1 stainings show antibody specific staining at both phases of the disease. (B) Histogram of CD68, iNOS, MRC-1, FRβ immunohistochemistry and (C) iNOS/MRC-1 – ratio indicate significantly increased expression of iNOS positivity at chronic phase compared to acute phase. Positive staining area is normalized to lesion hemisphere area (positive area %). Scale bar 50 µm. Key:* = $P \leq 0.05$, NS = $P \geq 0.05$ (Modified from Study II).

Table 5. Correlation of FR-β immunostaining to iNOS, MRC-1, CD68 and iNOS/MRC-1 immunostainings and to ^{18}F-FOL and ^{11}C-PBR28 radiotracer uptake in *f*DTH-EAE rats.

	INOS		**MRC-1**		**FR-B**		**CD68**		**INOS/MRC-1**	
	R^2	*P*	R^2	*P*	R^2	*P*	R^2	*P*	R^2	*P*
^{18}F-FOL	0.43	0.076	0.22	0.24	0.13	0.37	0.60	*	0.23	0.23
FR-B	0.017	0.38	0.53	***	—		0.45	**	0.39	***
^{11}C-PBR28	0.24	0.26	0.37	0.15	0.01	0.81	0.48	0.64	0.16	0.37

Key: *= $P < 0.05$, **= $P < 0.01$, ***= $P < 0.001$

5.3.1 Comparison of ^{18}F-FOL and ^{11}C-PBR28 radioligands

In the Study II, both ^{18}F-FOL and ^{11}C-PBR28 radioligands showed favorable properties for imaging neuroinflammationin in the rat model of MS representative of type I immunopathology. First, *in vitro* autoradiography of ^{18}F-FOL indicated that the binding was specific to FR as brain cryosections pre-treated with folate glucosamine blocking agent showed significantly lower binding compared to non-blocked sections (blocked, 0.44 ± 0.17 vs. non-blocked, 22 ± 1.2, $P < 0.0001$). ^{18}F-FOL was able to visualize the inflammatory CNS lesions in acute and chronic phases of inflammation *in vivo*, *ex vivo* and *in vitro*. In addition, ^{18}F-FOL enabled the separation of acute and chronic inflammatory lesions only with digital *ex vivo* autoradiography (Figure 10A). The *in vivo* uptake of ^{18}F-FOL co-localized with corresponding lesions observed in MRI (Figure 11A & B). Although, ^{18}F-FOL binding managed to show significant difference compared to ^{11}C-PBR28 at the chronic phase ($P = 0.016$), the differentiation of disease stages with the ^{18}F-FOL imaged *f*DTH-EAE rats was not possible *in vivo* (Figure 11C).

^{11}C-PBR28 was able to visualize acute and chronic phase lesions *ex vivo* and *in vivo*. The uptake was present in the areas of corresponding MRI lesions as with ^{18}F-FOL. However, ^{11}C-PBR28 lacked the ability to detect any differences between acute and chronic lesions both *ex vivo* and *in vivo* (Figure 10B & 11). To support the *in vivo* findings, a significant relationship was observed between *ex vivo* and *in vivo* measurements of both ^{18}F-FOL ($P = 0.0004$) and ^{11}C-PBR28 ($P = 0.037$) tracers.

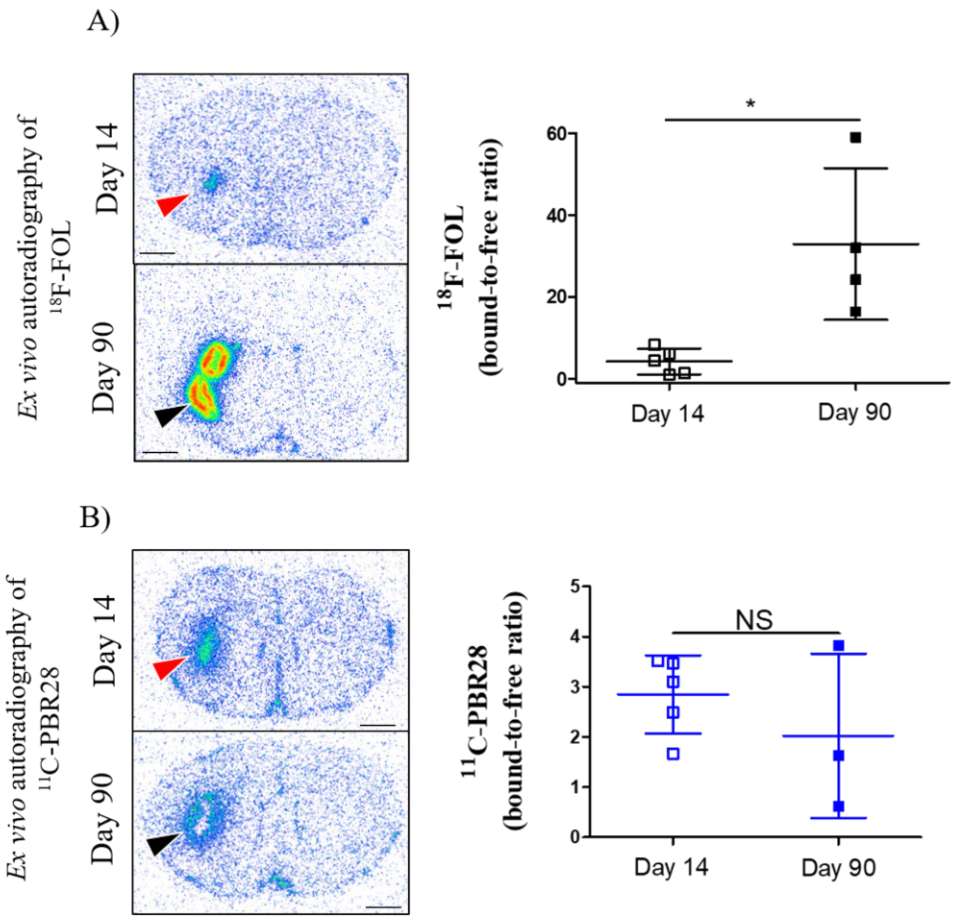

Figure 10. *Ex vivo* autoradiography of ^{18}F-FOL and ^{11}C-PBR28 PET imaging agents. A) *Ex vivo* autoradiography indicates high binding of ^{18}F-FOL in the lesion hemisphere compared to the contralateral hemisphere during acute inflammation (red arrow). ^{18}F-FOL binding is significantly more extensive during chronic inflammation (black arrow). *Ex vivo* images are supported by ^{18}F-FOL quantification data. B) *Ex vivo* autoradiography exhibits binding of ^{11}C-PBR28 in lesion hemisphere compared to contralateral hemisphere during acute inflammation (red arrow). ^{11}C-PBR28 binding shows no significant difference between acute inflammation and chronic inflammation (black arrows). *Ex vivo* images are supported by ^{11}C-PBR28 quantification data. Scale bar=2 mm. Key:* = $P \leq 0.05$, NS = $P \geq 0.05$ (Modified from Study II).

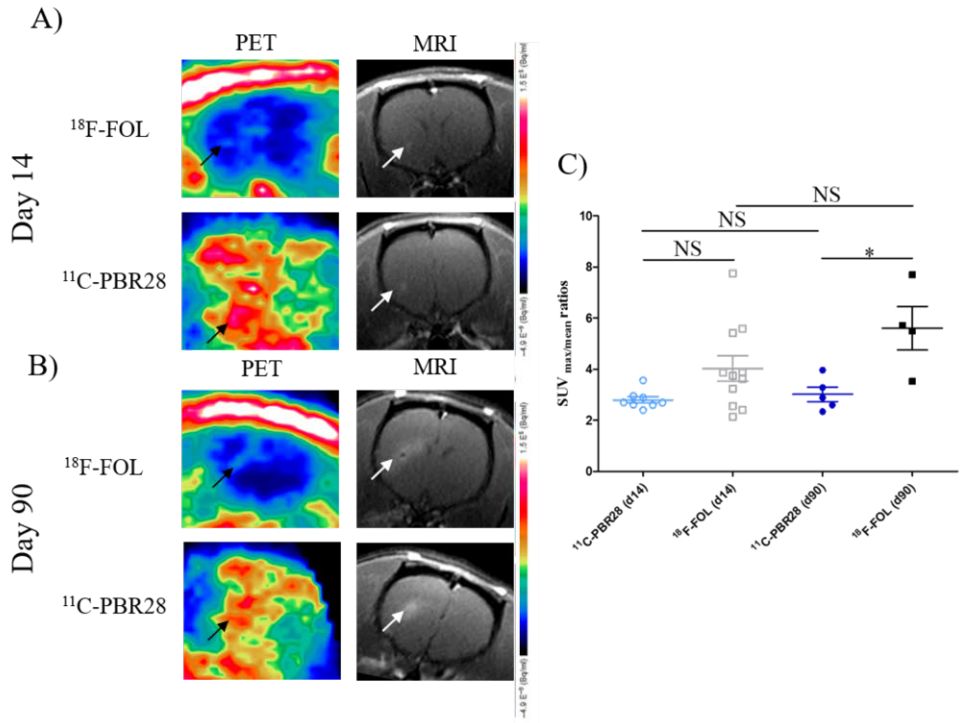

Figure 11. *In vivo* PET images and MR images of *f*DTH-EAE rat brain on acute (day 14) and chronic (day 90) phases of CNS inflammation with quantitative data. A) Representative coronal ^{18}F-FOL, ^{11}C-PBR28 PET and MRI images during the acute phase. B) Representative coronal ^{18}F-FOL, ^{11}C-PBR28 PET and MRI images during chronic phase. C) *In vivo* PET quantitative data are presented as SUV-ratios ($SUV_{max,\ lesion}/SUV_{mean,\ contralateral}$). Black and white arrows display the lesion site. Error bars denote standard deviation. Key:* = $P \leq 0.05$, NS = $P \geq 0.05$ (Modified from Study II).

5.4 Folate aminopterin intervention and evaluation of ^{68}Ga-FOL in acute and chronic *f*DTH-EAE

EC2319, folate aminopterin drug-conjugate, treatment showed efficacy in the chronic phase of inflammation in *f*DTH-EAE as observed from immunofluorescence and histology in the study III. The anti-FR-β positivity was significantly lowered in EC2319-treated rats compared to saline-treated ($P < 0.05$) and the lesion size was also significantly reduced in rats treated with EC2319 compared to saline treated rats ($P < 0.01$). However, the area of CD68-positive macrophages/microglia ($P = 0.093$) and lymphocyte count densities ($P = 0.065$) demonstrated reduction for rats in EC2319 treatment group to that of saline treated rats, but the reductions did not result in significant difference. The immunofluorescence indicated significantly lowered iNOS/MRC-1-ratio ($P < 0.01$).

In vitro assay of ^{68}Ga-FOL revealed significantly lower binding for ^{68}Ga-FOL when the brain samples from chronic phase were pre-incubated with the folate glucosamine compared to total binding in which the samples had no pre-incubation. In addition, ^{68}Ga-FOL binding was significantly reduced in brain samples that were EC2319-treated compared to saline-treated ($P < 0.01$). Although *in vivo* PET/CT and *ex vivo* autoradiography of ^{68}Ga-FOL enabled the visualization of inflammatory lesions, these methods were unable to monitor the EC2319 therapy efficacy otherwise observed by anti-FR-β immunofluorescence and histology.

For the acute phase of inflammation in *f*DTH-EAE, the corresponding immunofluorescence data indicated no differences in FR-β, CD68, iNOS or MRC-1 positivity between EC2319 and saline treated groups. There was also no difference in iNOS/MRC-1-ratio, amount of lymphocytes and lesion size between EC2319-treated rats and saline-treated rats. *In vitro* ^{68}Ga-FOL assay, *in vivo* PET/CT imaging and *ex vivo* autoradiography revealed no differences between treatment groups. The EC2319 intervention data of acute and chronic *f*DTH-EAE rats is presented in more detail in Table 6.

5.4.1 Expression of FR-β in human post-mortem MS brain and normal brain samples

Immunohistochemistry of FR-β in the study III confirmed the presence of FR-β cells in brain parenchyma of patients with MS. The paraffin-fixed post-mortem MS brain sections showed FR-β positivity in areas of NAWM and in the chronic active lesions, which typically include vast amounts of activated microglia and macrophages, compared to normal brain sections that lacked the expression of FR-β in corresponding anatomical locations of NAWM (Figure 12). The immunofluorescence data support this assumption as FR-β expression in the MS brain is largely co-localized with CD68, iNOS (marker for M1 proinflammatory microglia/macrophages) and MRC-1 (marker for M2 anti-inflammatory microglia/macrophages) positivity (data not shown). This indicates that the results obtained from the *f*DTH-EAE are translatable to human MS to some extent. On the other hand, FR-β expression was very weak or absent in normal appearing grey matter (NAGM) and in chronic inactive lesions both know to have insignificant amounts of activated microglia and macrophages. The expression of FR-β was also very weak or negative in NAGM in normal brain samples (Figure 12 A).

5.4.2 Modelling of ^{18}F-FOL and ^{68}Ga-FOL PET data

In the Study II and III, the radiotracers ^{18}F-FOL and ^{68}Ga-FOL remained relatively stable in rat blood circulation (^{18}F-FOL; 88% ± 0.12% intact tracer vs. ^{68}Ga-FOL;

89% ± 2.81% at 30min post-injection) and the tracer uptake kinetics in the brain were well described by the Logan model for reversible binding.

However, distribution volume ratio (DVR) for Logan analysis showed no significant difference in between ^{18}F-FOL and ^{68}Ga-FOL imaged *f*DTH-EAE rats at day 14 (P = 0.50) and at day 90 (P = 0.66). Additionally, brain to blood-ratios indicated no significant difference between ^{18}F-FOL and ^{68}Ga-FOL imaged *f*DTH-EAE rats at acute phase of inflammation (at day 14, P = 0.47) and at chronic phase of inflammation (at day 90, P = 0.95).

Interesting though, the DVR acquired from reversible Logan model for kinetic analysis (DVR_{Logan}) correlated well with SUV-ratio of ^{18}F-FOL imaged rats at the acute phase (R^2 = 0.73, P < 0.05) and of ^{68}Ga-FOL imaged rats at the chronic phase (R^2 = 0.74, P < 0.05). The data is presented in Table 7.

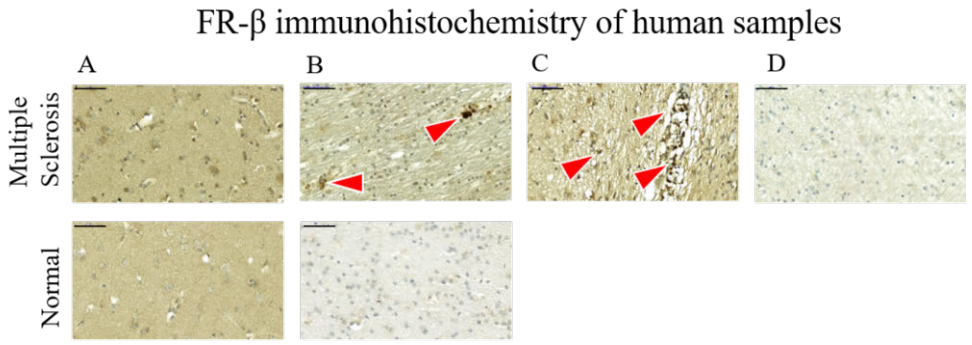

Figure 12. Anti- FR-β immunohistochemical staining of formalin-fixed paraffin embedded human brain sections from MS and normal brain. FR-β staining A) of NAGM from SPMS patient and normal brain, B) of NAWM from SPMS patient and normal brain, C) of chronic active lesion and, D) of chronic inactive plaque. Red arrows display FR-β positivity. Scale bar is 50 µm.

Table 6. Results of immunofluorescence, histology and ^{68}Ga-FOL analyses from acute phase or chronic phase of *f*DTH-EAE rats treated with EC2319 or saline.

	***f*DTH-EAE Day 14 (Saline)**	***f*DTH-EAE Day 14 (EC2319)**	**P value**	***f*DTH-EAE Day 90 (Saline)**	***f*DTH-EAE Day 90 (EC2319)**	**P value**
FR-β (mm^2)	0.0030 ± 0.00088	0.0024 ± 0.0013	0.24	0.0064 ± 0.0016	0.0019 ± 0.00067	*
CD68 (mm^2)	0.0098 ± 0.0039	0.015 ± 0.0042	0.28	0.010 ± 0.0021	0.0053 ± 0.0011	0.093
iNOS (mm^2)	0.015 ± 0.0069	0.027 ± 0.0093	0.34	0.025 ± 0.011	0.0016 ± 0.0012	0.10
MRC-1 (mm^2)	0.0044 ± 0.0012	0.0040 ± 0.0016	0.89	0.0015 ± 0.00051	0.0022 ± 0.00065	0.63
iNOS/ MRC-1	7.96 ± 5.80	8.62 ± 4.54	0.69	15.59 ± 2.24	0.63 ± 0.29	**
Lesion (mm^2)	0.16 ± 0.043	0.71 ± 0.42	0.66	0.26 ± 0.098	0.055 ± 0.018	**
Lymphocytes (cells/mm^2)	956.4 ± 120.5	986.5 ± 118.6	0.89	729.80 ± 146.00	393.30 ± 84.66	0.065
***In vitro* (bound-to-free)**	12.19 ± 0.77	13.97 ± 0.83	0.11	4.93 ± 0.43	2.47 ± 0.45	**
***Ex vivo* (bound-to-free)**	3.95 ± 0.98	10.16 ± 5.25	0.96	3.76 ± 1.75	0.75 ± 0.19	0.11
***In vivo* (SUV)**	4.01 ± 0.30	4.77 ± 0.27	0.10	3.79 ± 0.28	4.04 ± 0.30	0.55

*= P<0.05, **=P<0.01, ***=P<0.001.

Table 7. Logan plot analysis and associations between SUV-ratios and DVR_{Logan} of ^{18}F-FOL and ^{68}Ga-FOL uptake in *f*DTH-EAE rats.

	^{18}F-FOL	**^{68}Ga-FOL**	**^{18}F-FOL**	**^{68}Ga-FOL**	**^{18}F-FOL**	**^{68}Ga-FOL**
	DVR Lesion/ Contralateral	**DVR Lesion/ Contralateral**	**Brain-to-Blood ratio Lesion/ Contralateral**	**Brain-to-Blood ratio Lesion/ Contralateral**	**Correlation (R^2) of SUV-ratio and (DVR_{Logan})**	**Correlation (R^2) of SUV-ratio and (DVR_{Logan})**
Day 14	1.19 ± 0.26	1.18 ± 0.18	1.18 ± 0.28	1.11 ± 0.17	0.73	0.19
P	0.50		0.47		< 0.05	0.66
Day 90	1.28 ± 0.30	1.22 ± 0.13	1.33 ± 0.32	1.32 ± 0.18	0.70	0.74
P	0.66		0.95		0.19	< 0.05

6 Discussion

6.1 Main findings of the studies

In the Study I, we showed for the first time that the membrane-bound form of VAP-1 is actively associated with the development of inflammatory lesions representative of type I and antibody-mediated type II immunopathology. Inhibition of membrane-bound VAP-1 activity with a small molecular inhibitor LJP1586 prohibited the lymphocyte recruitment into lesion in the brain parenchyma during the acute inflammation in type II rat model of MS, but restored to same levels as without the LJP1586 treatment after the acute inflammation subsided at the remission phase. *Ex vivo* autoradiography results display that ^{68}Ga-DOTA-Siglec-9 enabled detection of lesions that have evolved to traditional inflammatory lesions with active demyelination, lymphocyte recruitment, presence of activated macrophages and compromising of intact BBB. Luminal VAP-1 was not present during "pre-active" lesion development, which suggested that ^{68}Ga-DOTA-Siglec-9 might not be considered as a promising radiotracer in early evaluation of MS-like pathologies. Thus, luminal VAP-1 was most likely expressed in lesion vasculature only after developed inflammatory lesions required amplification of immune response at the site of inflammation and the expression of VAP-1 remained on the lesion vasculature after the first active relapse during BBB restoration. In *f*MOG-EAE lesions the endothelium appeared to undergo a structural transformation from regular flat-walled endothelium to HEV-like endothelium as the endothelial cells in *f*DTH-EAE lesions mostly displayed flat-walled morphology. The role of the luminal VAP-1 in EAE and possibly in MS might be related to amplifying inflammation in active demyelinating lesions and the function of VAP-1 in driving new lesion formation showed to be less significant of importance.

In the Study II, we discovered the presence of FR-β expression in activated macrophages and microglia during the development of acute and chronic type I CNS inflammatory lesions in EAE. The FR-β expression was mostly detected in borderline of these lesions, which are known to have activated macrophages, ongoing demyelination and remyelination. Both of the studied radiotracers, ^{18}F-FOL and ^{11}C-PBR28 were able to identify the CNS lesions in acute and chronic phase of *f*DTH-EAE, but only ^{18}F-FOL was able to separate between acute phase and chronic

phase lesions compared to ^{11}C-PBR28. ^{18}F-FOL exhibited also a significantly lower background than ^{11}C-PBR28 overcoming a major limitation that conventional TSPO-targeted imaging still possesses especially during studies regarding neuroinflammation. Immunofluorescence and correlation data supported the view that FR-β expression is more prominent in MRC-1 positive macrophages and microglia (anti-inflammatory) than in iNOS positive macrophages and microglia (proinflammatory) in EAE. FR-β expression is also suggestive of equilibrium in iNOS/MRC-1 ratio known to be associated with milder inflammation in EAE. The ^{18}F-FOL binding was shown to be at highest in areas of the densest anti-MRC-1 positivity, which indicates that ^{18}F-FOL uptake could be located in the areas related to tissue remodeling and remyelination in neuroinflammation.

In the III study, we examined the treatment efficacy of novel folate conjugate EC2319 for acute and chronic DTH-type lesions in EAE and the ability of ^{68}Ga-FOL to visualize inflammatory lesions *in vitro*, *ex vivo* and *in vivo*, and demonstrate therapy efficacy of EC2319. The EC2319 was effective when administered at chronic phase of inflammation by reducing FR-β expression, iNOS/MRC-1 –ratio, lesion size, and also ^{68}Ga-FOL binding in *in vitro* assay of brain sections. However, ^{68}Ga-FOL showed no significant change in *in vivo* and *ex vivo* uptake at either the chronic phase or the acute phase. In addition, the therapy efficacy observed at chronic phase was absent during acute phase of EAE. With regards to iNOS/MRC-1 equilibrium post EC2319 treatment at chronic inflammation, the EC2319 might aid in the regulation of CNS inflammatory processess and therefore could introduce new therapeutic indications for folate aminopterin therapies outside the traditional scope of peripheral inflammatory disorders. This concept was very tempting as there have been very few approved therapies for primary progressive MS. However, it was noteworthy that the long-term efficacy and safety remained to be determined as EC2319 therapy reduced the number of FR-β positive cells required to FR-mediated endocytosis of the drug molecule.

6.2 Evaluation of VAP-1 targeted ^{68}Ga-Siglec-9 for PET imaging of MS-like lesions

Based on the Study I, we can determine that luminal translocation of VAP-1 occurs in the vasculature of developed inflammatory lesions in rat models of MS that depict type I and II immunopathology and luminal VAP-1 can be used as a molecular target for imaging neuroinflammation. The data obtained from the digital *ex vivo* autoradiography suggests that ^{68}Ga-DOTA-Siglec-9 can bind and visualize the inflammatory brain lesions positive for VAP-1 although the molar mass of ^{68}Ga-DOTA-Siglec-9 ($C_{10}4H_{17}4N_{30}O_{32}S_2$, molecular weight 2.4202 kDa) exceeds 500 Da described in Lipinski's rule (Virtanen et al., 2015, Oprea et al., 2001). This could be

explained by location of the molecular target, VAP-1, which is on the surface of the endothelium in blood vessels at the site of inflammation in the brain in *f*DTH-EAE and *f*MOG-EAE rats. The utility of ^{68}Ga-DOTA-Siglec-9 has also been proven in previous preclinical studies in *in vivo* imaging of animal models of peri-implant infections, synovitis, atherosclerosis and tumor xenografts (Ahtinen et al., 2014, Virtanen et al., 2015, Silvola et al., 2016, Siitonen et al., 2019). The relatively abundant expression of membrane-bound VAP-1 during inflammatory processes in peripheral tissues is most certainly beneficial for the use of VAP-1 targeting radiotracers like ^{68}Ga-DOTA-Siglec-9 in PET imaging of peripheral conditions compared to PET imaging of CNS inflammatory disorders.

Our data in the study I suggested that VAP-1 expression is not found in the pre-active lesions in *f*DTH-type lesions that typically lack the features of traditional CNS inflammatory lesions visible in MRI, such as ongoing demyelination, BBB disruption, macrophage and lymphocyte recruitment (Serres et al., 2009). Due to this ^{68}Ga-DOTA-Siglec-9 has very limited capacity for PET imaging of newly forming inflammatory MS-like lesions. This finding is unfortunate as tissue samples from early lesions in MS are challenging to obtain from living MS patients and discovery of molecular imaging marker for early stage lesions would be an important finding in the diagnostic field of MS (Pirko & Johnson, 2008). In contrast to early stage MS-like lesions, ^{68}Ga-DOTA-Siglec-9 was found to be successful in detecting lesions at the acute phase with widespread inflammation accompanied with BBB disruption in both type I and type II rat models of MS and lesions that show evidence of BBB restoration after the first acute relapse. Because perivascular lymphocyte and macrophage recruitment and BBB disruption occur during the relapse in MS (Alvarez et al., 2011, Minagar & Alexander, 2003), this discovery may be translatable to MS during relapses. Therefore, ^{68}Ga-DOTA-Siglec-9 might have the ability to detect the inflammation-related alterations in the lesion after relapses and identify lesions, which could potentially show signs of progression during periods between relapses in MS.

Most importantly, we found that anti-VAP-1 positivity of immunofluorescence data and *ex vivo* autoradiography of ^{68}Ga-DOTA-Siglec-9 binding in *f*MOG-EAE was reduced 14 days after the inhibition of VAP-1 activity with LJP1586 indicating that ^{68}Ga-DOTA-Siglec-9 is also capable of detecting the therapy effect of VAP-1 targeting anti-inflammatory therapies. However, the autoradiography data at the acute phase revealed unexpected outcomes as ^{68}Ga-DOTA-Siglec-9 binding increased for LJP1586 treated *f*MOG-EAE rats. In case of LJP1586, it is acknowledged that LJP1586 only inhibits enzymatic activity of VAP-1/SSAO (Stolen et al., 2005). Hence the binding of ^{68}Ga-DOTA-Siglec-9 to its target, luminal VAP-1, could be independent of LJP1586 inhibitory activity at lest in the early phases of treatment, although lymphocyte infiltration to inflammation site has found

to be reduced. Another reason for this increased binding of ^{68}Ga-DOTA-Siglec-9 could be the ability of LJP1586 to alter the conformation of luminal VAP-1 during the treatment period.

Interestingly, we found in the study I that the CNS lesion area expanded in LJP1586-treated rats at the remission phase, which might be explained by unfavorable timing of the VAP-1 inhibiting therapy. *FMOG-EAE* rats are designed to model acute widespread inflammation and cortical demyelination, which spontaneously recover over time and this acute pathogen-clearing inflammatory process should not be intervened (Merkler et al., 2006). On the other hand, the treatment of EAE in SJL mice with another SSAO/VAP-1 inhibitor, LJP1207, has mitigated the incidence and inhibited the development of clinical disability in EAE when the therapy was initiated after the first peak of the disease (O'Rourke et al., 2007). This contradicts with the results observed in the study I with *f*MOG-EAE showing that the efficacy of SSAO/VAP-1 targeting therapy is dependent at least on the type of EAE model used and the onset of the intervention. As VAP-1 targeting therapies have these limitations in treating acute EAE and VAP-1 appeared to be upregulated rather in the hypercellular core of lesions than in microglia-rich NAWM around the inflammatory lesions, these limitations will also have negative influence on the potential of ^{68}Ga-DOTA-Siglec-9 in monitoring lesion progression and inflammatory status in EAE. As activated microglia are believed to be the driving force behind ongoing demyelination in MS, but not necessarily in EAE, these features may potentially limit the clinical utility of ^{68}Ga-DOTA-Siglec-9 for imaging MS patients. However, the clinical first-in-human studies with healthy individuals could aid in promoting the translation of ^{68}Ga-DOTA-Siglec-9 PET imaging into clinical use.

6.3 Evaluation of FR-β-targeted ^{18}F-FOL for PET imaging of MS-like lesions

In the study II, the prominent expression of FR-β during acute and chronic neuroinflammation in *f*DTH-EAE rat model provides a promising target for FR-based molecular imaging agents, such as ^{18}F-FOL, to monitor neuroinflammation. In addition, it has been confirmed that specific FR-targeting folate aminopterin therapies can modulate the course of the disease in EAE (Lu et al., 2014) indicating that FRs can play an important role in progression of the MS-like lesions and ^{18}F-FOL could be useful in evaluating this disease progression. When ^{18}F-FOL was compared to the standard TSPO targeting tracer, ^{11}C-PBR28, it could visualize both the acute and chronic phase inflammatory EAE lesions as could ^{11}C-PBR28, but to the extent that ^{18}F-FOL enabled the differentiation *ex vivo* between the acute inflammatory lesions and larger chronic inflammatory lesions with more severe

inflammation and lesion burden. This feature of ^{18}F-FOL is largely contributed by the significantly lower background signal than current microglia and macrophage detecting TSPO targeting radiotracers including ^{11}C-PBR28 has (Imaizumi et al., 2008, Harberts et al., 2012, Datta et al., 2017). Another beneficial attribute in ^{18}F-FOL is the use of 18-fluorine label, which has shorter positron range than 11-carbon increasing the spatial resolution 18-fluorine can provide for PET images (Miller et al., 2010). However, the ^{18}F-FOL *in vivo* PET showed insufficient sensitivity in detecting the changes during lesion progression from the acute to chronic phase. Unfortunately, that was most likely due to too low spatial resolution (1.6mm^3) of Inveon small animal PET camera (Goertzen et al., 2012) complicating the *in vivo* imaging of smaller acute lesions with average lesion size of approximately 0.06 mm^2 measured using histological evaluation. In the clinical setting, however, the median lesion size for MS patients is considered to be 30 – 40 mm^2 in MRI considering that only 20% of brain lesions have nominal diameters less than 3.5 mm (Wang et al., 1997 & Davis, 2013) With the performance of new digital PET/CT cameras, it is possible to acquire a spatial resolution of 2.7 mm^3 indicating that these existing restrictions in pre-clinical PET imaging of focal EAE models might not apply with modern clinical PET imaging devices in patients with MS (Chicheportiche et al., 2020). Therefore, ^{18}F-FOL may overcome the observed limitations and it may support the translation of pre-clinical imaging protocols into clinical use. The ideal goal wth ^{18}F-FOL would be to enable the detection of the lesion progression *in vivo* and identify the dominant polarization patterns of macrophages and microglia during CNS inflammation in MS

According to the data obtained from the Study II, we found a positive correlation and co-localization of anti-MRC-1 and anti-FR-β positivity from correlation analysis and immunofluorescence stainings during the chronic phase of EAE. In addition, the anti-FR-β positivity correlated with decreased iNOS/MRC-1 –ratio as previously reported. On the other hand, anti-iNOS positivity showed weak correlation with FR-β positivity. Previous studies are in line with our studies that ^{18}F-FOL clearly binds more to MRC-1-positive macrophages than to iNOS-positive macrophages (Silvola et al., 2018) and FR-β expression is densest in areas of known ongoing remyelination and macrophage recruitment (Lassmann et al., 2007, Miron et al., 2013). Based on this assumption that MRC-1 expressing macrophages and microglia express more of FR-β than iNOS-expressing macrophages and microglia and anti-FR-β positivity is indicative for milder inflammation in EAE (Mikita et al., 2011), the FR-β targeting ^{18}F-FOL could potentially be used to evaluate the dominant polarization patterns of macrophages and microglia *in vivo* and predict the inflammation severity in the CNS lesions. Because MRC-1 positive (M2) phenotype is known to be associated with tissue remodeling and remyelination in MS (Miron et al., 2013, Nagai et al., 2006), one could suspect if ^{18}F-FOL would have the potential to be utilized in *in vivo*

imaging of demyelination, remyelination and inflammation burden in MS. This could have implications in earlier identification of MS patients with increased risk of disease progression and inflammation severity, but limited potential in optimizing MS therapies as there are currently no approved therapies directly targeting demyelination or remyelination (U.S. Food and Drug Administration news release, 2019).

The ^{18}F-FOL tracer uptake kinetics in the brain was successfully represented with kinetic Logan analysis for reversible binding rather than with kinetic Patlak analysis (data not shown) for irreversible binding. Based on previous studies on folate radioconjugates, the rate of tracer internalization could vary vastly among folate targeted tracers and disease models used (Muller et al., 2013). As FRs normally get internalized after binding to its ligand (Low et al., 2007) one would expect the irreversible portion of the ^{18}F-FOL uptake to be significant in the brain, but instead the data obtained from Logan analysis showed significant reversible uptake of ^{18}F-FOL. According to DVR and brain-to-blood values in Table 7, the uptake of ^{18}F-FOL is still higher in the lesion side than in the contralateral side of the brain. It is known that distribution volume obtained from the graphical Logan analysis is independent of perfusion and should not influence to increased uptake in the lesion (Logan et al., 1990). Hence, this increased uptake may be due to increased binding of ^{18}F-FOL to plasma proteins or transporters in close proximity of the lesion in the brain, which are unable to internalize the radiotracer. In addition, compromised BBB could possibly increase the distribution volume of ^{18}F-FOL in *f*DTH-EAE rats.

It must be taken into consideration that ^{18}F-FOL is not FR-β specific and it can also bind to the other isoform of FR (FR-α) complicating the diagnostic *in vivo* PET imaging of FR-β positive MS-like inflammatory lesions. As FR-α is expressed in low concentrations in some structures of the brain (Low et al., 2007), the binding of the ^{18}F-FOL could introduce bias in attempt to provide accurate information on FR-β positive CNS lesions.

Taken together, ^{18}F-FOL could provide an alternative tool to acquire information with *in vivo* PET imaging on inflammatory status and lesion load in the brain during CNS inflammation and supplement with information that is not attainable using conventional TSPO-targeted PET.

6.4 Evaluation of FR-β-targeted ^{68}Ga-FOL for PET imaging of MS-like lesions

In the Study III, we evaluated the effectiveness of FR-β targeted folate aminopterin conjugate EC2319 therapy in treating MS-like lesions in acute and chronic *f*DTH-EAE and examined the utility of ^{68}Ga-FOL to measure the therapy effect in *f*DTH-EAE. Although EC2319 showed efficacy in reducing FR-β expression, lesion

volume and iNOS/MRC-1–ratio in chronic phase of inflammation, ^{68}Ga-FOL showed insufficient signal-to-background ratio, sensitivity and binding to CNS inflammatory lesions both at acute and chronic phase of CNS inflammation to differentiate lesion progression and therapy efficacy between EC2319-treated and saline-treated lesions *in vivo* and *ex vivo*. However, the sensitivity of ^{68}Ga-FOL was adequate enough to visualize the focal DTH-EAE lesions during the entire time course of the disease and to distinguish brain sections *in vitro* treated with EC2319 at chronic phase of inflammation. In addition to the limitations observed with ^{18}F-FOL, the lack of sensitivity in detecting the treatment effect may results from the use of 68-gallium as a radiolabel for ^{68}Ga-FOL radiotracer. ^{68}Ga has larger positron range than commonly used ^{18}F considerably reducing the spatial resolution than can be provided with ^{68}Ga-FOL especially during small animal PET imaging when high resolution PET/CT cameras are used (Li & Conti, 2010). This is especially counterproductive if the relatively long positron range is combined with 1) the limited *in vivo* binding of ^{68}Ga-FOL to FRs because of excessive plasma protein and transporter binding, and 2) the scarce overall availability of the target, FR-β, due to EC2319 therapy effect in the inflammatory brain lesions.

The 1.6 mm^3 spatial resolution of small animal Inveon multimodality PET/CT undoubtedly limits the *in vivo* detection of subtle changes in FR-β expression with ^{68}Ga-FOL (Goertzen et al., 2012). In the Study III, the lesion size was reduced by 0.2 mm^2 on average between EC2319-treated and saline-treated rats at chronic phase. In theory, this difference is very difficult to observe even if NOTA-Folate radiotracer would have been labeled with shorter positron range ^{18}F in order to synthetize ^{18}F-FOL (Li & Conti, 2010). In addition, FRβ-expression was significantly reduced in the rats treated with EC2319 at chronic phase. This further reduces the availability of FR-β for ^{68}Ga-FOL binding and complicates the detection of therapy effects and detection of the CNS lesion itself.

Despite the drawbacks ^{68}Ga-FOL arguably has compared to ^{18}F-FOL, it still has potential to overcome the limitations traditional TSPO imaging possesses, such as, too high background, low receptor affinity, lack of selectivity towards macrophages and microglia and dependency for onsite cyclotron (Kreisl et al., 2010, Ching et al., 2012, Aljammaz et al., 2014).

The kinetic Logan analysis data for ^{68}Ga-FOL in the Study III was in line with corresponding analysis performed with ^{18}F-FOL in the Study II. The kinetic data obtained for ^{68}Ga-FOL showed no differences in DVR_{Logan} and in brain-to-blood ratios between ^{18}F-FOL and ^{68}Ga-FOL imaged *f*DTH-EAE rats (Table 7.). This indicates that ^{68}Ga labeling of NOTA-Folate has minimal interference with tracer kinetics. However, the correlation data in table 7 showed very weak correlation between SUV–ratios and DVR_{Logan} at acute phase of inflammation. This could be explained by both significantly lower lesions size of *f*DTH-EAE rats during acute

phase, which is limiting the capability of ^{68}Ga-FOL to detect inflammatory lesions, and by lower spatial resolution in PET images caused by larger positron range in ^{68}Ga-FOL (Li & Conti, 2010).

Regarding the clinical potential of ^{68}Ga-FOL, it would be a tempting idea to use an optimal radiotracer in patients with MS that could evaluate lesion progression, inflammatory severity and predict disease progression without the need for onsite cyclotron (Aljammanz et al., 2014). However, the observed disadvantages of ^{68}Ga-FOL in this work have demonstrated that the individual benefit ^{68}Ga-FOL may provide for *in vivo* PET imaging of MS patients is the independency from the cyclotron alone.

6.5 Limitations of the studies

These studies indicated that blocking of VAP-1/SSAO activity with small molecular inhibitor LJP1586 impaired the transmigration of lymphocytes into sites of inflammation in the brain during the acute inflammation in rats with *f*MOG-EAE. However, we have disregarded the role of soluble VAP-1 (sVAP-1) during the LJP1586 intervention. For example, it is known that the serum levels of sVAP-1 are increased in patients with active RRMS and absence of sVAP-1 in the CSF of RRMS patients indicate that soluble VAP-1 may be originated from its luminal form of VAP-1 (Airas et al., 2006). In addition, sVAP-1 levels might aid in regulation of VAP-1-dependent transmigration of leukocytes from bloodstream into site if inflammation without compromising the immunodefensive functions (Stolen et al., 2005). The lack of sVAP-1 data in this work limits the evaluation of the role of sVAP-1 in regulating lymphocyte trafficking and LJP1586 therapy efficacy in EAE. Investigating the relationship between sVAP-1 and luminal VAP-1 in EAE would have provided valuable insights in regulatory roles of both forms of VAP-1 and possibly supported the translation of these findings to pathophysiology in human MS. Furthermore, it could have revealed mechanisms that possibly would have explained the efficacy or lack of efficacy of LJP1586 in treating CNS inflammation.

Both of the EAE rat models used in the study I display some limitations when compared to conventional disseminated models of EAE (Svensson et al., 2002, Lyons et al., 1999). The *f*DTH-EAE and *f*MOG-EAE will form only an individual focal lesion whereas most EAE models will create new lesions in random and variable manner during the entire disease course. Therefore, *f*DTH-EAE and *f*MOG-EAE models are not suitable for studying formation of new neighboring lesions, which is an essential component in MS (Waubant et al., 1997). Furthermore, the immunopathology of EAE lesions is typically dependent on the location of lesions, and on used animal, strain and antigen (Gold et al., 2006, Foster et al., 2008). For example, if EAE is induced in C57BL/6 mice using MOG-peptides in CFA for

immunization and pertussis toxin for activation of immune response, this will create a monophasic EAE without any relapses and $CD4^+$ dominated inflammatory lesions prominently present in spinal cord (Steinman et al., 2006, Dal Canto et al., 1995). On the other hand, Swiss James Lambert mice immunized with MBP of MOG will establish a chronic relapsing-remitting EAE with active demyelination and inflammatory events in the brain (Mix et al., 2010). Furthermore, *f*DTH-EAE has shown lack of similarity for rarer pattern III and IV of demyelination in MS (Lucchinetti et al., 2005). In case of *f*DTH- and *f*MOG type EAE, the inflammatory cells mainly consist of $CD8^+$ and macrophage dominant lesions with extensive remyelinating capacity after acute demyelination and antibodies involved in disease pathology of MOG induced EAE (Merkler et al., 2006, Serres et al., 2009). Certain types of MOG peptide fragments have implications to characteristic of the disease and to experimental designs that can be conducted (Lyons et al., 1999). In addition, the small size of the individual acute lesions in *f*DTH-EAE may exacerbate the limitations caused by the relatively low expression levels of molecular targets, such as VAP-1 and FR-β, available for PET imaging agents. Despite of vast amount of restrictions when creating an EAE model, we chose the most suitable models for our purpose to study the onset and development of EAE and to study the efficacy of novel therapeutics and utility of novel PET imaging agents in acute and chronic CNS inflammation (Anthony et al., 2014, Lyons et al., 2002). These models, however, require intracranial injection for the induction of the disease and the injection may cause inflammation at the injection site and possibly affect also the contralateral side of the brain. As non-operated healthy intact rats were only used in the study III, therefore, it can be regarded as a limitation in this work.

The study results are also limited by lack of valid MRI data during the Study II and III, because due to random coil failures or malfunction in the clinical MRI device. High quality MRI would provide high resolution images, which could be used as anatomical reference for various areas of the brain supporting, validating or complementing the data acquired from PET imaging and aid in co-registration of PET and MR images. In addition, rat brain MR images can be used as a tool to evaluate BBB permeability during various stages of CNS inflammation and as an alternative method to demonstrate therapy effects of novel therapies (Jiang et al., 2005). This would have been a robust method per se as it is currently used in clinical practices when evaluating therapies in patients with MS (Siffrin et al., 2010).

7 Conclusions

The main goal of the thesis was to assess novel molecular imaging probes targeting alternative markers, FR and VAP-1, for *in vivo* PET imaging of neuroinflammation and EAE disease progression, respectively. In detail, we aimed to investigate the role of VAP-1 and FR-β in development of EAE lesions and the utility of VAP-1 targeted PET radiotracer, ^{68}Ga-DOTA-Sigle-9, and the feasibility of FR-targeted radiotracers, ^{18}F-FOL and ^{68}Ga-FOL, in monitoring CNS inflammation and progression of the disorder in EAE compared to second generation TSPO targeting radiotracer. In addition, we evaluated if VAP-1 and FR targeted PET probes enabled monitoring of the treatment efficacy in EAE rats. Finally, MRI, *ex vivo* autoradiography, immunofluorescence and immunohistochemistry were used to both acquire novel findings and confirm the findings obtained from *in vivo* PET imaging. According to the data shown in this thesis, the following conclusions can be drawn:

1. 3T clinical MRI combined with rat-dedicated brain coil provides a feasible method for evaluating traditional CNS inflammatory lesions in rat models of MS without the use of high-resolution MRI.
2. Luminal VAP-1 is involved in the development of acute MS-like lesions and remains to be expressed on lesion vasculature during remissions. ^{68}Ga-DOTA-Sigle-9 is capable of detecting neuroinflammation in the active MS-like lesions that present leukocyte infiltrates, but may not be suitable for evaluating new lesion formation and efficacy of therapies.
3. FR-β is expressed on activated macrophages/microglia on EAE lesions and also in chronic MS lesions. FR targeting PET probe ^{18}F-FOL can be used to assess EAE lesion development and acquire information that cannot be obtained with TSPO-targeted imaging.
4. Novel folate aminopterin was effective only during chronic inflammation in EAE. ^{68}Ga-FOL could visualize acute and chronic lesions, but lacked the ability to detect efficacy of therapies. FR-B may be a potential target for *in vivo* PET imaging of MS patients and development of novel therapeutics for MS patients.

Acknowledgements

This study was conducted at the Turku PET Centre and Department of Clinical Physiology and Nuclear Medicine in Turku University Hospital and University of Turku during the years 2015–2020. I want to express my gratitude to Jaakko Hartiala (Head of the Department of Clinical Physiology and Nuclear Medicine during the initial years of my studies), Adjunct Professor Jukka Kemppainen (Head of the Department of Clinical Physiology and Nuclear Medicine after Jaakko Hartiala since May 2016), Professor Juhani Knuuti (Director of Turku PET Centre) for providing me up-to-date facilities and welcoming environment to work in. This study was financially supported by personal grants and awards from Finnish MS Foundation, the Finnish Brain Foundation, Turku University Foundation, Instrumentarium Foundation, the Finnish Society of Nuclear Medicine, the State Research Funding of Turku University Hospital, the Alfred Kordelin Foundation, the Orion Foundation and finally the Drug Research and Doctoral Programme of the University of Turku Graduate School.

I want to show my deepest gratitude to my awesome supervisors, Professor Anne Roivainen, Professor Laura Airas and Academician, Professor Sirpa Jalkanen who have provided me with excellent support and guidance in my work. Your academic expertise and professional knowledge has been irreplaceable. I especially appreciate Anne's strong expertise in biochemistry, preclinical imaging concepts and producing high-quality scientific articles. This has greatly expanded my abilities to write academic texts in the level required. You have also been close and available to assist me in whatever I have encountered. Sirpa's experience and career has been quite unique including the discovery of VAP-1. I have felt privileged in working with you during my studies, because there are quite few people who have been appointed as Academy Professors in Finland. Your excellent up-to-date and in-depth knowledge on scientific information, especially in the field of immunology, has given me and my articles a tremendous value that I would perhaps never discovered on my own. I believe you have been and will be a great example for young scientist in their careers. Laura has a very broad spectrum of knowledge and experience in neuroimmunology and in clinical studies related to MS. It has helped me to understand the translational potential of my studies and the importance of my work in clinical context. I admire

her enthusiasm, ambition and creativity for MS research and the reputation that she has acquired during her career. I have had multiple opportunities to grow my professional network because of knowing Laura and I am very grateful of this. I want to thank my follow-up committee member, Ullamari Pesonen, who provided assist and guidance during this study. I wish to thank Professor Mika Scheinin, former Director of FinPharmaNet, Professor Markku Koulu, former Director of Drug Research Doctoral Programme and Associate Professor Eriika Savontaus, Director of Drug Research Doctoral Programme for enabling my doctoral studies in their doctoral programme at University of Turku. In addition, I want to thank Eeva Valve, coordinator for Drug Research Doctoral Programme, for assisting me in practical matters and providing friendly atmosphere in meetings during my time in DRDP.

I wish to give special thanks to all of my co-authors and colleagues who have worked in my research projects. I wish to thank Xiang-Guo Li, Olli Moisio, Semi Helin, Maxwell Miner and Meeri Käkelä who have provided me with high quality radiotracers irrespective of the radioactive label or time of the day to enable my PET imaging studies. Your ability to solve occasional and unprecedented issues with radiosynthesis has been very important part of completing all studies. I have also had great time with you in lab meetings and coffee breaks. I want to thank Heidi Liljenbäck and Jenni Virta for being always available to help me with animal experiments and imaging days, which sometimes were stretched beyond regular workday hours. I want to thank Jarmo Teuho, Kalle Koskensalo and Virva Saunavaara for their expertise in MRI protocols and their positive attitude, flexibility and curiosity towards my studies. I also want to thank Sina Tadayon for interest in doing his MSc thesis related to my research projects and the opportunity mentor and share laughs with you. I would like to thank Tibor Verez, Aida Steiner, Antti Saraste, Vesa Oikonen and Päivi Marjamäki for proving me with both excellent technical and scientific support. I want to also thank Philiph Low, Madduri Srinivasarao, June Lu and Qingshou Chen from the USA. They helped with the essential material and analyses for doing my research articles.

I wish to thank the personnel at Turku PET Centre, especially Minna Aatsinki and Marko Seppänen for scheduling the imaging studies and the rest of the personnel to help me with the practical work at the lab. I thank Aake Honkaniemi for performing practical PET imaging studies with me and organizing the schedules conveniently to complete all the studies. Marko Tirri is acknowledged in assisting with PET imaging if needed and educate for radiation safety. I want to thank Rami Mikkola and Marko Tättäläinen for professional help in IT related issues. I want to warmly thank Erica Nyman, Marja-Riitta Kaajala, Timo Kattelus and Sari Mäki for high quality technical work and laboratory experiments for my doctoral thesis.

I wish to thank my all former and current colleagues in the pre-clinical research group Helena, Riikka, Mia, Maria, Miikka, Max, Maxwell, Olli, Arghavan,

Andriana, Senthil and Erika that shared the same office space in PET or in Teutori and the great atmosphere you guys create in the work. My doctal thesis has felt better and more joyable because of good team spirit and peer support.

I am also grateful for having good friends outside my core pre-clinical research group. I want to thank Minna, Simona, Milena, Kumar and Priyanka for their friendship, humor, and positive attitude for life, science and life sciences. I want to thank Miikka Honka, Luiz Eduardo and Prince “Mr. Muscle” Dadson for forming a male gym quartet to keep us in fit, mentally and physically, during good and hard times throughout my doctoral studies and sharing intercontinental cultural differences in humoristic way. Especially, Prince has shared a lot of thoughts and ideas with me and helped me in multiple areas of life. Furthermore, I want to thank all of my friends outside work for spending great time with me.

I want to sincerely give my appreciation to my mother Maritta Elo and my brother Miikka Elo for your presence and care throughout my doctoral studies and in life in general. You have always been supporting me whatever I have done. Most of all, I want to express my love and gratitude for my fiancée Maria Metsämäki. You have been taking care of my wellbeing, work life and free time balance, stress, listened my worries, assisting me with my analysis while I had to attend meetings or congresses, cheering up me after an exhausting work periods, keeping “discipline” during coronavirus lockdown and be there when I need it the most. I know that I can rely on you now and in the future and we are going to have an amazing adventure ahead of us.

Turku, September, 2020
Petri Elo

References

Aalto, K., Autio, A., Kiss, E.A., Elima, K., Nymalm, Y., Veres, T.Z., Maksimow, M., Marttila-Ichihara, F., Elovaara, H., Saanijoki, T., Crocker, P.R., Maksimow, M., Bligt, E., Salminen, T.A., Salmi, M., Roivainen, A., Jalkanen, S. 2011. Siglec-9 is a novel leukocyte ligand for vascular adhesion protein-1 and can be used in PET imaging of inflammation and cancer. *Blood,* 118, p. 3725–3733.

Ahtinen, H., Kulkova, J., Lindholm, L., Eerola, E., Hakanen, A.J., Mortiz, N., Söderström, M., Saanijoki, T., Jalkanen, S., Roivainen, A., Aro, H.T. 2014. ^{68}Ga-DOTASiglec-9 PET/CT imaging of peri-implant tissue responses and staphylococcal infections. *EJNMMI Res,* 4, p. 45.

Airas, L., Mikkola, J., Vainio, J.M., Elovaara, I., Smith, D.J. 2006. Elevated serum soluble vascular adhesion protein-1 (VAP-1) in patients with active relapsing remitting multiple sclerosis. *J Neuroimmunol,* 117(1-2), p. 132–135.

Airas, L., Dickens, A.M., Elo, P., Marjamäki, P.M., Johansson, J., Eskola, O., Jones, P.A., Trigg, W., Solin, O., Haaparanta-Solin, M., Anthony, D.C., Rinne, J. 2015. In vivo positron emission tomography imaging demonstrates diminished microglial activation after fingolimod treatment in an animal model of multiple sclerosis. *J Nucl Med*, (56), p. 305–310.

Alam, M, Lee, J., Lee, S-Y. 2017. Recent Progress in the Development of TSPO PET Ligands for Neuroinflammation Imaging in Neurological Diseases. *Nucl Med Mol Img,* 51, p. 283–296.

Aljammaz, I., Al-Otaibi, B., Al-Hokbany, N., Amer, S., Okarvi, S. 2014. Development and pre-clinical evaluation of new ^{68}Ga-NOTA-folate conjugates for PET imaging of folate receptor-positive tumors. *Anticancer Res,* 34, p. 6547–6556.

Allen, I.V., McQuid, S., Miradkhur, M., Nevin, G. 2001. Pathological abnormalities in the normal-appearing white matter in multiple sclerosis. *Neurol Sci*, 22, p. 141–144.

Alvarez JI, Cayrol R, Prat A. 2011. Disruption of central nervous system barriers in multiple sclerosis. *Biochim Biophys Acta*, 1812, p. 252–264.

Anthony, D.C., Couch, Y. 2014. The systemic response to CNS injury. *Exp Neurol,* 258, p. 105-111.

Anthony, D.C., Miller, K.M., Fearn, S., Townsend, M.J., Opdenakker, G., Wells, G.M.A, Clements, J.M., Chandler, S., Gearing, A.J.H, Perry, V.H. 1998. Matrix metalloproteinase expression in an experimentally-induced DTH model of multiple sclerosis in the rat CNS. *J Neuroimmunol,* (87), p. 62–72.

Autio A, Jalkanen S, Roivainen A. 2013. Nuclear imaging of inflammation: homing-associated molecules as targets. *EJNMMI Res,* 3:1.

Auvity, S., Tonietto, M., Caillé, F., Bodini, B., Bottlaender, M., Tournier, N., Kuhnast, B., Stankoff, B. 2020. Repurposing radiotracers for myelin imaging: a study comparing ^{18}F-florbetaben, ^{18}F-florbetapir, ^{18}F-flutemetamol, ^{11C}-MeDAS, and ^{11}C-PiB. *Eur J Nucl Med Mol Img,* 47, p. 490–501.

Bailey, S.L., Carpentier, P.A., McMahon, E.J., Begolka, W.S., Miller, S.D. 2006. Innate and adaptive immune responses of the central nervous system. *Crit Rev Immunol*, 26(2), p. 149–188.

Bakshi, R., Thompson, A.J., Rocca, M.A., Pelletier, D., Dousset, V., Barkhof, F., Inglese, M., Guttmann, C.R., Horsfield, M.A., Filippi, M. 2008. MRI in multiple sclerosis: current status and future prospects. *Lancet Neurol*, 7, p. 615–625.

Barkhof F. 2002. The clinico-radiological paradox in multiple sclerosis revisited. *Curr Opin Neurol,* 15, p. 239–245.

Barnett MH, Prineas JW. 2004. Relapsing and remitting multiple sclerosis: pathology of the newly forming lesion. *Ann Neurol,* 55, p. 458–468.

McBride, W.J., Sharkey, R.M., Karacay, H., D'Souza, C.A., Rossi, E.A., Laverman, P., Goldenberg, D.M. 2009. A novel method of ^{18}F radiolabeling for PET. *J Nucl Med,* 50, p. 991–998.

Bo, L., Vedeler, C.A., Nyland, H., Trapp, B.D., Mork, S.J. 2003. Intracortical multiple sclerosis lesions are not associated with increased lymphocyte infiltration. *Mult Scler*, 9, p. 323–331.

Bogie, J.F., Stinissen, P., Hendriks, J.J. 2014. Macrophage subsets and microglia in multiple sclerosis. *Acta Neuropathol,* 128, p. 191–213.

Brosnan, C.F., Raine, C.S. 2013. The astrocyte in multiple sclerosis revisited. *Glia,* 61, p. 453–465.

Browne P, Chandraratna D, Angood C, Tremlett H, Baker C, Taylor BV, & Thompson AJ., 2014. Atlas of Multiple Sclerosis: A growing global problem with widespread inequity. *Neurology*, 83(11), p. 1022–1024.

Bruck, W., Porada, P., Poser, S., Rieckmann, P., Hanefeld, F., Kretzschmarch, HA. Lassmann, H. 1995. Monocyte/macrophage differentiation in early multiple sclerosis lesions. *Annals of Neurology*, 38, p. 788–796.

Carlos, T.M., Harlan, J.M. 1994. Leukocyte-endothelial adhesion molecules. *Blood,* 84, p. 2068 - 2101.

Castillo, V., Lizcano, J.M., Visa, J., Unzeta, M. 1998. Semicarbazide-sensitive amine oxidase (SSAO) from human and bovine cerebrovascular tissues: biochemical and immunohistological characterization. *Neurochem Int,* 33, p. 415–423.

Chan, L., Sitoh, Y., Chong, J., See, S., Umapathi, T. N., Lim, S. & Ong, B. 2007. Application of the McDonald MRI criteria in multiple sclerosis. *Annals-Academy of Medicine Singapore,* 36, p. 647–654.

Chen, Q., Meng, X., McQuade, P., Rubins, D., Lin, S., Zeng, Z., Low, P.S. 2016. Synthesis and preclinical evaluation of Folate-NOTA-Al^{18}F for PET imaging of folate-receptor-positive tumors. *Mol Pharm,* 13, p. 1520–1527.

Chauveau, F., Boutin, H., Van Camp, N., Dolle, F., Tavitian, B. 2008. Nuclear imaging of neuroinflammation: a comprehensive review of [^{11}C]PK1195 challengers. *Eur J Nucl Med Mol Imaging,* 35, p. 2304–2319.

Cherry, S., Shao, Y., Silverman, R., Meadors, K., Siegel, S., Chatziioannou, A., Young, J., Jones, W., Moyers, J. & Newport, D. 1997. MicroPET: a high resolution PET scanner for imaging small animals. *Nuclear Science,* (44), p. 1161–1166.

Chicheportiche, A., Marciano, R., Orevi, M. 2020. Comparison of NEMA characterizations for Discovery MI and Discovery MI-DR TOF PET/CT systems at different sites and with other commercial PET/CT systems. *Eur J Nucl Med Mol I Phys,* 7(1), p.4

Ching, A.S.C., Kuhnast, B., Damont, A., Roeda, D., Tavitian, B., Dollé, F. 2012. Current paradigm of the 18-kDa translocator protein (TSPO) as a molecular target for PET imaging in neuroinflammation and neurodegenerative diseases. *Insights Imaging,* 3(1), p. 1–9.

Comi, G., Filippi, M., Barkhof, F., Durelli, L., Edan, G., Fernandez, O., Hartung, H.P., Seeldrayers, P., Sorensen, P.S., Rovaris, M., Martinelli, V., Hommes, O.R. 2001. Effect of early interferon treatment on conversion to definite multiple sclerosis: a randomised study. *Lancet,* (357), p. 1576–1582.

Compston, A., Coles, A., 2008. Multiple sclerosis. *Lancet*, 372(9648), p. 1502– 1517.

Confavreux C, Vukusic S, Moreau T, Adeleine P. 2000. Relapses and progression of disability in multiple sclerosis. *N Engl J Med*, 343, p. 1430–1438.

Corboy, J.R., Goodin, D.S., Frohman, E.M. 2003. Disease-modifying therapies for multiple sclerosis. *Current Treatment Options in Neurology,* 5(1), p. 35–54.

Dal Canto, M.C., Melvold, R.V., Kim, B.S., Miller, S.D. 1995. Two models of multiple sclerosis: Experimental allergic encephalomyelitis (EAE) and theiler's murine encephalomyelitis virus (TMEV) infection. A pathological and immunological comparison. *Microsc Res Techniq,* 32(3), p. 215–229.

Datta, G., Colasanti, A., Kalk, N., Owen, D., Scott, G., Rabiner, E.A., Gunn, R.N., Lingford-Hughes, A., Malik, O., Ciccarelli, O., Nicholas, R., Nei, L., Battaglini, M., Stefano, N.D., Matthews, P.A. 2017. ^{11}C-PBR28 and ^{18}F-PBR111 Detect White Matter Inflammatory Heterogeneity in Multiple Sclerosis. *J Nucl Med,* 58(9), p. 1477–1482.

Davis, F.A. 2014. The clinico-radiological paradox in multiple sclerosis: novel implications of lesion size. *Mult Scler J*, 20(4), p. 515–516.

DeLuca, G.C., Williams, K., Evangelou, N., Ebers, G.C., Esiri, M.M. 2006. The contribution of demyelination to axonal loss in multiple sclerosis. *Brain*, 129, p. 1507–1516.

De Paula Faria, D., Copray, S., Dierckx, Buchpiguel, C., Dierckx, R., De Vries, E. 2014. PET imaging in multiple sclerosis. *J Neuroimmun Pharm,* 9, p. 468–482.

Dickens, A.M., Vainio, S., Marjamäki, P., Johansson, J., Lehtiniemi, P., Rokka, J., Rinne, J., Solin, O., Haaparanta-Solin, M., Jones, P.A., Trigg, W., Anthony, D.C., Airas, L. 2014. Detection of Microglial Activation in an Acute Model of Neuroinflammation Using PET and Radiotracers ^{11}C-(R)-PK11195 and ^{18}F-GE-18. *J Nucl Med,* 55, p. 466–472.

Ebers, G.C. PRISMS (Prevention of Relapses Disability by Interferon b-1a Subcutaneously in Multiple Sclerosis) Study Group. 1998. Randomised double-blind placebo controlled study of interferon b-1a in relapsing/remitting multiple sclerosis. *Lancet,* 352, p. 1498–1504.

Elnakat, H., Ratnam, M. 2004. Distribution, functionality and gene regulation of folate receptor isoforms: implications in targeted therapy. *Advanced Drug Delivery Reviews,* 56(8), p. 1067–1084.

Evangelou, N., DeLuca, G.C., Owens, T., Esiri, M.M. 2005. Pathological study of spinal cord atrophy in multiple sclerosis suggests limited role of local lesions. *Brain*, 128, p. 29–34.

Farges, R, Joseph-Liauzun, E., Shire, D., Caput, D., LeFur, G., Ferrara, P. 1994. Site-directed mutagenesis of the peripheral benzodiazepine receptor: identification of amino acids implicated in the binding site of Ro5-4864. *Mol Pharmacol,* 46, p. 1160–1167.

Feng, Y., Shen, J., Streaker, E.D., Lockwood, M., Zhu, Z., Low, P.S., Dimitrov, D.S. 2011. A folate receptor beta-specific human monoclonal antibody recognizes activated macrophage of rheumatoid patients and mediates antibodydependent cell-mediated cytotoxicity. *Arthritis Res Ther,* 13, p. 1–12.

Ferguson, B., Matyszak, M.K., Esiri, M.M., Petty, V.H. 1997. Axonal damage in acute multiple sclerosis lesions. *Brain,* 120, p. 393–399.

Fazekas, F., Soelberg-Sorensen, P., Comi. G., Filippi, M. 2007. MRI to monitor treatment efficacy in multiple sclerosis. *J Neuroimaging,* 17(1), p. 50–55.

FDA approves new oral drug to treat multiple sclerosis. 2019. https://www.fda.gov/NewsEvents/Newsroom/PressAnnouncements/ucm634469.htm (Accessed on February 13, 2020).

FDA approves new oral treatment for multiple sclerosis. 2019. https://www.fda.gov/news-events/press-announcements/fda-approves-new-oral-treatment-multiple-sclerosis. Accessed on February (13, 2020).

Fisniku, L.K., Chard, D.T., Jackson, J.S., Anderson, V.M., Altmann, D.R., Miszkiel, K.A., Thompson, A.J., Miller, D.H. 2008. Gray matter atrophy is related to long-term disability in multiple sclerosis. *Ann Neurol,* 64, p. 247–254.

Foster, C.A., Mechtcheriakova, D., Storch, M.K., Balatoni, B., Howard, L.M., Bornancin, F., Wlachos, A., Sobanov, J., Kinnunen, A., Baumruker, T. 2008. FTY720 rescue therapy in the dark agouti rat model of experimental autoimmune encephalomyelitis: expression of central nervous system genes and reversal of blood-brain-barrier damage. *Brain Pathol,* 19, p. 254–266.

Freedman, M.S., Selchen, D., Arnold, D.L. Prat, A., Banwell, B., Yeung, M. 2013. Treatment optimization in MS: Canadian MMS working group updated recommendations. *Can J Neurosci,* 40, p. 307–323.

Freund, J., Stern, E.R., Pisani, T.M. 1947. Isoallergic encephalomyelitis and radiculitis in guinea pigs after one injection of brain and mycobacteria in water-in-oil emulsion. *J Immunol,* 57, p. 179–194.

Frischer, J.M., Bramow, S., Dal-Bianco, A., Lucchinetti, C.F., Rauschka, H., Schmidbauer, H., Laursen, H., Sorensen, P.S., Lassmann, H. 2009. The relation between inflammation and neurodegeneration in multiple sclerosis brains. *Brain*, 132, p. 1175–1189.

Frohman, E.M., Racke, M.K., Raine, C.S. 2006. Multiple sclerosis–the plaque and its pathogenesis. *N Engl J Med,* 354, p. 942–955.

Gay, F.W., Drye, T.J., Dick, G.W., & Esiri, M.M. 1997. The application of multifocal cluster analysis in the staging of plaques in early multiple sclerosis. Identification and characterization of primary demyelinating lesiosn. *Brain,* 120, p. 1461–1483.

Genain, C.P., Nguyen, M.H., Letvin, N.L., Pearl, R., Davis, R.L., Adelman, M., Lees, M.B., Linington, C., Hauser, S.L. 1995. Antibody facilitation of multiple sclerosis-like lesions in a nonhuman primate. *J Clin Invest,* 96, p. 2966–2974.

Girard, J.P., Springer, T.A. 1995. High endothelial venules (HEV's): specialized endothelium for lymphocyte migration. *Immunol Today,* 16, p. 449–457.

Goertzen, A.L., Bao, Q., Bergeron, M., Blankemeyer, E., Blinder, S., Canadas, M., Chatziioannou, A.F., Dinelle, K., Elhami, E., Jans, H.S., Lage, E., Lecomte, R., Sossi, V., Surti, S., Tai, Y.C., Vaquero, J.J., Vicente, E., Williams, D.A., Laforest, R. 2012. NEMA NU 4- 2008 comparison of preclinical PET imaging systems. *J Nucl Med,* 53, p. 1300–1309.

Gold, R., Linington, C., Lassmann, H., 2006. Understanding pathogenesis and therapy of multiple sclerosis via animal models: 70 years of merits and culprits in experimental autoimmune encephalomyelitis research. *Brain,* 129, p. 1953–1971.

Goverman, J., Woods, A., Larson, L., Weiner, L.P., Hood, L., Zaller, D.M. 1993. Transgenic mice that express a myelin basic protein-specific T cell receptor develop spontaneous autoimmunity. *Cell,* 72, p. 551–560.

Harberts, E., Datta, D., Chen S., Wohler, J.E., Oh, U., Jacobson, S. 2012. Translocator Protein 18 kDa (TSPO) Expression in Multiple Sclerosis Patient. *J Neuroimmune Pharmacol,* 8, p. 51–57.

Hartung, H.P., Gonsette, R., Konig, N., Kwiecinski, H., Guseo, A., Morrissey, S.P., Krapf, H., Zwingers, T. 2002. Mitoxantrone in progressive multiple sclerosis: a placebo-controlled, double-blind, randomised, multicentre trial. *Lancet,* 360(9350), p. 2018–2025.

Hauser, S.L., Chan, J.R., Oksenberg, J.R. 2013. Multiple sclerosis: prospects and promise. *Ann Neurol,* 74, p. 317–327.

Havrdova, E., Galetta, S., Stefoski, D., Comi, G. 2010. Freedom from disease activity in multiple sclerosis. *Neurology,* 74(3), p. S3–S7.

Hilgenbrink, A.R., Low, P.S. 2005. Folate receptor-mediated drug targeting: from therapeutics to diagnostics. *J Pharm Sci,* 94, p. 2135–46.

Hochmeister, S., Grundtner, R., Bauer, J., Engelhardt, B., Lyck, R, Gordon, G., Korosec, T., Kutzelnigg, A., Berger, J., Bradl, M., Bittner, R.E., Lassmann, H. 2006. Dysferlin is a new marker for leaky brain blood vessels in multiple sclerosis. *J Neuropath Exp Neurol*, 65, p. 855–865.

Horng, S., Therattil, A., Moyon, S., Gordon, A., Kim, K., Argaw, A.T., Hara, Y., Mariani, J.N., Sawai, S., Flodby, P., Crandall, E.D., Borok, Z., Sofroniew, M.V., Chapouly, C., John, G.R. 2017. Astrocytic tight junctions control inflammatory CNS lesion pathogenesis. *J Clin Invest,* 127, p. 3136–3151.

Huseby, E.S., Liggitt, D., Brabb, T., Schnabel, B., Ohle´n, C., Goverman, J. 2001. A pathogenic role for myelin-specific CD8+ T cells in a model for multiple sclerosis. *J Exp Med,* 194, p. 669–676.

Imaizumi, M., Briard, E., Zoghbi, S.S., Gourley, J.P., Hong, J., Musachio, J.L., Gladding, R., Pike V.W., Innis R.B., Masahiro, F. 2007. Kinetic evaluation in nonhuman primates of two new PET ligands for peripheral benzodiazepine receptors in brain. *Synapse,* 61, p. 595–605.

Imaizumi, M., Briard, E., Zoghbi, S.S., Gourley, J.P., Hong, J., Fujimura, Y., Pike, V.W., Innis, R.B., Fujita, M. 2008. Brain and whole-body imaging in nonhuman primates of [^{11}C]PBR28, a promising PET radioligand for peripheral benzodiazepine receptors. *NeuroImage,* 39(3), p. 1289–1298.

Jacobsen, C.O., Farbu, E. 2014. MRI evaluation of grey matter atrophy and disease course in multiple sclerosis: an overview of current knowledge. *Acta Neurologica Scandinavica*, 129, p. 32–36.

Janssen, B., Vugts, D.J., Windhorst, A.D., Mach, R.H. 2018. PET imaging of microglial activation-beyond targeting TSPO. *Molecules,* 23, p. 607.

Jiang, Q., Ewing, J.R., Ding, G.L., Zhang, L., Zhang, Z.G., Li, L., Whitton, P., Lu, M., Hu, J., Li, Q.J., Knight, R.A., Chopp, M. 2005. Quantitative Evaluation of BBB Permeability after Embolic Stroke in Rat Using MRI. *J Cerebr Blood F Met,* 25(5), p. 583–592.

Geurts, J.J.G, Bo, L., Roosendaal, S.D., Hazes, T., Danie¨ls, R., Barkhof, F., Witter, M.P., Huitinga, I., Van Der Valk, P. 2007. Extensive Hippocampal Demyelination in Multiple Sclerosis. *J Neuropathol Exp Neurol,* 66, p. 819–827.

Kieseier, B. C. 2011. The mechanism of action of interferon-β in relapsing multiple sclerosis. *CNS drugs,* 25, p. 491–502.

Kiessling, F., Pichler, B., Hauff, P. 2017. How to choose the right imaging modality. *Small Animal Imaging,* p. 155–161.

Kiferle, L., Politis, M., Muraro, P.A. 2011. Positron emission tomography imaging in multiple sclerosis-current status and future applications. *Eur J Neurol,* 18, p. 226–231.Kivi, E., Elima, K., Aalto, K., Nymalm, Y., Auvinen, K., Koivunen, E., Otto, D.M., Crocker, P.R., Salminen, T.A., Salmi, M., Jalkanen, S. 2009. Human Siglec-10 can bind to vascular adhesion protein-1 and serves as its substrate. *Blood,* 114, p. 5385–5392.

Kreisl, W.C., Fujita, M., Fujimura, Y., Kimura, N., Jenko, K.J., Kannan, P., Jacobson, S.. 2010. Comparison of [^{11}C]-(R)-PK 11195 and [^{11}C]PBR28, two radioligands for translocator protein (18 kDa) in human and monkey: implications for positron emission tomographic imaging of this inflammation biomarker. *Neuroimage,* 49, p. 2924–2932.

Kremenchutzky, A. 2003. Primary progressive MS. *International Multiple Sclerosis Journal*, 10, p. 89–95.

Kuhlmann, T., Ludwin, S., Prat, A., Antel, J., Bruck, W., Lassmann, H. 2017. An updated histological classification system for multiple sclerosis lesions. *Acta Neuropathol*, 133, p. 13–24.

Kurtzke JF. 1983. Rating neurologic impairment in multiple sclerosis: an expanded disability status scale (EDSS). *Neurology,* 33, p. 1444–1452.

Kutzelnigg, A., Lucchinetti, C.F., Stadelmann, C., Brück, W., Rauschka, H., Bergmann, M., Schmidbauer, M., Parisi, J.E., Lassmann, H. 2005. Cortical demyelination and diffuse white matter injury in multiple sclerosis. *Brain*, 128(11), p. 2705–12.

Kutzelnigg, A., Lassmann, H. 2014. Pathology of multiple sclerosis and related inflammatory demyelinating diseases. *Handbook of Clinical Neurology*, 122, p. 15–58.

Laatsch, R.H., Kies, M.W., Gordon, S., Alvord, E.C. 1962. The encephalomyelitic activity of myelin isolated by ultracentrifugation. *J. Exp. Med,* 115, p. 77–88.

Lassmann, H. 1999. The pathology of multiple sclerosis and its evolution. *Philosophical Transactions of the Royal Society B: Biological Sciences,* 354, p. 1635-40.

Lassmann H, Brück W, Lucchinetti C. 2007. The immunopathology of multiple sclerosis: an overview. *Brain Pathol*, 17, p. 210–218.

Lassmann, H., Van Horssen, J., Mahad, D. 2012. Progressive multiple sclerosis: pathology and pathogenesis. *Nat Rev Neurol*, 8, p. 647–656.

Lassmann, H. 2014. Mechanisms of White Matter Damage in Multiple Sclerosis. *Glia,* 62, p. 1816–1830.

Lavisse, S., Guillermier, M., Hérard, A.S., Petit, F., Delahaye, M., Van Camp, N., Ben Haim, L., Lebon, V., Remy, P., Dollé, F., Delzescaux, T., Bonvento, G., Hantraye, P., Escartin, C. 2012. Reactive astrocytes overexpress TSPO and are detected by TSPO positron emission tomography imaging. *J Neurosci,* 32, p. 10809–10818.

Leary SM, Thompson AJ. 2005. Primary progressive multiple sclerosis: current and future treatment options. *CNS Drugs,* 19, p. 369–376.

Li, Z., Conti, P.S. 2010. Radiopharmaceutical chemistry for positron emission tomography. *Adv Drug Deliv Rev,* 62(11), p. 1031–1051.

Logan, J., Fowler, J.S., Volkow, N.D., Wolf, A.P., Dewey, S.L., Schlyer, D.J., MacGregor, R.R., Hitzemann, R., Bendriem, B., Gatley, S.J., Christman, D.R. 1990. Graphical Analysis of Reversible Radioligand Binding from Time—Activity Measurements Applied to [N-^{11}C-Methyl]-(−)-Cocaine PET Studies in Human Subjects. *J Cerebr Blood F Met,* 10(5), p. 740–747.

Low, P.S., Antony, A.C. 2004. Folate receptor-targeted drugs for cancer and inflammatory diseases. Adv. *Drug Delivery Rev,* 56, p. 1055–1231.

Low, P.S., Henne, W.A., Doorneweerd, D.D. 2007. Discovery and development of folicacid-based receptor targeting for imaging and therapy of cancer and inflammatory diseases. *Acc Chem Res,* 41, p. 120–129.

Lu, Y., Wollak, K.N., Cross, V.A., Westrick, E., Wheeler, L.W., Stinnette, T.W., Vaughn, J.F., Hahn, S.J., Xu, L.C., Vlahov, I.R., Leamon, C.P.2014. Folate receptor-targeted aminopterin therapy is highly effective and specific in experimental models of autoimmune uveitis and autoimmune encephalomyelitis. *Clin Immunol,* 150, p. 64–77.

Lublin, F.D., Reingold, S.C. 1996. Defining the clinical course of multiple sclerosis: results of an international survey. *Neurology*, 46, p. 907–911.

Lublin, F.D., Reingold, S.C, Cohen, J.A., Cutter G.R., Sørensen P.S., Thompson A.J., Wolinsky, J.S., Balcer, L.J., Banwell, B., Barkhof, F., Bebo, B., Calabresi, P.A., Clanet, M., Comi, G., Fox, R.J., Freedman, M.S., Goodman, A.D., Inglese, M., Kappos, L., Kieseier, B.C., Lincoln, J.A., Lubetzki, C., Miller, A.E., Montalban, X., O'Connor, P.W., Petkau, J., Pozzilli, C., Rudick, R.A., Sormani, M.P., Stüve, O., Waubant, E., Polman, C.P. 2014. Defining the clinical course of multiple sclerosis: the 2013 revisions. *Neurology,* 83, p. 278–286.

Lucchinetti, C.F., Bruck, W., Parisi, J., Scheithauer, B., Rodriguez, M., Lassmann, H. 1999. A quantitative analysis of oligodendrocytes in multiple sclerosis lesions: A study of 113 cases. *Brain,* 122(12), p. 2279–2295.

Lucchinetti, C.F., Bruck, W., Parisi, J., Scheithauer, B., Rodriguez, M., Lassmann, H. 2000. Heterogeneity of multiple sclerosis lesions: Implications for the pathogenesis of demyelination. *Ann Neurol,* 47(6), p. 707–717.

Lucchinetti, C. F., Parisi, J. & Bruck, W. 2005. The pathology of multiple sclerosis. *Neurologic clinics,* 23, p. 77–105.

Luus, C., Hanani, R., Reynolds, A., Kassiou, M. 2010. The development of PET radioligands for imaging the translocator protein (18 kDa): What have we learned. *J Label Compd Radiopharm,* 53, p. 501–510.

Lyons, J.A., Ramsbottom, M.J., Cross, A.H. 2002. Critical role of antigen-specific antibody in experimental autoimmune encephalomyelitis induced by recombinant myelin oligodendrocyte glycoprotein. *Eur J Immunol,* 32, p. 1905–1913.

Lyons, J.A., San, M., Happ, M.P., Cross, A.H. 1999. B cells are critical to induction of experimental allergic encephalomyelitis by protein but not by a short encephalitogenic peptide. *Eur J Immunol,* 29, p. 3432–3439.

Mahad, D., Ziabreva, I., Lassmann, H., Turnbull, D. 2008. Mitochondrial defects in acute multiple sclerosis lesions. *Brain,* 131, p. 1722–1735.

Marrie, R. A. 2004. Environmental risk factors in multiple sclerosis aetiology. *The Lancet Neurology,* 3, p. 709–718.

McDonald, W.I., Compston, A., Edan, G., Goodkin, D., Hartung H.P., Lublin, F.D., McFarland, H.F., Paty, D.W., Polman, C.P., Reingold, S.C., Sandberg-Wollheim, M., Sibley, W., Thompson, A., Van Den Noort, S., Weinshenker, B.Y., Wolinsky, J.S. 2001. Recommended diagnostic criteria for multiple sclerosis: guidelines from the International Panel on the diagnosis of multiple sclerosis. *Ann Neurol*, 50, p. 121–127.

Merkler, D., Ernsting, T., Kerschensteiner, M., Brück, W., Stadelmann, C. 2006. A new focal EAE model of cortical demyelination: multiple sclerosis-like lesions with rapid resolution of inflammation and extensive remyelination. *Brain,* 129(8), p. 1972–1983.

Meyer-Moock, S., Feng, Y.S., Maeurer, M., Dippel, F.W., Kohlmann, T. 2014. Systematic literature review and validity evaluation of the Expanded Disability Status Scale (EDSS) and the Multiple Sclerosis Functional Composite (MSFC) in patients with multiple sclerosis. *BMC Neurol,* 14, p. 58.

Mikita, J., Dubourdieu-Cassagno, N., Deloire, M.S., Vekris, A., Biran, M., Raffard, G., Brochet, B., Canron, M.H., Franconi, J.M., Boiziau, C., Petry, K.G. 2011. Altered M1/M2 activation patterns of monocytes in severe relapsing experimental rat model of multiple sclerosis. Amelioration of clinical status by M2 activated monocyte administration. *Mult Scler,* 17, p. 2–15.

Miller, D.H., Albert, P.S., Barkhof, F., Francis, G., Frank, J.A., Hodgkinson, S., Lublin, F.D., Paty, D.W., Reingold, S.C., Simon, J. 1996. Guidelines for the use of magnetic resonance techniques in monitoring the treatment of multiple sclerosis. US National MS Society Task Force. *Ann Neurol,* 39(1), p. 6–16.

Miller, D.H., Leary, S.H. 2007. Primary progressive multiple sclerosis. *Lancet Neurol,* 6, p. 903–12.

Miller, W., deMello, P.J., Anthony, A.D.G. 2010. Application of Microfluidics to the Ultra-Rapid Preparation of Fluorine-18 Labelled Compounds. *Curr Radiopharm,* 3(3), p. 254–262.

Minagar A, Alexander JS. 2003. Blood-brain barrier disruption in multiple sclerosis. *Mult Scler,* 9, p. 540–549.

Miron, V.E., Boyd, A., Zhao, J.W., Yuen, T.J., Ruckh, J.M., Shadrach, J.L., Wijngaarden, P., Wagers, A.J., Williams, A., Franklin, R.J.M., French-Constant, C. 2013. M2 microglia and macrophages drive oligodendrocyte differentiation during CNS remyelination. *Nat Neurosci,* (16), p. 1211–1218.

Mix, E., Meyer-Rienecker, H., Hartung, H. P. & Zettl, U.K. 2010. Animal models of multiple sclerosis—Potentials and limitations. *Progress in neurobiology,* 92, p. 386–404.

Mollison, D., Sellar, R., Bastin, M., Mollison, D., Chandran, S., Wardlaw, J., Connick, P. 2017 The clinico-radiological paradox of cognitive function and MRI burden of white matter lesions in people with multiple sclerosis: A systematic review and meta-analysis. *PLoS One,* 12(5), p. e0177727.

Montalban, X., Hauser, S.L., Kappos, L, Arnold, D.L, Bar-Or, A., Comi, G., de Seze, J., Giovannoni, G., Hartung, H.P., Hemmer, B., Lublin, F., Rammohan, K.W. 2017. Ocrelizumab versus placebo in primary progressive multiple sclerosis. *N Engl J Med*, 376(3), p. 209–220.

Muller, C., Struthers, H., Winiger, C., Zhernosekov, K., Schibli, R. 2013. DOTA Conjugate with an Albumin-Binding Entity Enables the First Folic Acid–Targeted ^{177}Lu-Radionuclide Tumor Therapy in Mice. *J Nucl Med,* 53(1), p. 124–131.

Munoz, J.J., Bernard, C.C., Mackay, I.R., 1984. Elicitation of experimental allergic encephalomyelitis (EAE) in mice with the aid of pertussigen. *Cell Immunol*, 83, p. 92–100.

Muzi, M., O'Sullivan, F., Mankoff, D.A., Doot, R.K., Pierce, L.A., Kurland, B.F., Linden, H.M., Kinahan, P.E. 2012. Quantitative assessment of dynamic PET imaging data in cancer imaging. *Magnetic Resonance Imaging,* 30(9), p. 1203–1215.

Nagai, T., Tanaka, M., Tsuneyoshi, Y., Matsushita, K., Sunahara, N., Matsuda, T., Yoshida, H., Komiya, S., Onda, M., Matsuyama, T. 2006. *In vitro* and *in vivo* efficacy of a recombinant immunotoxin against folate receptor beta on the activation and proliferation of rheumatoid arthritis synovial cells. *Arthritis Rheum,* 54, p. 3126–3134.

Niino, M. 2012. Multiple sclerosis treatment: current best practice. *Expert Review of Clinical Immunology,* 8, p. 505–507.

Oprea, T.I., Davis, A.M., Teague, S.J., Leeson, P.D. 2001. Is there a difference between leads and drugs? A historical perspective. *J Chem Inf Comput Sci, 41,* p. 1308–15.

O'Rourke, A.M., Wang, E.Y., Salter-Cid, L., Huang, L., Miller, A., Podar, E., Gao, H.F., Jones, D.S., Linnik, M.D. 2007. Benefit of inhibiting SSAO in relapsing experimental autoimmune encephalomyelitis. *J Neural Transm,* 114, p. 845–849.

Orton, S.M., Herrera, B.M., Yee, I.M., Waldar, W., Ramagopalan, S.V., Sadovnik, A.D., Ebers, G.C., 2006. Sex ratio of multiple sclerosis in Canada: a longitudinal study. *Lancet Neurol*, 5, p. 932–936.

Pirko I, Johnson AJ. 2008. Neuroimaging of demyelination and remyelination models. *Adv Mult Scler Exp Dem Dis*, p. 241-266.

Polman, C. H., Reingold, S. C., Banwell, B., Clanet, M., Cohen, J. A., Filippi, M., Fujihara, K., Havrdova, E., Hutchinson, M. & Kappos, L. 2011. Diagnostic criteria for multiple sclerosis: 2010 revisions to the McDonald criteria. *Annals of neurology,* 69, p. 292–302.

Polman, C. H., Reingold, S. C., Edan, G., Filippi, M., Hartung, H. P., Kappos, L., Lublin, F. D., Metz, L. M., Mcfarland, H. F. & O'connor, P. W. 2005. Diagnostic criteria for multiple sclerosis: 2005 revisions to the "McDonald Criteria". *Annals of neurology,* 58, p. 840–846.

Ponath, G., Ramanan, S., Mubarak, M., Housley, W., Seunghoon, L., Sahinkaya, R.F., Vortmeyer, A., Raine, C.S., Pitt, D. 2017. Myelin phagocytosis by astrocytes after myelin damage promotes lesion pathology. *Brain,* 140, p. 399–413.

Popescu, V., Agosta, F., Hulst, H.E., Sluimer, I.C., Knol, D.L. Sormani, M.P., Enzinger, C., Ropele, S., Alonso, J., Sastre -Garriga, J., Rovira, A., Montalban, X., Bodini, B., Ciccarelli, O., Khaleeli, Z., Chard, DT., Matthews, L., Palace, J., Giorgio, A., Stefano, N.D., Eisele, P., Gass, A., Polman C.H., Uitdehaag, B.M.J., Messina, M.J., Comi, G., Filippi, M., Barkhof, F., Vrenken, H. 2013. Brain atrophy and lesion load predict long term disability in multiple sclerosis. *J. Neurol. Neurosurg. Psychiatry,* 84, p. 1082–1091.

Poser, C. M., Paty, D. W., Scheinberg, L., Mcdonald, W. I., Davis, F. A., Ebers, G. C., Johnson, K. P., Sibley, W. A., Silberberg, D. H. & Tourtellotte, W. W. 1983. New diagnostic criteria for multiple sclerosis: guidelines for research protocols. *Annals of neurology,* 13, p. 227–231.

Prescribing information Mavenclad (cladribine) tablets. https://www.accessdata.fda.gov/drugsatfda_docs/label/2019/022561s000lbl.pdf (Accessed on February 13, 2020).

Prineas, J.W., Kwon, E.E., Cho, E.S., Sharer, L.R., Barnett, M.H., Oleszak, E.L., Hoffman, B., Morgan B.P. 2001. Immunopathology of secondary-progressive multiple sclerosis. *Ann Neurol*, 50, p. 646–657.

Prineas, J.W., Parrat, J.D.E. 2012. Oligodendrocytes and early multiple sclerosis lesion. *Ann Neurol,* 72(1), p. 18–31.

Qiu, A., Jansen, M., Sakaris, A., Min, S.H., Chattopadhyay, S., Tsai, E., Sandoval, C., Zhao, R., Akabas, M.H., Goldman, I.D. 2006. Identification of an intestinal folate transporter and the molecular basis for hereditary folate malabsorption. *Cell,* 127, p. 917–928.

Racke, M.K. 2008. The role of B cells in multiple sclerosis: rationale for B-cell-targeted therapies. *Curr Opin Neurol,* 21, p. 9–18.

Ransohoff, R.M. 2006. A mighty mouse: building a better model of multiple sclerosis. *J. Clin. Invest,* 116, p. 2313–2316.

Ransohoff, R. M. 2012. Animal models of multiple sclerosis: the good, the bad and the bottom line. *Nature Neuroscience,* 15, p. 1074–1077.

Rissanen, E., Virta, J.R., Paavilainen, T., Tuisku, J., Helin, S., Luoto, P., Parkkola, R., Rinne, J.O., Airas, L. 2013. Adenosine A_2A Receptors in Secondary Progressive Multiple Sclerosis: A [^{11}C] TMSX Brain PET Study. *J Cerebral Blood F Met,* 33(9), p. 1394–1401.

Rovaris, M., Confavreux, C., Furlan, R., Kappos, L., Comi, G. & Filippi, M. 2006. Secondary progressive multiple sclerosis: current knowledge and future challenges. *Lancet Neurol*, 5, p. 343–354.

Rovira, A., Leon, A. 2008. MR in the diagnosis and monitoring of multiple sclerosis: An overview. *Eur J Radiol,* 67, p. 409–414.

Salmi, M., Kalimo, K., Jalkanen, S. 1993. Induction and function of vascular adhesion protein-1 at sites of inflammation. *J Exp Med,* 178 (6), p. 2255–2260.

Schumacher, G. A., Beebe, G., Kibler, R. F., Kurland, L. T., Kurtzke, J. F., Mcdowell, F., Nagler, B., Sibley, W. A., Tourtellotte, W. W. & Willmon, T. L. 1965. Problems of experimental trials of

therapy in multiple sclerosis: report by the panel on the evaluation of experimental trials of therapy in multiple sclerosis. *Ann NY Acad Sci,* (122), p. 552–568.

Schweitzer, P.J., Fallon, B.A., Mann, J.J., Kumar, J.S. 2010. PET tracers for the peripheral bendiazepine receptor and uses thereof. *Drug Discov Today,* 15, p. 933–942.

Serres, S., Anthony, D. C., Jiang, Y., Campbell, S. J., Broom, K. A., Khrapitchev, A. & Sibson, N. R. 2009. Comparison of MRI signatures in pattern I and II multiple sclerosis models. *NMR in Biomed,* 22, p. 1014–1024.

Sica A, Mantovani A. 2012. Macrophage plasticity and polarization: *in vivo* veritas. *J Clin Invest,* 122(3), p. 787–795.

Siffrin, V., Vogt, J., Radbruch, H., Nitsch, R. & Zipp, F. 2010. Multiple sclerosis–candidate mechanisms underlying CNS atrophy. *Trends Neurosci*, 33, p. 202–210.

Siitonen, R., Peuhu, E., Autio, A., Liljenbäck, H., Mattila, E., Metsälä, O., Käkelä, M., Saanijoki, T., Dijkgraaf, I., Jalkanen, S., Ivaska, J., Roivainen, A. 2019. ^{68}Ga-DOTA-E[c(RGDfK)]2 Positron Emission Tomography Imaging of SHARPIN-Regulated Integrin Activity in Mice. *J Nucl Med,* 60, p. 1380–1387.

Silvola, J.M.U., Li, X.G., Virta, J., Marjamäki, P., Liljenbäck, H., Hytönen, J.P., Tarkia, M., Saunavaara, V., Hurme, S., Palani, S., Hakovirta, H., Ylä-Herttuala, S., Saukko, P., Chen, Q., Low, P.S., Knuuti, J., Saraste, A., Roivainen, A. 2018. Aluminum fluoride-18 labeled folate enables in vivo detection of atherosclerotic plaque inflammation by positron emission tomography. *Sci Rep,* 9720, p.1–15.

Silvola, J.M.U, Virtanen, H., Siitonen, R., Hellberg, S., Liljenbäck, H., Metsälä, O., Ståhle, M., Saanijoki, T., Käkelä, M., Hakovirta, H., Ylä-Herttuala, S., Saukko, P., Jauhiainen, M., Veres, T.Z., Jalkanen, S., Knuuti, J., Saraste, A., Roivainen, A. 2016. Leukocyte trafficking-associated vascular adhesion protein 1 is expressed and functionally active in atherosclerotic plaques. *Sci Rep,* 6, 35089.

Sirotnak, F.M., Tolner, B. 1999. Carrier-mediated membrane transport of folates in mammalian cells. *Annu Rev Nutr,* 19, p. 91–122.

Sofroniew, M.V. 2015. Astrocyte barriers to neurotoxic inflammation. *Nat Rev Neurosci*, 16, p. 249–263.

Sofroniew, M.V., Vinters, H.V. 2010. Astrocytes: biology and pathology. *Acta Neuropathol,* 119, p. 7–35.

Sormani, M.P., & Bruzzi, P. 2013. MRI lesions as a surrogate for relapses in multiple sclerosis: a meta-analysis of randomised trials. *Lancet Neurol*, (12), p. 669–676.

Sriram, S. & Steiner, I. 2005. Experimental allergic encephalomyelitis: a misleading model of multiple sclerosis. *Ann Neurol,* 58, 939–945.

Steinman, L., Zamvil, S.S. 2006. How to successfully apply animal studies in experimental allergic encephalomyelitis to research on multiple sclerosis. *Ann Neurol,* 60(1), p. 12–21.

Stolen, C.M., Martilla-Ichihara, F., Koskinen, K., Yegutkin, G.G., Turja, R., Bono, P., Skurnik, M., Hanninen, A., Jalkanen, S., Salmi, M. 2005. Absence of the endothelial oxidase AOC3 leads to abnormal leukocyte traffic in vivo. *Immunity,* 22, p. 105–15.

Sumelahti, M.L., Tienari, P.J., Hakama, M., Wikström, J. 2003. Multiple sclerosis in Finland: incidence trends and differences in relapsing remitting and primary progressive disease courses. *J Neurol Neurosurg Psychiatry*, 74, p. 25–28.

Svensson, L., Abdul-Majid, K.B., Bauer, J., Lassmann, H., Harris, R.A., Holmdahl, R. 2002. A comparative analysis of B cell-mediated myelin oligodendrocyte glycoprotein-experimental autoimmune encephalomyelitis pathogenesis in B cell-deficient mice reveals an effect on demyelination. *Eur J Immunol,* 32, p. 1939–1946.

Tallantyre, E.C., Whittam, D.H., Jolles, S., Paling, D., Constantinesecu, C., Robertson, N.P., Jacob, A. 2018. Secondary antibody deficiency: a complication of anti-CD20 therapy for neuroinflammation. *J Neurol,* 265(5), p. 1115–22.

The IFN-β Multiple Sclerosis Study Group. 1993. Interferon beta-1b is effective in relapsing-remitting multiple sclerosis. Clinical results of a multicenter, randomized, double-blind, placebo-controlled trial. *Neurology,*43, p. 655–661.

Thompson, A.J., Banwell, B.L., Barkhof, F., Carroll, W.M., Coetzee, T., Comi, G., Correale, J., Fazekas, F., Filippi, M., Freedman M.S., Fujihara, K., Galetta, S.L., Hartung, H.P., Kappos, L., Lublin, F.D., Marrie, R.A., Miller, A.E., Miller, D.H., Cohen, J.A. 2018. Diagnosis of multiple sclerosis: 2017 revisions of the McDonald criteria. *Lancet,* 17(2), p. 162–173.

Thorkildsen, O., Myhr, K.M., Bo, L. 2016. Disease-modifying treatments for multiple sclerosis – a review of approved therapies. *Eur J Neurol,* 23, p. 18–27.

Trapp, B.D., Peterson, J., Ransohoff, R.M., Rudick, R., MOrk, S., Bo, L. 1998. Axonal transection in the lesions of multiple sclerosis. *New Engl J Med,* 338, p. 278–285.

Turk, M.J., Breur, G.J., Widmer, W.R., Paulos, C.M., Xu, L.C., Grote, L.A., Low, P.S. 2002. Folate targeted imaging of activated macrophages in rats with adjuvant-induced arthritis. *Arthritis Rheum,* 46, p. 1947–55.

Turkington, T.G. 2001. Introduction to PET Instrumentation. *J Nucl Med Technol,* 29, p. 1–8.

Virtanen, H., Autio, A., Siitonen, R., Liljenbäck, H., Saanijoki, T., Lankinen, P., Mäkilä, J., Käkelä, M., Teuho, J., Sasvisto, N., Jaakola, K., Jalkanen, S., Roivainen, A. 2015. ^{68}Ga-DOTA-Siglec-9 – a new imaging tool to detect synovitis. *Arthritis Res Ther,* 17(17), p. 308.

Wang, L., Lai, H.M., Thompson, A.J. 1997. Survey of the distribution of lesion size in multiple sclerosis: Implication for the measurement of total lesion load. *J Neurol Neurosurg Psychiat,* 63, p. 452–455.

Wang, M., Yoder, K.K., Gao, M., Mock, B.H., Xu, X.M., Saykin, A.J., Hutchins, G.D., Zheng, Q.H. 2009. Fully automated synthesis and initial PET evaluation of [^{11}C]PBR28. *Bioorg Med Chem Lett,* 19(19), p. 5636–5639.

Waubant, E.L., Oksenberg, J.R., Goodkin, D.E. 1997. Pathophysiology of multiple sclerosis lesions. *Sci Med,* 4(6), p. 32.

Wekerle, H., Kojima, K., Lannes-Vieira, J., Lassmann, H., Linington, C. 1994. Animal models. *Ann. Neurol,* 36 (Suppl.), p. 47–53.

Wingerchuk, D.M., Carter, J.L. 2014. Multiple Sclerosis: Current and Emerging Disease-Modifying Therapies and Treatment Strategies. *Mayo Clin Proc,* 89(2), p. 225–240.

Witte, M.E., Bo, L., Rodenburg, R., Belien, J.A., Musters, R., Hazes, T., Wintjes, L., Smeitink, J.A., Geurts, J.J., de Vries, H.E., Van der Valk, P., Van Horssen, J. 2009. Enhanced number and activity of mitochondria in multiple sclerosis lesions. *J Pathol*, 2, p. 193–204.

Yamasaki, K., Kira, J., Kawano, Y., Kobayashi, T., Kanai, T., Nishimura, Y., Matsushita S, Hasuo, K., Tobimatsu, S. 1996. Western versus Asian types of multiple sclerosis: immunogenetically and clinically distinct disorders. *Ann Neurol,* 40, p.569–574.

Young, P.Y, Lederer, C., Eder, K., Daumer, M., Neiss, A., Polman, C., Kappos, L. 2006. Relapses and subsequent worsening of disability in relapsing-remitting multiple sclerosis. *Neurology*, 67, p. 804–808.

UNIVERSITY OF TURKU

Painosalama Oy, Turku, Finland 2020

ISBN 978-951-29-8181-6 (PRINT)
ISBN 978-951-29-8182-3 (PDF)
ISSN 0355-9483 (Print)
ISSN 2343-3213 (Online)